Lipokine 5-PAHSA Is Regulated by Adipose Triglyceride Lipase and Primes Adipocytes for De Novo Lipogenesis in Mice

Veronika Paluchova,[1] Marina Oseeva,[1] Marie Brezinova,[1] Tomas Cajka,[1] Kristina Bardova,[1] Katerina Adamcova,[1] Petr Zacek,[2] Kristyna Brejchova,[1] Laurence Balas,[3] Hana Chodounska,[4] Eva Kudova,[4] Renate Schreiber,[5] Rudolf Zechner,[5] Thierry Durand,[3] Martin Rossmeisl,[1] Nada A. Abumrad,[6] Jan Kopecky,[1] and Ondrej Kuda[1]

Diabetes 2020;69:1–13 | https://doi.org/10.2337/db19-0494

Branched esters of palmitic acid and hydroxystearic acid (PAHSA) are anti-inflammatory and antidiabetic lipokines that connect glucose and lipid metabolism. We aimed to characterize involvement of the 5-PAHSA regioisomer in the adaptive metabolic response of white adipose tissue (WAT) to cold exposure (CE) in mice, exploring the cross talk between glucose utilization and lipid metabolism. CE promoted local production of 5- and 9-PAHSAs in WAT. Metabolic labeling of de novo lipogenesis (DNL) using $^{2}H_2O$ revealed that 5-PAHSA potentiated the effects of CE and stimulated triacylglycerol (TAG)/fatty acid (FA) cycling in WAT through impacting lipogenesis and lipolysis. Adipocyte lipolytic products were altered by 5-PAHSA through selective FA re-esterification. The impaired lipolysis in global adipose triglyceride lipase (ATGL) knockout mice reduced free PAHSA levels and uncovered a metabolite reservoir of TAG-bound PAHSAs (TAG estolides) in WAT. Utilization of ^{13}C isotope tracers and dynamic metabolomics documented that 5-PAHSA primes adipocytes for glucose metabolism in a different way from insulin, promoting DNL and impeding TAG synthesis. In summary, our data reveal new cellular and physiological mechanisms underlying the beneficial effects of 5-PAHSA and its relation to insulin action in adipocytes and independently confirm a PAHSA metabolite reservoir linked to ATGL-mediated lipolysis.

The dysregulation of both glucose and lipid metabolism in white adipose tissue (WAT) contributes to the development of obesity-associated type 2 diabetes, which represents one of the most serious health threats. However, the mechanistic links between altered glucose and lipid metabolism in the WAT of obese patients and the development of systemic insulin resistance are not fully explored. De novo lipogenesis (DNL) converts carbohydrates to energy-dense neutral lipids both in the liver and in WAT (1–4). Although hepatic DNL is usually associated with systemic insulin resistance, DNL in WAT correlates with insulin sensitivity and obesity resistance (5–8). We recently demonstrated in WAT that DNL, when combined with triacylglycerol (TAG)/fatty acid (FA) cycling activity, contributes to a lean phenotype in mice (6). This supports the notion that adipose tissue–specific regulation of DNL is critical for metabolic homeostasis (reviewed in Yilmaz et al. [4]).

DNL in WAT might also serve as a source of signaling molecules, i.e., bioactive lipids (lipokines), including palmitoleate (5), alkyl ether lipids (9), and FA esters of hydroxy FAs (FAHFAs), namely, palmitic acid hydroxystearic acids (PAHSAs) (8), molecules that promote insulin sensitivity and ameliorate insulin resistance. Structurally, FAHFAs consist of an FA (e.g., palmitic acid) esterified to a hydroxy FA (e.g., hydroxystearic acid), and the position of the branching carbon defines the regioisomer (e.g.,

[1]Institute of Physiology of the Czech Academy of Sciences, Prague, Czech Republic
[2]Proteomics Core Facility, Faculty of Science, Charles University, and Division BIOCEV, Institute of Molecular Genetics of the Czech Academy of Sciences, Vestec, Czech Republic
[3]Institut des Biomolécules Max Mousseron, UMR 5247, CNRS, Université Montpellier, and Faculté de Pharmacie, ENSCM, Montpellier, France
[4]Neurosteroids, Institute of Organic Chemistry and Biochemistry of the Czech Academy of Sciences, Prague, Czech Republic
[5]Institute of Molecular Biosciences, University of Graz, Graz, Austria
[6]Department of Medicine, Washington University School of Medicine, St. Louis, MO

Corresponding author: Ondrej Kuda, ondrej.kuda@fgu.cas.cz

Received 17 May 2019 and accepted 30 November 2019

This article contains Supplementary Data online at http://diabetes.diabetesjournals.org/lookup/suppl/doi:10.2337/db19-0494/-/DC1.

5-PAHSA, positional isomer). Many families of regioisomers have been identified in humans, rodents, and plants (8,10,11). The 5- and 9-PAHSA regioisomers have been the most studied for their anti-inflammatory and insulin-sensitizing effects (12,13).

During cold exposure (CE), adipose triglyceride lipase (ATGL) catalyzes TAG hydrolysis in WAT and the released FAs fuel thermogenesis in brown adipose tissue (14) while TAGs in WAT are replenished by DNL from glucose (6). Here, we explored the potential involvement of 5-PAHSA in the adaptive metabolic response of WAT to CE in mice. We tested the hypothesis that CE could associate with increased generation of PAHSA that affects both DNL and TAG/FA recycling and influences the metabolic profile of WAT.

RESEARCH DESIGN AND METHODS

Reagents

All chemical reagents were from Sigma-Aldrich (St. Louis, MO) unless stated otherwise. FAHFA standards were from Cayman Europe (Tallinn, Estonia), and 5-PAHSA (Supplementary Fig. 1) was synthesized as previously described (15). Heavy water (^2H_2O) was from CortecNET (Voisins-le-Bretonneux, France), and ^{13}C-labeled glucose and glutamine and ^2H-labeled glucose were from Cambridge Isotope Laboratories (Tewksbury, MA). TAG estolide tag 16:0/16:0/9-PAHSA [*sn*-3-((9-(palmitoyloxy)octadecanoyl)oxy)propane-1,2-diyldipalmitate] was synthesized from 1,2-dipalmitoyl glycerol and 9-PAHSA (Sigma) using 1-ethyl-3-(3-dimethylaminopropyl)carbodiimide and 4-dimethylaminopyridine in CH_2Cl_2.

Animal Studies

Two-month-old male B6 (C57BL/6JBomTac; Taconic Biosciences, Ejby, Denmark) mice fed standard chow were maintained close to thermoneutrality (TN) at 30°C for 1 week. Thereafter, subgroups of mice were either maintained at 30°C (control animals) or exposed to cold (CE animals) at 6°C for 7 days before killing (6). After 3 days, mice were further divided into subgroups and received an oral gavage of 5-PAHSA or saline (in a polyethylene glycol 400/TWEEN 80 formulation [8]) (Fig. 1). The 5-PAHSA dose was 45 mg/kg. EDTA plasma and various tissues were collected, including liver and epididymal WAT (eWAT). Samples were flash frozen and stored in liquid nitrogen. Global ATGL knockout (AKO) mice were generated as previously described (14). Female AKO mice and wild-type (WT) littermates fed standard chow were fasted for 12 h before dissection (fed vs. fasted state) or sacrificed at ad libitum fed state (acute and chronic CE) (14).

In Vivo Lipid Synthesis in Murine eWAT

Two days prior to dissection, mice were injected intraperitoneally with a bolus of ^2H_2O in saline (3.5 mL of 0.9% NaCl w/v in 99.9%-enriched ^2H_2O/100 g body weight) and 10% of their drinking water was replaced with ^2H_2O for the rest of the experiment to stabilize ^2H_2O content in body water as previously described (6). Deuterium enrichment of mouse plasma was assayed by exchange with acetone using GC×GC-TOFMS (two-dimensional gas chromatography time-of-flight mass spectrometry) (16). Total lipids from eWAT were extracted using the methanol/methyl *tert*-butyl ether/water protocol and the TAGs purified by solid-phase extraction (17,18). An aliquot of the TAG extract was hydrolyzed in KOH, the free FA converted to methyl esters, and free glycerol derivatized with N,O-bis(trimethylsilyl)trifluoroacetamide before analysis using GC×GC-TOFMS (19). The fractional synthesis of FA from ^2H_2O was calculated according to mass isotopomer analysis (20). A separate aliquot of the lipid extract was processed for lipidomics and metabolomics.

Cell Culture

3T3-L1 murine adipocytes were differentiated according to a standard protocol and mature adipocytes kept in DMEM complete medium (25 mmol/L glucose, 10% calf serum, 850 nmol/L insulin, penicillin/streptomycin) (10).

In Vitro Lipid Synthesis

3T3-L1 adipocytes were maintained in DMEM complete medium prepared from powder (D5648; Sigma-Aldrich), ^2H_2O, and water for cell cultures (50/50, v/v) (21) for 3 days. Total lipids were extracted as above and processed for lipidomics, and the raw data were analyzed with MS-DIAL version 2.52 software (22). Data from labeling experiments (^{13}C and ^2H) were adjusted for C, H, and O natural abundance and tracer purity using IsoCor 2.0.5 (23), and the fractional synthesis of intact lipids was estimated according to the mass isotopomer analysis (20,24). Parallel reaction monitoring and tandem mass spectrometry (MS/MS) scanning modes of the Q Exactive Plus mass spectrometer (Thermo Fisher Scientific, Bremen, Germany) were used to confirm M+3 isotopologue identity and glycerol backbone labeling.

Glucose Uptake and PAHSA Treatment

Mature 3T3-L1 adipocytes were grown in full DMEM for 3 days in the absence or presence of 5-PAHSA, similar to the duration of 5-PAHSA gavage in mice. Adipocytes were serum starved in DMEM with 0.1% (w/v) BSA for 15 h, washed, and kept in DMEM without glucose and glutamine (A1443001; Gibco) for 30 min. Cells were then labeled with $^{13}C_6$-glucose (5.5 mmol/L in A144301 medium) in the presence or absence of 40 μmol/L 5-PAHSA for 0, 5, 10, and 15 min in a reverse time course fashion, similar to that described by Krycer et al. (25). Metabolism was quenched in a water bath (0°C), and cells were washed twice with ice-cold PBS, lysed in the methanol/water fraction of the methyl *tert*-butyl ether extraction mixture chilled at −20°C, and frozen in liquid nitrogen. Alternatively, cells were preincubated with 10 nmol/L insulin in the glucose-free media and labeled with $^{13}C_6$-glucose (5.5 mmol/L final) with or without 10 nmol/L insulin, and the metabolism was quenched after 10 min.

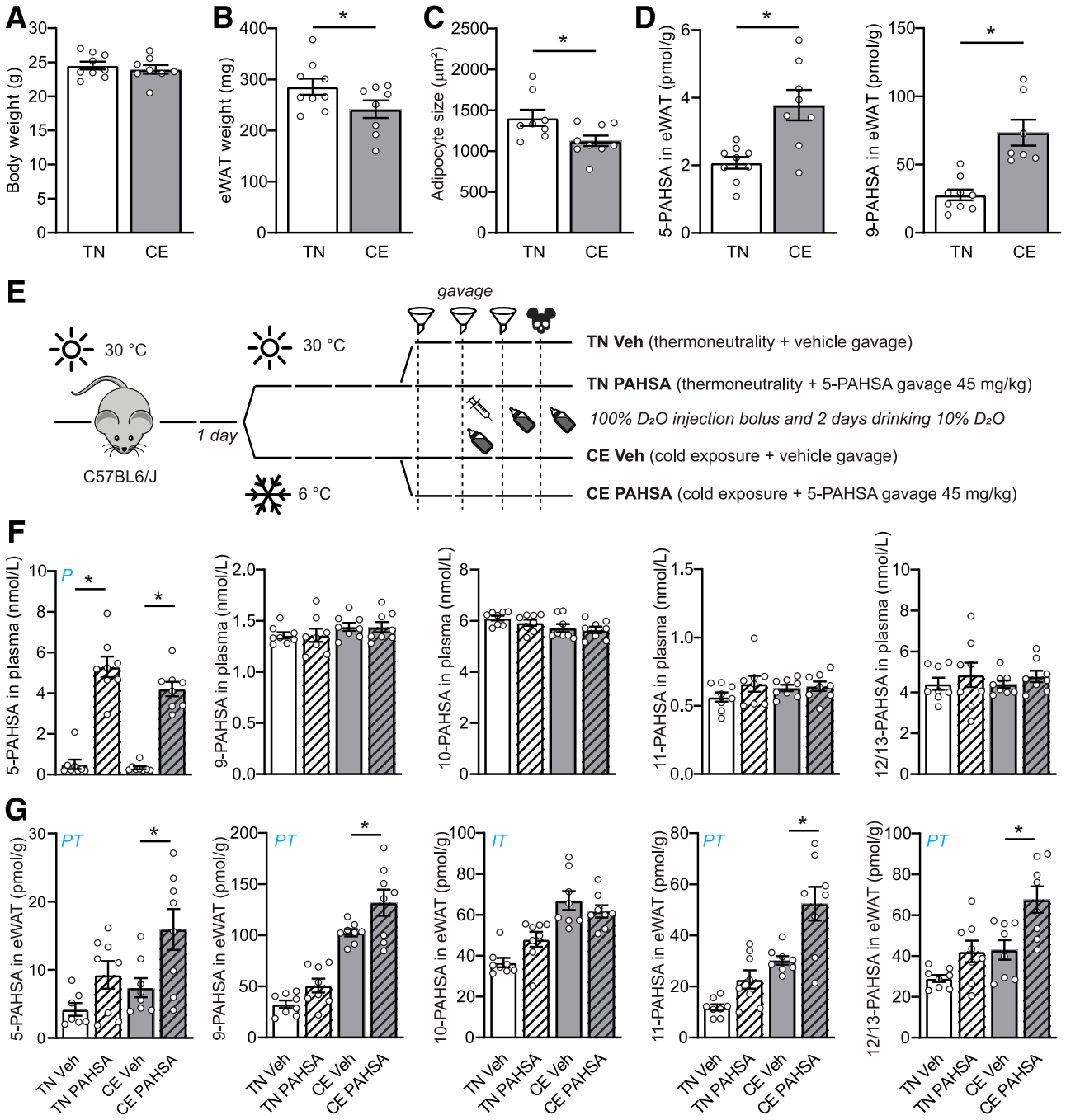

Figure 1—PAHSA levels were increased in cold. *A*: Body weight of male C57BL/6J mice maintained at TN (30°C) and then either kept at TN or exposed to cold (6°C) for 7 days. *B*: Weight of eWAT. *C*: Size of adipocytes in eWAT. *D*: Concentration of 5- and 9-PAHSA in eWAT. Data are means ± SEM (n = 8–9). *$P < 0.05$ by Student t test. *E*: Experiment combining TN, CE, gavage of 5-PAHSA, and deuterium metabolic labeling. *F*: Levels of PAHSA regioisomers in plasma. *G*: Levels of PAHSA regioisomers in eWAT. Two-way ANOVA with multiple comparison test (Sidak) was used. Letters within the graphs denote a statistically significant effect of 5-PAHSA (*P*), temperature (*T*), or interaction of factors (*I*). Data are means ± SEM (n = 8–9). *Planned multiple comparison of the effect of 5-PAHSA at the given temperature statistically different at $P < 0.05$. D_2O, heavy water; Veh, vehicle.

To explore the contribution of glutamine carbons, the labeling media were supplemented with 5.5 mmol/L glucose and 4 mmol/L $^{13}C_5$-glutamine, and the metabolism was quenched after 10 min of glucose uptake.

FAHFA Analysis

Plasma, eWAT, cells, and media were processed according to published methods (10,18) with special attention paid to known methodological issues (26,27).

Metabolomics, Lipidomics, Bioinformatics, and Statistical Analyses

The liquid chromatography (LC)-MS system consisted of a Vanquish UHPLC System (Thermo Fisher Scientific) coupled to a Q Exactive Plus mass spectrometer. See Supplementary Data for details.

LC-MS and LC-MS/MS data were processed through the software MS-DIAL, version 2.52 (22), using its isotope tracking features. Metabolites were annotated using an in-house retention time charge/mass ratio (*m/z*) library and using MS/MS libraries available from public sources (MassBank of North America [MoNA]). Normalized (locally estimated scatterplot smoothing procedure, Python script) peak heights/data from labeling experiments (^{13}C and ^{2}H) were adjusted for C, H, and O natural abundance and tracer purity using IsoCor 2.0.5 (23) when needed. An in silico library of theoretical TAG estolides was calculated using EnviPat (28) and in-house Python scripts. GraphPad Prism 8.0.2 software was used to compare groups (Student *t* test, ANOVA, etc.).

Data and Resource Availability

The data sets generated and/or analyzed during the current study are available from the corresponding author upon reasonable request. No applicable resources were generated or analyzed during the current study.

RESULTS

PAHSA Levels Are Increased by CE

We previously showed that induction of DNL in WAT during CE was associated with a lean phenotype in mice (6). To explore the involvement of PAHSAs in this metabolic adaptation, we examined mice kept at TN or exposed to cold for 7 days. In response to CE, body weight was not affected, while the weight of eWAT and adipocyte size decreased (Fig. 1*A–C*), similar to previous studies (6,29). Levels of both 5- and 9-PAHSA in eWAT were elevated by CE (Fig. 1*D*). Therefore, we explored the effect of 5-PAHSA, administered by gavage for 3 days, on DNL in eWAT of mice kept either at TN or exposed to cold for 7 days. In these studies heavy water ($^{2}H_2O$) was used as a tracer for lipogenesis (Fig. 1*E*). The 5-PAHSA gavage led to an approximately fivefold increase in plasma 5-PAHSA levels with no changes in other PAHSA regioisomers at either TN or cold temperature (Fig. 1*F*). Intriguingly, we noticed that the levels of nearly all PAHSA regioisomers were increased in eWAT after 5-PAHSA gavage, especially in CE animals (Fig. 1*G*), suggesting a modulation of DNL. Of note, the

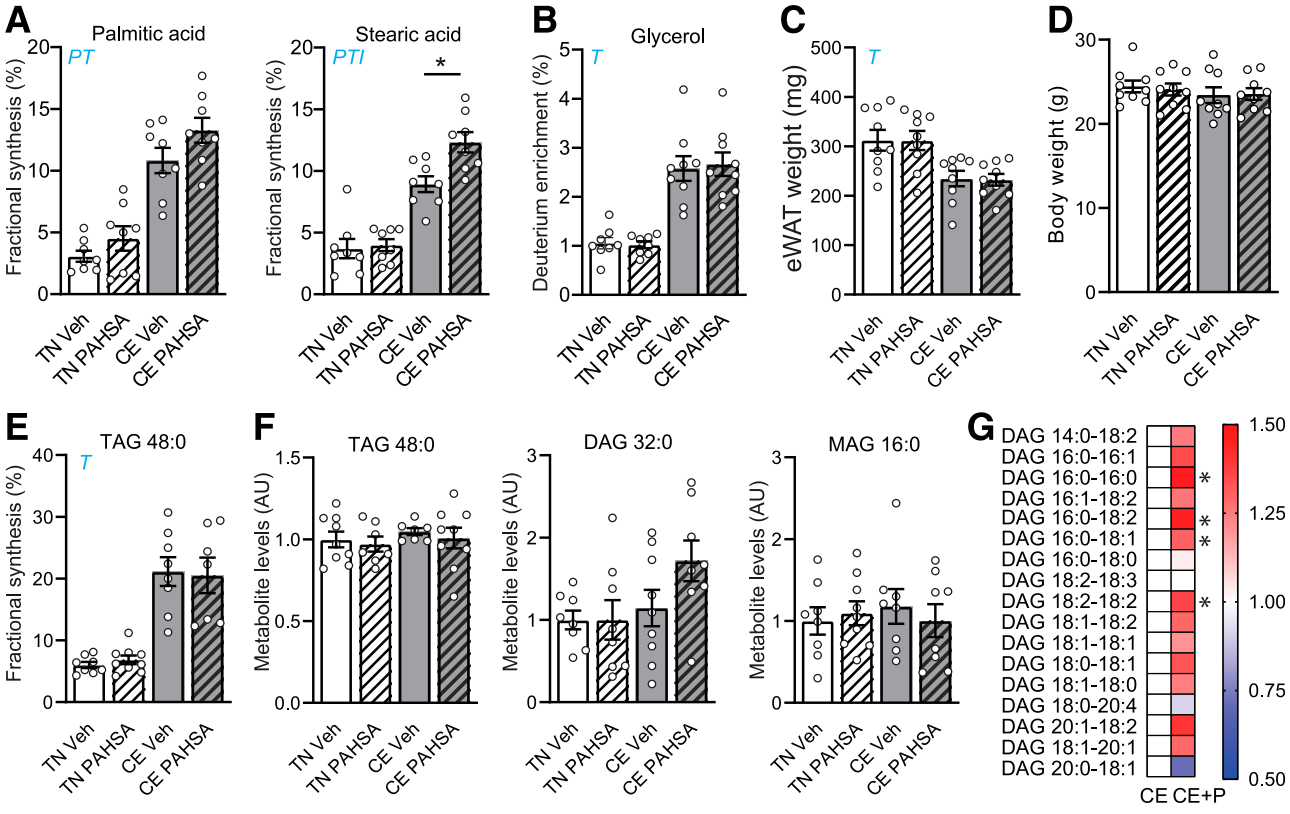

Figure 2—5-PAHSA stimulated DNL in eWAT during CE. *A*: Fractional synthesis of palmitic and stearic acid measured in hydrolysates of the TAG fraction of eWAT (see experiment in Fig. 1*E*). Two-way ANOVA with multiple comparison test (Sidak) was used. Letters within the graphs denote a statistically significant effect of 5-PAHSA (*P*), temperature (*T*), or interaction of factors (*I*). *Planned multiple comparison of the effect of 5-PAHSA at the given temperature statistically different at $P < 0.05$. *B*: Deuterium enrichment of glycerol measured in hydrolysates as above. *C*: Weight of eWAT. *D*: Body weight of animals. *E*: Fractional synthesis of TAG 48:0 (TAG 16:0_16:0_16:0). *F*: Relative levels of TAG 48:0, DAG 32:0 (16:0_16:0), and MAG 16:0. *G*: Profile of DAGs comparing CE and CE 5-PAHSA (CE + P) groups. Data are means ± SEM. *$P < 0.05$ by Student *t* test (n = 8–9). AU, arbitrary units; Veh, vehicle.

concentration and ionization efficiency of 5-PAHSA is lower compared with other PAHSAs. Therefore, the variations between experiments are larger than for other PAHSA regioisomers.

5-PAHSA Stimulates DNL and Lipid Remodeling in eWAT During CE

We took advantage of the in vivo deuterium labeling of cellular lipids in both TN and CE mice (see above) and analyzed (gas chromatography–mass spectrometry) the deuterium enrichment of *1*) FAs liberated by hydrolysis of eWAT lipid extract and *2*) plasma water to calculate the fractional rate of palmitate and stearate synthesis (Fig. 2*A*). The palmitate synthesis data showed a clear uptrend in both TN and CE mice, while the stearate data showed that 5-PAHSA stimulated DNL in the CE mice but not in the TN mice. Glycerol deuterium enrichment (Fig. 2*B*) and eWAT weight (Fig. 2*C*) were only affected by CE and not by 5-PAHSA treatment, indicating an effect independent of glyceroneogenesis. In addition, body weight was unaffected (Fig. 2*D*), leading us to conclude that the 5-PAHSA stimulation of DNL promoted not lipid storage but, rather, a form of energy-consuming DNL and TAG/FA remodeling.

We then performed a lipidomic analysis of deuterium-labeled intact lipids extracted from eWAT using LC-MS. Many lipid species were found to be enriched with deuterium, but the TAGs with shorter-chain FAs, especially TAG 16:0_16:0_16:0 (TAG 48:0) and 16:0_16:0_16:1 (TAG 48:1), were the most labeled species. In the CE mice, the fractional synthesis of TAG 48:0 was significantly higher than with the TN mice (Fig. 2*E*). The absolute levels of TAG 48:0 were similar in all the groups, but the levels of diacylglycerol (DAG) 16:0_16:0 (DAG 32:0), the lipolytic product of TAG 48:0, tended to be higher in the CE PAHSA group, while there was no difference in monoacylglycerol (MAG) 16:0 levels (Fig. 2*F*). The same pattern applied to TAG 48:1 (Supplementary Fig. 2*A*). Detailed analysis of DAG levels in the CE animals showed that 5-PAHSA induced a global increase in acylglycerol remodeling (Fig. 2*G* and Supplementary Fig. 2*B*).

FAHFAs Are Liberated From TAG Estolides During Lipolysis via ATGL

Yore et al. (8) reported the puzzling findings that levels of PAHSA increased during fasting while being associated with DNL during refeeding. Here, we observed that PAHSA levels were also elevated during CE when eWAT metabolism balances lipolysis and lipogenesis. Moreover, when we tried to measure PAHSA synthesis using the $^{2}H_2O$ approach during fasting in mice, we were unable to detect any deuterium enrichment of PAHSAs. This observation suggests that PAHSAs were released from a specific cellular pool during lipolysis. We hypothesized that the best chemical form for FAHFA storage would be a TAG estolide, a TAG-like molecule containing esterified FAHFA (30). To test this, we analyzed mouse eWAT lipid extracts and focused our LC-MS/MS measurement on the higher m/z range. Indeed, we found several analytes matching our in silico library and were able to identify them by the number of carbons and double bonds (Table 1). The structure of TAG-estolide 16:0_18:2_18:0-(O-16:0) and the minor components containing 16:0/18:0/18:1/18:2 and -(O-18:1) acyls was assigned based on the structure and fragmentation patterns of a synthetic standard (Fig. 3*A* and *B* and Supplementary Fig. 3). It was identical to a recently reported PAHSA-containing TAG species (31). Several coeluting analytes were identified as FAHFA-containing TAG estolides, but further method development will be needed for detailed structural analysis including the position of acyl chains and hydroxy FA branching carbon of the isomers. We hypothesized that the FAHFAs might be released via lipolysis. When 3T3-L1 adipocytes differentiated in vitro were stimulated with forskolin, free FAHFA levels increased, while the ATGL inhibitor atglistatin (32) prevented the release of glycerol, FAs, and FAHFAs (Fig. 3*C*). Therefore, we explored this further using eWAT of ATGL-deficient (AKO) mice in the fed and fasted state (Fig. 3*D*). Interestingly, TAG estolides were higher in the fasted than in the fed state in WT animals, while this regulation was absent in the AKO mice and also the TAG EST levels were minimal in the AKO mice. Furthermore, the levels of free 5- and 9-PAHSA followed the same pattern (Fig. 3*E*). We also analyzed

Table 1—List of TAG estolides containing an FAHFA regioisomer detected in mouse eWAT

RT (min)	*m/z*	ID
5.67	1,126.9990	TAG EST 68:4
5.83	1,129.0135	TAG EST 68:3
5.96	1,131.0292	TAG EST 68:2
5.68	1,153.0143	TAG EST 70:5
5.84	1,155.0234	TAG EST 70:4
5.95	1,157.0442	TAG EST 70:3
5.83	1,157.0435	TAG EST 70:3
5.97	1,159.0581	TAG EST 70:2
5.68	1,179.0291	TAG EST 72:6
5.81	1,181.0447	TAG EST 72:5
5.94	1,183.0615	TAG EST 72:4
5.69	1,181.0448	TAG EST 72:5
5.83	1,183.0594	TAG EST 72:4
5.96	1,185.0747	TAG EST 72:3
6.01	1,187.0918	TAG EST 72:2
5.66	1,205.0460	TAG EST 74:7
5.69	1,207.0609	TAG EST 74:6
5.82	1,209.0753	TAG EST 74:5
5.95	1,211.0929	TAG EST 74:4

Identification is based on the number of carbons and double bonds, *m/z* as ammonium adducts $[M + NH_4]^+$, retention time (RT), MS/MS spectra, and fragmentation patterns of the synthetic standard TAG EST 16:0/16:0/9-PAHSA. EST, estolide; ID, identifier.

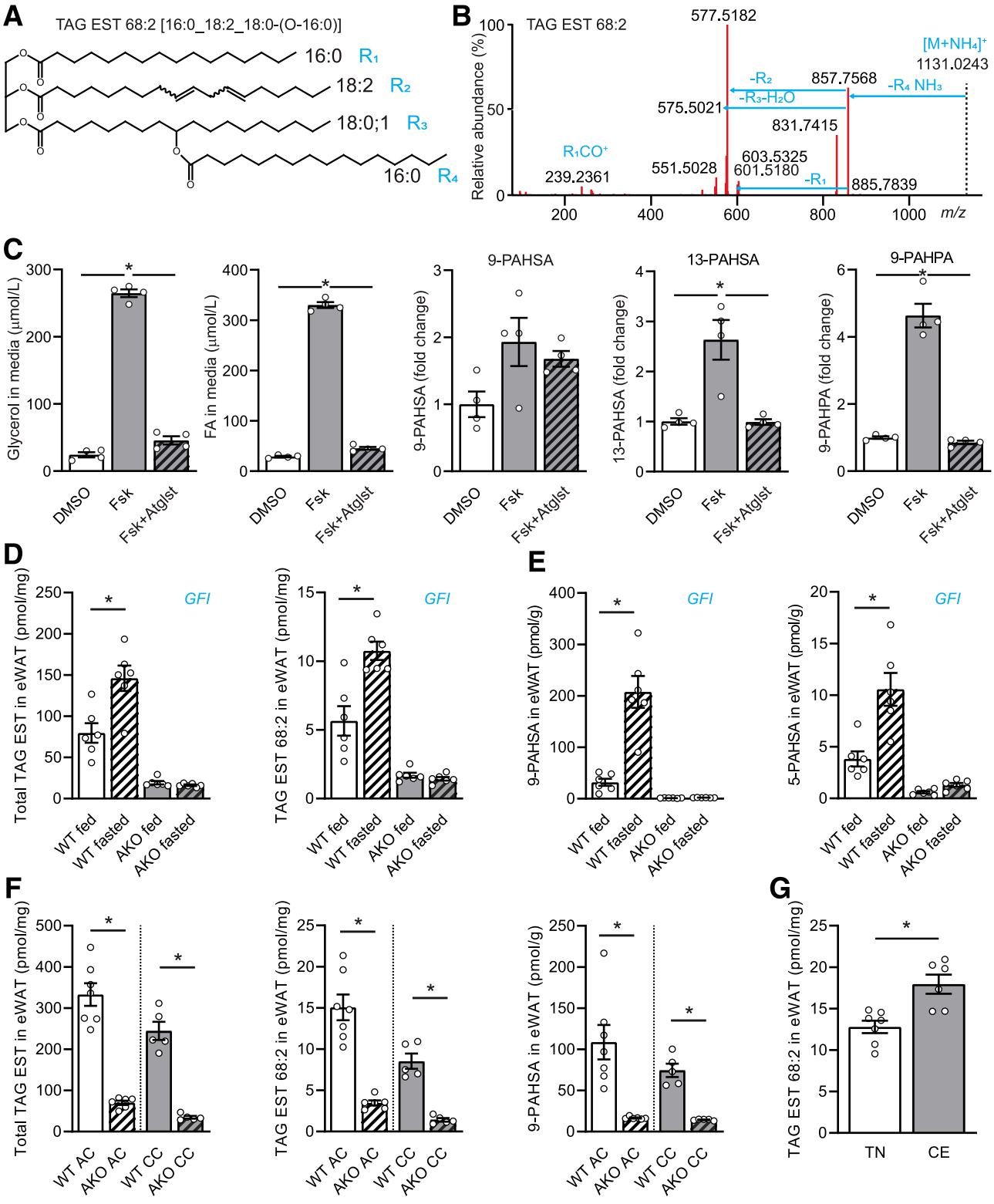

Figure 3—FAHFAs are liberated from TAG estolides during lipolysis. *A*: Tentative structure of a TAG estolide containing 9-PAHSA. This structure was deduced from MS/MS spectra observed in eWAT mouse extracts. The technique does not allow us to assign acyl position, double-bond position, and geometry. *B*: MS/MS spectrum of the measured analyte (see Supplementary Fig. 3 for annotations). *C*: 3T3-L1 adipocytes were preincubated with or without atglistatin (Atglst) and stimulated with forskolin (Fsk) for 2 h, and levels of glycerol and free FAs were determined in the media. Cells and media were extracted, and levels of free FAHFAs were measured using LC-MS/MS. DMSO indicates control cells incubated with DMSO. Data are means ± SEM ($n = 4$). One-way ANOVA with multiple comparison test (Dunnett) was used to compare means with the mean of the Fsk group. *Statistically different at $P < 0.05$. *D*: eWAT samples from WT and AKO mice were harvested in the fed and fasted state and analyzed using LC-MS/MS. Levels of TAG estolides containing PAHSAs (TAG EST 68:2 as a representative) and total levels of TAG EST are shown. *E*: Levels of free 9-PAHSA and 5-PAHSA in eWAT of WT and AKO mice analyzed in the same extract

TAG estolides and 9-PAHSA in WT and AKO animals exposed to acute cold (6 h) and chronic cold adaptation (3 weeks) (14) (Fig. 3*F*) as well as in TN and CE mice (Fig. 3*G*). Acute cold increased total levels of TAG estolides above those in the fasting state, and levels remained high in cold-adapted WT animals. In AKO mice, total TAG estolide levels slightly increased in response to cold, but values were much lower compared with WT mice (Fig. 3*F*). A difference in the changes in total TAG estolide levels, TAG estolide 68:2, and 9-PAHSA (as the representatives of all isomers) suggested that free FAHFA levels were increased through ATGL-mediated release from TAG estolides and that multiple levels of substrate specificity are involved.

5-PAHSA Modulates Both Lipogenesis and Lipolysis

Not all DAGs were affected the same way by 5-PAHSA (Fig. 2*G*), so we investigated whether there was an FA-specific metabolic pattern. Differentiated 3T3-L1 adipocytes were grown in a culture medium containing 50% $^{2}H_2O$ for 3 days with or without 5-PAHSA. The deuterium enrichment of TAGs showed that 5-PAHSA–treated cells incorporated more deuteria into shorter and saturated/monounsaturated "nascent" TAGs (Fig. 4*A*), but there were also differences in the position of incorporated deuteria within the molecule. Both the TAG acyl chains and the glycerol backbone can be labeled with deuterium through different pathways (33). We observed that TAG 48:0 was labeled mainly on the acyl chains (produced through DNL) and not as the M+3 isotopologue, which represents the TAG glycerol backbone labeled during glycolysis (Fig. 4*B* and Supplementary Fig. 4 for MS/MS spectra explanation).

Both lipolysis and FA esterification contribute to eWAT lipid metabolism during CE, balancing effects of catecholamines and insulin. Catecholamines stimulate release of FAs from WAT to supply brown adipose tissue heat production. The mice had access to food and therefore, in parallel, insulin stimulated glucose uptake into WAT to promote DNL and the TAG/FA cycle to buffer lipolysis. We examined the effect of 5-PAHSA on both pathways. 3T3-L1 adipocytes were grown with or without 5-PAHSA for 3 days, serum starved, preincubated with 10 nmol/L insulin or 5-PAHSA for 30 min, and subsequently exposed to forskolin for 2 h. Glycerol release into the medium showed that insulin partially countered lipolysis but 5-PAHSA slightly enhanced the effect of forskolin. Release of FAs was completely inhibited by insulin, while the effect of 5-PAHSA was not significant (Fig. 4*C*). Similar effects were observed with acute 5-PAHSA stimulation and isoproterenol on cultured and freshly isolated adipocytes (Supplementary Fig. 4*E* and *F*). Both markers of lipolysis suggested that 5-PAHSA affects FA re-esterification. Detailed analysis of media FA composition revealed a strong effect of 5-PAHSA on re-esterification of monounsaturated FA, especially 16:1 (i.e., palmitoleic acid), while the predominant FAs in TAGs (16:0, 18:1) accounted for net lipolysis (Fig. 4*D*). This effect was not observed using an acute preincubation with 5-PAHSA (Supplementary Fig. 4*G*). Furthermore, we tested the effect of combination of 5-PAHSA and insulin on isoproterenol-stimulated 3T3-L1 adipocytes (34) and found that 5-PAHSA stimulated glycerol release and counteracted insulin action (Fig. 4*E*). We conclude that 5-PAHSA significantly increased glycerol release and influenced FA release and re-esterification.

We added a $^{13}C_6$-glucose tracer in the forskolin experiment to explore metabolite labeling in the cells. We found that both insulin and 5-PAHSA prevented the decline during lipolysis of TAG 48:1, which proved to be a sensitive marker of DNL and lipid remodeling with the FA 16:1 (Fig. 4*F*). The M+3 isotopologue of TAG 48:1, corresponding to ^{13}C labeling of the glycerol backbone provided by glycolysis (Fig. 4*F* and Supplementary Fig. 4), proved that insulin drove glucose to the FA esterification pathway. In contrast, the levels of DAG 32:1, the lipolytic product of TAG 48:1, were higher in 5-PAHSA–treated cells, again pointing to TAG remodeling. Interestingly, the ^{13}C-labeling profile of citrate and its levels suggested that in contrast to insulin, 5-PAHSA directs glucose carbons to DNL instead of the glycerol backbone for esterification to TAGs (Fig. 4*F*).

5-PAHSA Primes Adipocytes for Glucose Metabolism and DNL

We next performed a glucose uptake experiment using $^{13}C_6$-glucose as a tracer and a major carbon source. Serum-starved 3T3-L1 adipocytes were preincubated with or without 5-PAHSA for 30 min, and then the metabolism of $^{13}C_6$-glucose was monitored for 0, 5, 10, and 15 min. The metabolites that were positively or negatively affected by 5-PAHSA are highlighted in green and red, respectively, in Fig. 5*A*. The levels of glucose and hexose 6-phosphates, which estimate glucose uptake, were higher in 5-PAHSA–treated cells, in agreement with previous data (8). 5-PAHSA stimulated ^{13}C enrichment and exchange of three carbon units within the lower part of the pentose phosphate pathway and glycolysis (Fig. 5*B*). In contrast, levels and labeling of

as above. Data are means ± SEM ($n = 6$). Two-way ANOVA with multiple comparison test (Tukey) was used. Letters in the graphs denote statistically significant effect of genotype (G), feeding status (F), or interaction of factors (I). *Multiple comparison of the effect of the condition with the given genotype statistically different at $P < 0.05$. Additional statistics are presented in Supplementary Table 1 for clarity. *F*: eWAT samples from WT and AKO mice were harvested in the fed state after acute cold (AC) (3 h) and chronic cold (CC) (3 weeks) and analyzed using LC-MS/MS. Levels of TAG estolides containing PAHSAs (TAG EST 68:2 as a representative), total levels of TAG EST, and levels of free 9-PAHSA are shown. Data are means ± SEM ($n = 5$–7). *$P < 0.05$ by Student *t* test. Vertical line separates AC and CC experiments. *G*: Levels of TAG EST 68:2 in eWAT samples from WT mice kept at TN or exposed to cold for 7 days as in Fig. 1. Data are means ± SEM ($n = 6$–7). *$P <$ 0.05 by Student *t* test. EST, estolide.

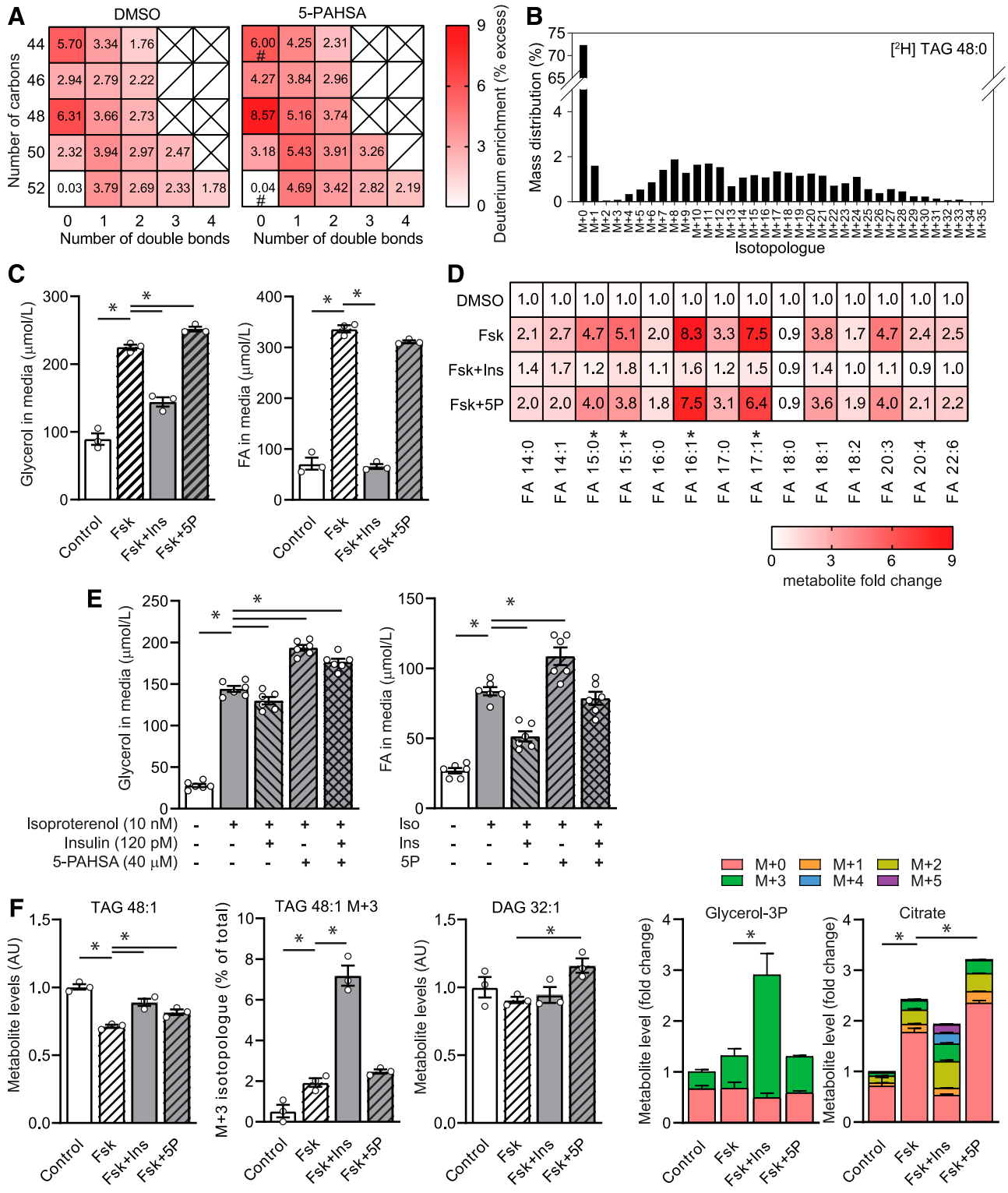

Figure 4—5-PAHSA–stimulated lipogenesis and selectively modulated lipolysis. *A*: 3T3-L1 adipocytes were grown in the presence or absence of 40 μmol/L 5-PAHSA for 3 days and labeled with 50% ^2H_2O. The deuterium enrichment of intact TAG molecules, marking the rate of lipogenesis, was measured using LC-MS/MS and is expressed as a heat map of TAGs sorted according to the number of carbons and double bonds. All fields were significantly different at $P < 0.05$ (Student *t* test, DMSO vs. 5-PAHSA) except for those marked with #, where the numbers in the fields are means ($n = 6$). *B*: Illustrative profile of deuterium-labeled TAG 48:0. *C*: Lipolysis: 3T3-L1 adipocytes were preincubated with insulin (Ins) or 40 μmol/L 5-PAHSA (5P) and stimulated with 1 μmol/L forskolin (Fsk). Glycerol and free FAs in media were measured using colorimetric kits. One-way ANOVA with multiple comparison test (Dunnett) comparing means with the mean of the Fsk group was used. Data are means ± SEM ($n = 3$). *Statistically different at $P < 0.05$. *D*: Lipolysis: levels of individual FAs in media were measured using LC-MS/MS; numbers in the fields are means ($n = 8$–9). *Statistically different at $P < 0.05$ by one-way ANOVA as above. *E*: Lipolysis: 3T3-L1 adipocytes were preincubated with 120 pmol/L Ins, 40 μmol/L 5P, or their combination and stimulated with 10 nmol/L isoproterenol

glycerol-3-phosphate were reduced by 5-PAHSA, consistent with the lipid-labeling data of Fig. 4. 5-PAHSA also channeled glucose carbons to the Krebs cycle through both pyruvate dehydrogenase and pyruvate carboxylase rather than to lactate. This was similar to the effect of insulin pretreatment on adipocytes, which primed metabolism for lipid synthesis and NADPH production through malate-pyruvate recycling (25). [4-^{2}H]glucose as a malic enzyme tracer confirmed that 5-PAHSA treatment significantly increased the ^{2}H-labeled fraction of cytosolic NADPH compared with control cells (Supplementary Fig. 5). The intermediates of the Krebs cycle decreased over time, probably due to of absence of glutamine in the medium and to lack of related anaplerotic reactions.

We then repeated the uptake experiment to test the effect of 10 nmol/L insulin (Fig. 5*C*) and quenched metabolism after 10 min, when the differences were maximal. Although insulin was a much stronger stimulant of glucose metabolism than 5-PAHSA, the specific 5-PAHSA pattern of three-carbon-unit metabolism was preserved. 5-PAHSA diverted carbon flux from glycerol-3-phosphate and rapid FA esterification downstream to the Krebs cycle.

Adipocytes use several carbon sources to supply the demands of DNL, and glutamine is an important player. Therefore, we repeated the glucose uptake experiment in the presence of 5.5 mmol/L glucose and 4 mmol/L $^{13}C_5$-glutamine and quenched metabolism after 10 min. When supply of major carbon sources was not limited, 5-PAHSA–treated adipocytes used significantly more carbon from glutamine (Fig. 6*A*). Interestingly, $^{13}C_5$-glutamine was metabolized both into succinate (M+4 labeling) and into M+5 citrate by reductive carboxylation, in good agreement with previously reported results (35) (Fig. 6*B* and *C*).

The above-described effects of 5-PAHSA on adipocyte metabolism are summarized in the scheme of Fig. 6*D*. While insulin (in red) stimulates glucose uptake and the utilization of glycerol-3-phosphate for rapid TAG synthesis, 5-PAHSA (in green) supports a longer, more energy-consuming path that involves DNL and TAG remodeling.

DISCUSSION

Here we demonstrate that 5-PAHSA, a lipokine with beneficial metabolic effects, primes adipocytes for glucose utilization and DNL while enhancing metabolically specific TAG/FA cycling. We used a combination of mouse experiments with metabolic labeling of lipogenesis and lipolysis together with dynamic metabolomics in cultured adipocytes to explore the pathways connecting glucose and lipid metabolism.

The energy-consuming combinations of TAG/FA cycling and DNL in adipocytes represent key components of a metabolically "healthy adipocyte" and are induced by CE (6,36). Our initial observation that CE increased PAHSA levels in eWAT suggested that these lipokines and DNL could be the mechanistic link underlying the metabolic changes. The experiment with 5-PAHSA oral gavage in mice at two housing temperatures with deuterium labeling of lipid synthesis proved that the effect of 5-PAHSA at TN is minimal, while CE is associated with higher PAHSA levels in eWAT. In addition, 5-PAHSA gavage increased levels of other PAHSA regioisomers in eWAT.

5-PAHSA stimulated DNL beyond the effect of CE, but it did not potentiate FA re-esterification with glucose-derived glycerol (direct TAG synthesis, fat accumulation). There was limited deuterium incorporation (only up to four deuteria) into palmitic and stearic acids in CE mice. Therefore, the effect observed at the level of FA hydrolyzed from TAGs was not clear at the level of intact lipids, where the deuterium tracer was diluted among all TAG FA combinations and insufficient tracer sensitivity was a limitation. Total metabolite level analysis suggested that 5-PAHSA affected lipid remodeling between TAGs and DAGs. The simplest interpretation is that 5-PAHSA stimulated de novo lipid synthesis from acetyl-CoA and acylglycerol remodeling, inducing a futile TAG/FA cycle that did not support lipid storage. In line with this, no effect on body weight was observed in mice chronically treated with PAHSAs (37). Our data suggest that two concurrent overlapping mechanisms were stimulated: *1*) futile (energy wasting) TAG/FA cycling (6), which builds and breaks TAG completely, and *2*) lipid remodeling of the TAG acyls, including FAHFAs and TAG estolides. Therefore, with respect to the metabolic rearrangements that are associated with obesity, 5-PAHSA positively affects adipocyte metabolism.

FAHFA levels rise during CE and with fasting in mice and rats (8,18). Because we were unable to detect any deuterium-labeled PAHSAs in either CE animals or fasted/refed mice, we looked for a metabolic storage pool from which PAHSA would be liberated during stimulated lipolysis. Using lipidomic profiling, we were able to identify several members of the TAG-estolide lipid class in which PAHSAs are esterified to the glycerol backbone alongside two other acyl chains. The structural patterns were confirmed using a synthetic standard. We estimate that there are dozens of TAG estolides that contain other FAHFAs, but a targeted analytical approach using multistage fragmentation (MS^4) will be needed to explore their complexity. It is difficult to separate all FAHFA regioisomers, and

(Iso). Glycerol and free FA in media were measured using colorimetric kits. One-way ANOVA with multiple comparison test (Dunnett) comparing means with the mean of the Iso-alone group was used. Data are means ± SEM ($n = 6$). *Statistically different at $P < 0.05$. *F*: Lipolysis: levels of metabolites related to TAG 48:1 (16:0_16:0_16:1) were measured in the harvested cells using LC-MS/MS. $^{13}C_6$-glucose was used as a tracer and citrate as a precursor of DNL. Data are means ± SEM ($n = 3$). *Statistically different at $P < 0.05$ by one-way ANOVA as above. AC, acute CE; AU, arbitrary unit; CC, chronic CE; Glycerol-3P, glycerol 3-phosphate.

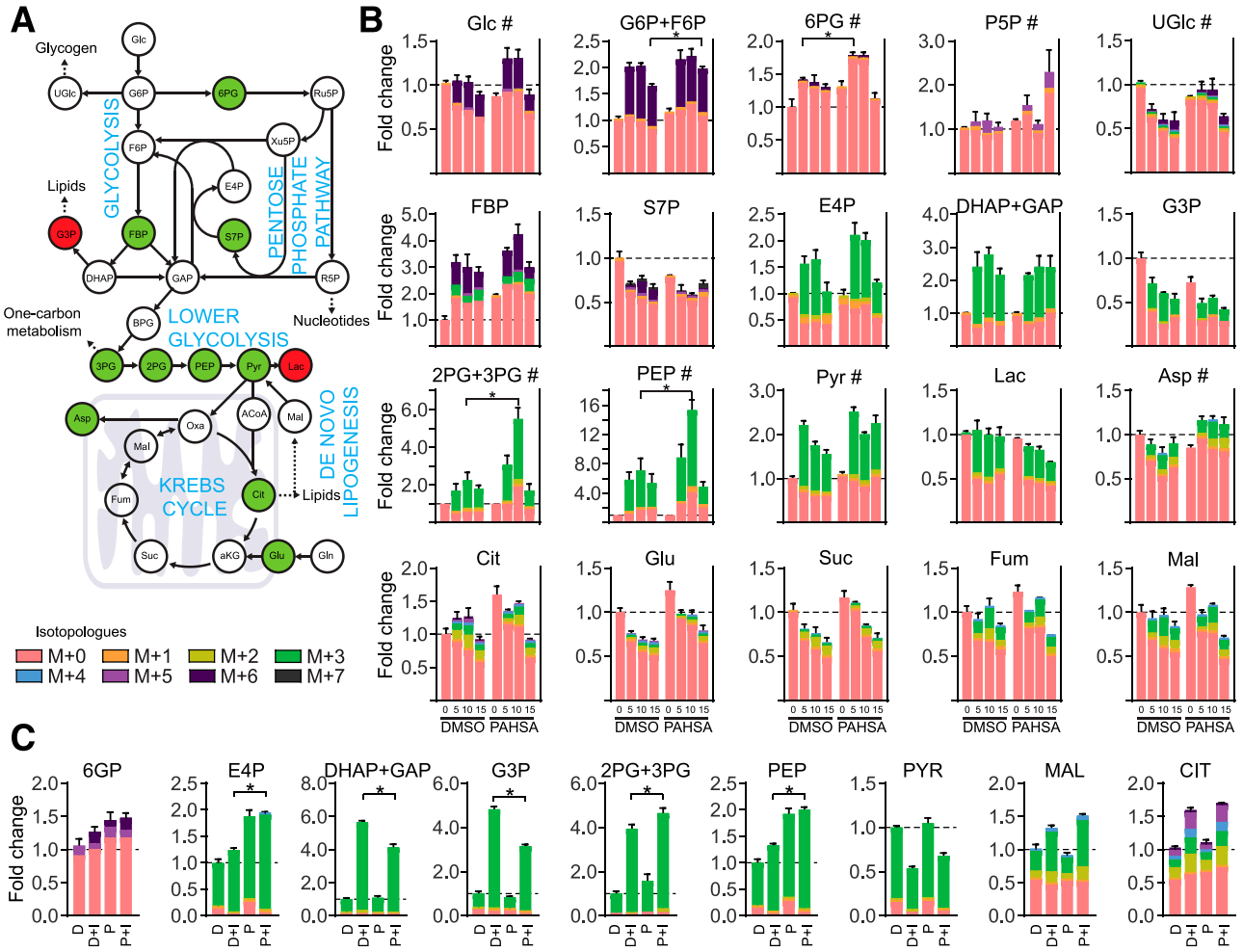

Figure 5—5-PAHSA primes adipocytes for glucose (Glc) utilization toward DNL and away from FA esterification. *A*: Glc uptake. Schematic representation of the metabolic pathways affected by 5-PAHSA treatment. Statistically significant differences between DMSO and 5-PAHSA treatments are highlighted in green (upregulation) and red (downregulation) (see below). Major pathways are labeled in blue. See Supplementary Table 2 for abbreviations of the metabolites. Once Glc enters the cell and is phosphorylated, the majority of the G6P is metabolized through glycolysis to three carbon units (e.g., GAP), but some Glc molecules are processed through ancillary pathways (e.g., the pentose phosphate pathway, glycogen synthetic pathway, lipid synthesis). GAP can be further metabolized to Pyr through the lower glycolysis pathway and converted to Lac or oxidized in the Krebs cycle. Mitochondrial Cit can be exported to the cytosol and serve as a substrate for DNL, while Pyr-Mal recycling generates NADPH to fuel the DNL. *B*: Glc uptake (UGlc): time profiles of isotopologues of selected metabolites. $^{13}C_6$-Glc uptake was measured in serum-starved 3T3-L1 adipocytes preincubated without DMSO or 5-PAHSA (40 μmol/L), and the metabolism was quenched at specific time points (0, 5, 10, and 15 min). Whole bars indicate means ± SEM of the total metabolite levels, and individual isotopologues are colored according to the key (n = 3). Glc was the only major source of carbons. Two-way repeated-measures ANOVA with Sidak multiple comparison test was performed on total metabolite levels: *statistically significant difference between DMSO and 5-PAHSA at the specific time point, #statistically significant interaction between time and treatment; additional statistics are presented in Supplementary Table 2 for clarity. *C*: Glc uptake: the same experiment was repeated with or without insulin (10 nmol/L), and cell metabolism was quenched at 10 min (n = 6). Whole bars indicate means ± SEM of the total metabolite levels, and individual isotopologues are colored according to the key (n = 6). Two-way ANOVA with Tukey multiple comparison test was performed on total metabolite levels: *Statistically significant difference between DMSO and 5-PAHSA in combination with insulin. For clarity, additional statistics are presented in Supplementary Table 3. D, DMSO; D+I, DMSO and insulin; P, 5-PAHSA; P+I, 5-PAHSA and insulin.

separation and structural analysis of low-abundance TAG estolides is at the edge of current technological limits. Our data are in agreement with and confirm those recently reported on FAHFA TAGs (identical to TAG estolides) (31).

Liberation of FAHFAs from TAG estolides during lipolysis and fasting/CE was prevented by inhibition or absence of ATGL. The FAHFA increase during fasting/CE is linked to the lipolytic activity of ATGL or hormone-sensitive lipase (31). Low levels of TAG estolides in AKO mice suggest that ATGL might also be involved in their metabolism via acyltransferase activity (38,39), independent of acyl CoA:DAG acyltransferases (31). The effect of atglistatin on forskolin-treated adipocytes was more pronounced on free FAHFA levels, and TAG estolides were not changed during this short incubation (data not shown), further

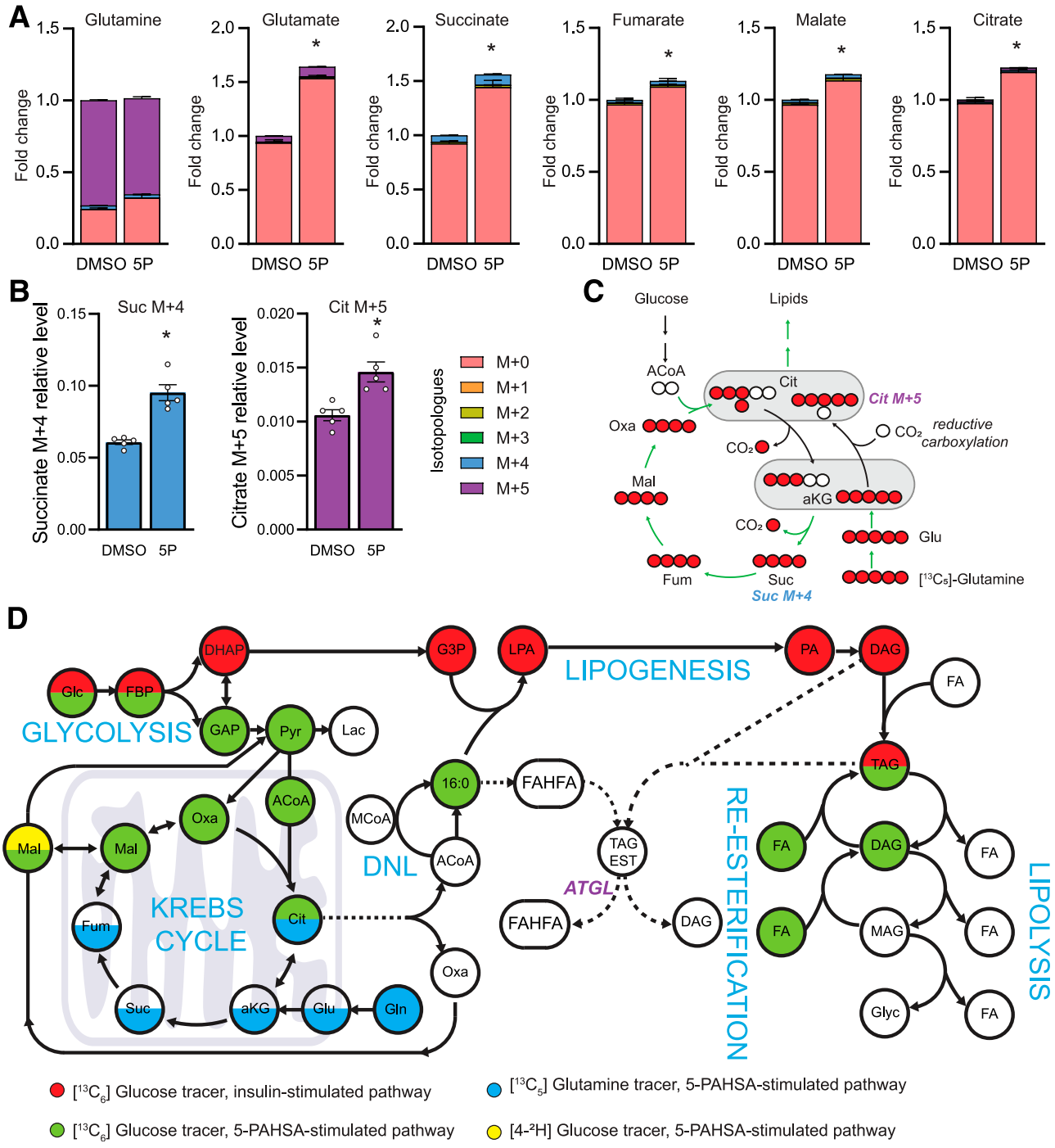

Figure 6—5-PAHSA promotes glutamine (Gln) utilization for DNL. *A*: Glucose (Glc) uptake II was measured in serum-starved 3T3-L1 adipocytes preincubated with or without 5-PAHSA (40 μmol/L), and metabolism was quenched at 10 min. $^{13}C_5$-Gln (4 mmol/L) was used as a tracer. Levels of traced metabolites and their isotopologue profiles are colored according to the key. Bars indicate means ± SEM of the total metabolite levels. *B*: Glc uptake II: ^{13}C-labeled intermediates of Krebs cycle, succinate (Suc), and citrate (Cit), illustrating the fate of Gln carbons. Data are means ± SEM ($n = 5$). *$P < 0.05$ by Student *t* test. *C*: Atom transition map depicting a model of carbon labeling within the first turn of the Krebs cycle. $^{13}C_5$-Gln carbons enter the Krebs cycle as α-ketoglutarate (aKG), produce $^{13}C_4$-Suc (Suc M+4 [as in *B*]), and label lipids (green path). Alternatively, Cit M+5 (as in *B*) is formed through a reductive carboxylation process. *D*: Metabolic scheme summarizing metabolite labeling data and the effects of 5-PAHSA. Dotted lines represent a sequence of reactions. ACoA, acetyl-CoA; LPA, lysophosphatidic acid; MCoA, malonyl-CoA; Oxa, oxaloacetate. See Supplementary Table 2 for abbreviations of the other metabolites.

supporting a dual role of ATGL in FAHFA metabolism. The new role of ATGL in controlling the release of FAHFAs from TAG-estolide stores in adipocytes, together with the stimulation of TAG/FA remodeling by FAHFAs that we describe, is compatible with the previously unexplained observation that ATGL is required for

stimulation of DNL, TAG/FA cycling, and mitochondrial electron transport by the β3-adrenergic pathway in adipose tissue (29). Innovative lipidomic analyses capable of quantifying individual TAG estolides and FAHFA isomers will be needed to explore substrate specificity of ATGL and its contribution to FAHFA metabolism.

A study of lipogenesis and lipolysis in 3T3-L1 adipocytes showed that the prolipogenic effect of 5-PAHSA is significant but does not promote excess lipid storage, in agreement with previous data (40). Newly synthesized short FAs are primarily incorporated into short-chain TAGs, probably on the surface of small lipid droplets, allowing high turnover. Intriguingly, although the effect of 5-PAHSA on net lipolysis was mild, the selective re-esterification of monounsaturated FAs highlighted fine-tuning of the TAG/FA remodeling cycle and the ability of 5-PAHSA to spare or rebuild specific TAGs, possibly also TAG estolides.

A comparison with the effect of insulin using the ^{13}C-tracer data, specifically involving the labeling pattern of glycerol-3-phosphate and citrate, prompted us to thoroughly explore the glucose utilization pathway. Dynamic metabolomic profiling of 3T3-L1 adipocytes preincubated with insulin showed how cells select specific metabolic pathways to optimize metabolic flux and secure NADPH-producing reactions for DNL (25). We performed an analogous experiment with 5-PAHSA preincubation and found that the lipokine activated similar pathways, with an important difference in the fate of glucose carbons. In contrast to insulin, 5-PAHSA specifically reduced carbon flux to glycerol-3-phosphate, away from TAG accumulation, while enhancing carbon flux to the Krebs cycle and DNL precursors. Although the effect of 5-PAHSA was small compared with the net effect of insulin, the critical metabolic pattern was observed even when both 5-PAHSA and insulin were present. The combination of insulin and PAHSA could potentially be used therapeutically in metabolic situations where glycolysis is dysregulated.

In contrast to Krycer et al. (25), we performed the labeling experiment in media with limited carbon sources to unmask 5-PAHSA effects. The addition of glutamine, which is an important lipogenic source in adipocytes, revealed that the flux toward DNL might be even higher when the Krebs cycle can use anaplerotic substrates. This alternative fate of glucose carbons might lower fat accumulation in WAT and contribute to other antidiabetic effects of PAHSAs (8).

In summary, we propose that FAHFAs are synthesized via DNL through hydroxylated intermediates (18) and stored as TAG estolides in lipid droplets. ATGL-mediated lipolysis releases free FAHFAs, which limit FA esterification into TAG while promoting TAG acylglycerol remodeling and the fine-tuning of lipolysis. These effects prime adipocytes for glucose metabolism, in a different way from insulin, once it becomes available, and promote metabolically "healthy adipose tissue."

Funding. This work was supported by grants from the Grantová Agentura České Republiky (17-10088Y), Ministerstvo Školství, Mládeže a Tělovýchovy (LTAUSA17173, LTAUSA18104), and the Czech Academy of Sciences (Lumina quaeruntur 2018) and by projects "BIOCEV (CZ.1.05/1.1.00/02.0109), RVO 61388963 and the equipment for metabolomic and cell analyses" (CZ.1.05/2.1.00/19.0400).

Duality of Interest. No potential conflicts of interest relevant to this article were reported.

Author Contributions. V.P., M.O., M.B., T.C., K.Br., and O.K. performed the LC-MS/MS analysis. V.P., M.B., K.Ba., and K.A. performed the animal studies. V.P., K.Br., and O.K. performed the cell culture experiments. V.P., J.K., and O.K. conceived, designed, and interpreted experiments. M.O., P.Z., and O.K. analyzed GC-MS data. L.B., H.C., E.K., and T.D. synthesized the PAHSAs and TAG-estolide. R.S. and R.Z. provided ATGL KO samples. R.Z., M.R., N.A.A., and J.K. reviewed the experiments and edited the manuscript. O.K. wrote the manuscript. All authors reviewed the manuscript. O.K. is the guarantor of this work and, as such, had full access to all the data in the study and takes responsibility for the integrity of the data and the accuracy of the data analysis.

References

1. Eissing L, Scherer T, Tödter K, et al. De novo lipogenesis in human fat and liver is linked to ChREBP-β and metabolic health. Nat Commun 2013;4:1528
2. Solinas G, Borén J, Dulloo AG. De novo lipogenesis in metabolic homeostasis: more friend than foe? Mol Metab 2015;4:367–377
3. Tang Y, Wallace M, Sanchez-Gurmaches J, et al. Adipose tissue mTORC2 regulates ChREBP-driven de novo lipogenesis and hepatic glucose metabolism. Nat Commun 2016;7:11365
4. Yilmaz M, Claiborn KC, Hotamisligil GS. De novo lipogenesis products and endogenous lipokines. Diabetes 2016;65:1800–1807
5. Cao H, Gerhold K, Mayers JR, Wiest MM, Watkins SM, Hotamisligil GS. Identification of a lipokine, a lipid hormone linking adipose tissue to systemic metabolism. Cell 2008;134:933–944
6. Flachs P, Adamcova K, Zouhar P, et al. Induction of lipogenesis in white fat during cold exposure in mice: link to lean phenotype. Int J Obes 2017;41:372–380
7. Herman MA, Peroni OD, Villoria J, et al. A novel ChREBP isoform in adipose tissue regulates systemic glucose metabolism. Nature 2012;484:333–338
8. Yore MM, Syed I, Moraes-Vieira PM, et al. Discovery of a class of endogenous mammalian lipids with anti-diabetic and anti-inflammatory effects. Cell 2014;159:318–332
9. Lodhi IJ, Yin L, Jensen-Urstad AP, et al. Inhibiting adipose tissue lipogenesis reprograms thermogenesis and PPARγ activation to decrease diet-induced obesity. Cell Metab 2012;16:189–201
10. Kuda O, Brezinova M, Rombaldova M, et al. Docosahexaenoic acid-derived fatty acid esters of hydroxy fatty acids (FAHFAs) with anti-inflammatory properties. Diabetes 2016;65:2580–2590
11. Zhu QF, Yan JW, Zhang TY, Xiao HM, Feng YQ. Comprehensive screening and identification of fatty acid esters of hydroxy fatty acids in plant tissues by chemical isotope labeling-assisted liquid chromatography-mass spectrometry. Anal Chem 2018;90:10056–10063
12. Lee J, Moraes-Vieira PM, Castoldi A, et al. Branched fatty acid esters of hydroxy fatty acids (FAHFAs) protect against colitis by regulating gut innate and adaptive immune responses. J Biol Chem 2016;291:22207–22217
13. Brezinova M, Kuda O, Hansikova J, et al. Levels of palmitic acid ester of hydroxystearic acid (PAHSA) are reduced in the breast milk of obese mothers. Biochim Biophys Acta Mol Cell Biol Lipids 2018;1863:126–131
14. Schreiber R, Diwoky C, Schoiswohl G, et al. Cold-induced thermogenesis depends on ATGL-mediated lipolysis in cardiac muscle, but not brown adipose tissue. Cell Metab 2017;26:753–763.e7
15. Balas L, Bertrand-Michel J, Viars F, et al. Regiocontrolled syntheses of FAHFAs and LC-MS/MS differentiation of regioisomers. Org Biomol Chem 2016;14:9012–9020

16. Yang D, Diraison F, Beylot M, et al. Assay of low deuterium enrichment of water by isotopic exchange with [U-13C3]acetone and gas chromatography-mass spectrometry. Anal Biochem 1998;258:315–321
17. Cajka T, Smilowitz JT, Fiehn O. Validating quantitative untargeted lipidomics across nine liquid chromatography-high-resolution mass spectrometry platforms. Anal Chem 2017;89:12360–12368
18. Kuda O, Brezinova M, Silhavy J, et al. Nrf2-mediated antioxidant defense and peroxiredoxin 6 are linked to biosynthesis of palmitic acid ester of 9-hydroxystearic acid. Diabetes 2018;67:1190–1199
19. Oseeva M, Paluchova V, Zacek P, et al. Omega-3 index in the Czech Republic: no difference between urban and rural populations. Chem Phys Lipids 2019;220:23–27
20. Lee WN, Bassilian S, Guo Z, et al. Measurement of fractional lipid synthesis using deuterated water (2H2O) and mass isotopomer analysis. Am J Physiol 1994; 266:E372–E383
21. Zhang Z, Chen L, Liu L, Su X, Rabinowitz JD. Chemical basis for deuterium labeling of fat and NADPH. J Am Chem Soc 2017;139:14368–14371
22. Tsugawa H, Cajka T, Kind T, et al. MS-DIAL: data-independent MS/MS deconvolution for comprehensive metabolome analysis. Nat Methods 2015;12:523–526
23. Millard P, Letisse F, Sokol S, Portais JC. IsoCor: correcting MS data in isotope labeling experiments. Bioinformatics 2012;28:1294–1296
24. Previs SF, Herath K, Nawrocki AR, et al. Using [^{2}H]water to quantify the contribution of de novo palmitate synthesis in plasma: enabling back-to-back studies. Am J Physiol Endocrinol Metab 2018;315:E63–E71
25. Krycer JR, Yugi K, Hirayama A, et al. Dynamic metabolomics reveals that insulin primes the adipocyte for glucose metabolism. Cell Rep 2017;21:3536–3547
26. Kuda O. On the complexity of PAHSA research. Cell Metab 2018;28:541–542
27. Syed I, Lee J, Peroni OD, et al. Methodological issues in studying PAHSA biology: masking PAHSA effects. Cell Metab 2018;28:543–546
28. Loos M, Gerber C, Corona F, Hollender J, Singer H. Accelerated isotope fine structure calculation using pruned transition trees. Anal Chem 2015;87:5738–5744
29. Mottillo EP, Balasubramanian P, Lee YH, Weng C, Kershaw EE, Granneman JG. Coupling of lipolysis and de novo lipogenesis in brown, beige, and white adipose tissues during chronic β3-adrenergic receptor activation. J Lipid Res 2014;55:2276–2286
30. McLean S, Davies NW, Nichols DS, Mcleod BJ. Triacylglycerol estolides, a new class of mammalian lipids, in the paracloacal gland of the brushtail possum (Trichosurus vulpecula). Lipids 2015;50:591–604
31. Tan D, Ertunc ME, Konduri S, et al. Discovery of FAHFA-containing triacylglycerols and their metabolic regulation. J Am Chem Soc 2019;141:8798–8806
32. Mayer N, Schweiger M, Romauch M, et al. Development of small-molecule inhibitors targeting adipose triglyceride lipase. Nat Chem Biol 2013;9: 785–787
33. Previs SF, McLaren DG, Wang SP, et al. New methodologies for studying lipid synthesis and turnover: looking backwards to enable moving forwards. Biochim Biophys Acta 2014;1842:402–413
34. Zhou P, Santoro A, Peroni OD, et al. PAHSAs enhance hepatic and systemic insulin sensitivity through direct and indirect mechanisms. J Clin Invest 2019;129: 4138–4150
35. Yoo H, Antoniewicz MR, Stephanopoulos G, Kelleher JK. Quantifying reductive carboxylation flux of glutamine to lipid in a brown adipocyte cell line. J Biol Chem 2008;283:20621–20627
36. Masoodi M, Kuda O, Rossmeisl M, Flachs P, Kopecky J. Lipid signaling in adipose tissue: connecting inflammation & metabolism. Biochim Biophys Acta 2015;1851:503–518
37. Syed I, Lee J, Moraes-Vieira PM, et al. Palmitic acid hydroxystearic acids activate GPR40, which is involved in their beneficial effects on glucose homeostasis. Cell Metab 2018;27:419–427.e4
38. Lake AC, Sun Y, Li JL, et al. Expression, regulation, and triglyceride hydrolase activity of Adiponutrin family members. J Lipid Res 2005;46:2477–2487
39. Jenkins CM, Mancuso DJ, Yan W, Sims HF, Gibson B, Gross RW. Identification, cloning, expression, and purification of three novel human calcium-independent phospholipase A2 family members possessing triacylglycerol lipase and acylglycerol transacylase activities. J Biol Chem 2004;279:48968–48975
40. Hammarstedt A, Syed I, Vijayakumar A, et al. Adipose tissue dysfunction is associated with low levels of the novel Palmitic Acid Hydroxystearic Acids. Sci Rep 2018;8:15757

Distinct roles of adipose triglyceride lipase and hormone-sensitive lipase in the catabolism of triacylglycerol estolides

Kristyna Brejchova[a,1], Franz Peter Walter Radner[b,1], Laurence Balas[c], Veronika Paluchova[a], Tomas Cajka[a], Hana Chodounska[d], Eva Kudova[d], Margarita Schratter[b], Renate Schreiber[b], Thierry Durand[c], Rudolf Zechner[b,e,2], and Ondrej Kuda[a,2]

[a]Institute of Physiology, Czech Academy of Sciences, 142 20 Prague 4, Czech Republic; [b]Institute of Molecular Biosciences, University of Graz, 8010 Graz, Austria; [c]Institut des Biomolécules Max Mousseron, UMR 5247, CNRS, École Nationale Supérieure de Chimie de Montpellier, Faculté de Pharmacie, Université de Montpellier, 34093 Montpellier, France; [d]Institute of Organic Chemistry and Biochemistry, Czech Academy of Sciences, 166 10 Prague 6, Czech Republic; and [e]BioTechMed-Graz, 8010 Graz, Austria

Contributed by Rudolf Zechner, November 13, 2020 (sent for review October 7, 2020; reviewed by Robert V. Farese Jr. and Stephen G. Young)

Branched esters of palmitic acid and hydroxy stearic acid are antiinflammatory and antidiabetic lipokines that belong to a family of fatty acid (FA) esters of hydroxy fatty acids (HFAs) called FAHFAs. FAHFAs themselves belong to oligomeric FA esters, known as estolides. Glycerol-bound FAHFAs in triacylglycerols (TAGs), named TAG estolides, serve as metabolite reservoir of FAHFAs mobilized by lipases upon demand. Here, we characterized the involvement of two major metabolic lipases, adipose triglyceride lipase (ATGL) and hormone-sensitive lipase (HSL), in TAG estolide and FAHFA degradation. We synthesized a library of 20 TAG estolide isomers with FAHFAs varying in branching position, chain length, saturation grade, and position on the glycerol backbone and developed an in silico mass spectra library of all predicted catabolic intermediates. We found that ATGL alone or coactivated by comparative gene identification-58 efficiently liberated FAHFAs from TAG estolides with a preference for more compact substrates where the estolide branching point is located near the glycerol ester bond. ATGL was further involved in transesterification and remodeling reactions leading to the formation of TAG estolides with alternative acyl compositions. HSL represented a much more potent estolide bond hydrolase for both TAG estolides and free FAHFAs. FAHFA and TAG estolide accumulation in white adipose tissue of mice lacking HSL argued for a functional role of HSL in estolide catabolism in vivo. Our data show that ATGL and HSL participate in the metabolism of estolides and TAG estolides in distinct manners and are likely to affect the lipokine function of FAHFAs.

ATGL | HSL | FAHFA | lipokine

Branched esters of palmitic acid and hydroxy stearic acid (PAHSAs) are antiinflammatory and antidiabetic lipokines (1–3). PAHSA serum and adipose tissue levels correlate with insulin sensitivity and are decreased in insulin-resistant humans (2, 4). PAHSAs increase glucose-stimulated insulin secretion by enhancing the production of the gut-derived incretin glucagon-like peptide-1 (5, 6). The antiinflammatory effects of PAHSA isomers (2, 7, 8) are mediated via free fatty acid receptor 4 (FFAR4, GPR120) and modulate both innate and adaptive immune responses in a mouse colitis model (1) and type-1 diabetes (6). Therefore, PAHSAs have beneficial effects on both metabolism and the immune system (9).

PAHSAs belong to the family of fatty acid (FA) esters of hydroxy FAs (HFAs) called FAHFAs, which are part of a much larger family of mono- or oligomeric FAHFA esters named estolides. Since FAHFAs contain only a single ester bond of one FA with one HFA (the estolide bond), they represent monoestolides (10). The position of the branching carbon atom defines the regioisomer (e.g., 5-PAHSA or 9-PAHSA). PAHSAs and other less-well-studied FAHFAs such as the oleic acid esters of hydroxy palmitic acid (OAHPAs) or the docosahexaenoic acid ester of 13-hydroxy linoleic acid (13-DHAHLA) derive from either dietary sources or de novo synthesis in adipose tissue and other organs (2, 11, 12). Nonesterified, free FAHFAs (free monoestolides) can be esterified to glycerol to form FAHFA acylglycerols, which in combination with other FAs result in the formation of triacylglycerol (TAG) estolides, diacylglycerol (DAG) estolides, or monoacylglycerol (MAG) estolides. TAG estolides represent a major storage form of bioactive free FAHFAs and are present in plant oils (e.g., castor oil) (13, 14) and adipose tissue of mice (3, 15) and humans (16).

Both the synthetic and catabolic pathways of FAHFAs and TAG estolides are insufficiently understood. The hydrolytic catabolism of FAHFAs and TAG estolides results in the generation of highly bioactive and physiologically relevant FAHFAs, HFAs, FAs, and DAGs. Given the structural and metabolic similarity between TAGs and TAG estolides, it seemed reasonable to suspect that canonical TAG lipases will be involved in FAHFA and TAG estolide degradation. Generally, the catabolism of TAGs in cells occurs in the cytosol (neutral lipolysis) or in lysosomes (acidic lipolysis). Neutral lipolysis represents the predominant pathway for the hydrolysis of lipid droplet-associated TAGs in adipocytes involving three major enzymes, adipose

Significance

Fat mass is controlled by the balance of triacylglycerol (TAG) degradation and synthesis. Adipose triglyceride lipase (ATGL) and hormone-sensitive lipase (HSL) are key players in TAG catabolism providing fatty acids (FAs) as energy substrates and metabolic intermediates. Here, we show that ATGL and HSL metabolize TAGs containing antidiabetic lipid mediators (FA esters of hydroxy FAs), distinctly controlling the release of bioactive lipids. Our paper connects lipolysis-mediated TAG metabolism with the regulation of antidiabetic signaling lipids.

Author contributions: R.Z. and O.K. designed research; K.B., F.P.W.R., L.B., V.P., T.C., H.C., E.K., M.S., R.S., T.D., and O.K. performed research; L.B., H.C., E.K., R.S., T.D., R.Z., and O.K. contributed new reagents/analytic tools; K.B., F.P.W.R., V.P., T.C., M.S., R.S., R.Z., and O.K. analyzed data; and K.B., F.P.W.R., L.B., T.C., E.K., R.S., T.D., R.Z., and O.K. wrote the paper.

Reviewers: R.V.F., Harvard Medical School; and S.G.Y., University of California, Los Angeles.

The authors declare no competing interest.

[1]K.B. and F.P.W.R. contributed equally to this work.

[2]To whom correspondence may be addressed. Email: rudolf.zechner@uni-graz.at or ondrej.kuda@fgu.cas.cz.

This article contains supporting information online at https://www.pnas.org/lookup/suppl/doi:10.1073/pnas.2020999118/-/DCSupplemental.

Published December 28, 2020.

triglyceride lipase (ATGL), hormone-sensitive lipase (HSL), and monoglyceride lipase (MGL). ATGL catalyzes the initial step of TAG hydrolysis, generating DAG and one FA (3, 17, 18). The enzyme belongs to the patatin-like phospholipase domain-containing (PNPLA) family of proteins comprising a number of lipid hydrolases (3, 15). ATGL is the most potent TAG hydrolase within this family but also exhibits some phospholipase, retinylesterase, and transacylase activities of undefined physiological relevance (17, 19, 20). For full TAG hydrolase activity, ATGL requires a coactivator named comparative gene identification-58 (CGI-58; also called α/β-hydrolase domain containing 5, ABHD5) (21–23). CGI-58 features α/β-hydrolase folds and also exerts some

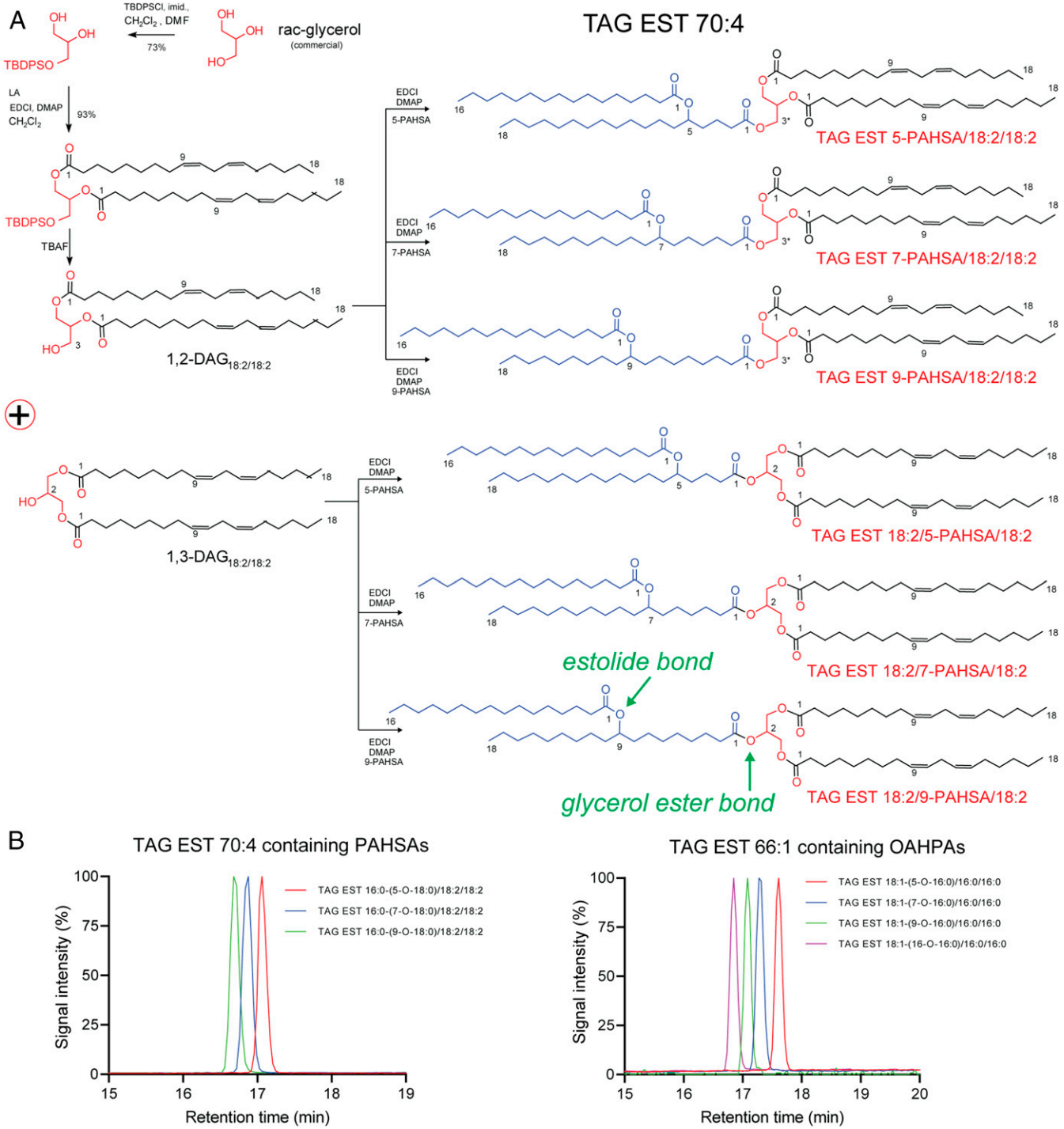

Fig. 1. Synthesis of TAG estolide 70:4 isomers. (*A*) Scheme of the organic synthesis of TAG estolide (TAG EST) 70:4 isomers. 1,2- and 1,3-dilinoleoyl glycerol (1,2/1,3-$DAG_{18:2/18:2}$) were esterified with palmitic acid ester of hydroxy stearic acid with branching positions at carbon atom 5, 7, or 9 (5-, 7-, or 9-PAHSA). Both *sn*-1 and *sn*-3 products were synthesized, as the starting glycerol (red structure) was a racemic mixture. The internal ester linkage within the PAHSA (blue structure) is the estolide bond (branching position). (*B*) Illustrative chromatograms of the TAG EST 70:4 and 66:1 isomers. The FAHFA (PAHSA or oleic acid ester of hydroxy palmitic acid [OAHPA]) is bound at the *sn*-1/3 position of the glycerol.

acyltransferase and protease activities (23–25). Yet, the physiological role of these activities remains elusive. ATGL exhibits unique regioselectivity for TAG substrates and preferentially hydrolyzes the *sn*-2 position of the glycerol chain of TAGs (26). Upon stimulation of ATGL by CGI-58 this regioselectivity broadens to the *sn*-1 but not the *sn*-3 position (26).

HSL is rate-limiting for the second step of TAG lipolysis converting DAG to one FA and MAG (27). The enzyme preferentially catalyzes DAGs at the *sn*-3 position and cholesteryl esters (28, 29) but also cleaves TAGs (*sn*-1 and *sn*-3 position), retinylesters (30), or medium- and short-chain carboxylic acid glycerol esters (29). The enzyme is structurally unrelated to ATGL and does not require enzyme coactivators. Hormonal stimulation of neutral lipolysis by β-adrenoreceptor agonists such as catecholamines activates both ATGL and HSL by promoting the molecular interaction of ATGL with CGI-58 on the surface of TAG-containing lipid droplets (21, 31) and the translocation of HSL from the cytoplasm to lipid droplets. These processes involve the protein kinase A-dependent phosphorylation of perilipin-1, CGI-58, and HSL (31–33).

Previous studies by Tan et al. (15) and our laboratory (3) demonstrated that ATGL and HSL are both able to hydrolyze FAHFA–glycerol ester bonds of TAG estolides. However, enzyme preferences for this reaction, the substrate requirements, or the contribution of these enzymes to hydrolyze the FA–HFA ester bond (estolide bond) in TAG estolides as well as in free FAHFAs remained unaddressed. Using a newly generated library of TAG estolides, we now show that ATGL and HSL play distinct roles in the formation of TAG estolides by transesterification reactions and the degradation of (TAG) estolides by hydrolysis reactions.

Results

Synthesis and Structural Analysis of a TAG Estolide Library. For the comprehensive analysis of the substrate requirements for TAG estolide hydrolysis by ATGL and HSL, we prepared a library of 20 TAG estolides with various FAHFAs esterified to the *sn*-1/3 or the *sn*-2 position of the glycerol backbone (*SI Appendix*, Fig. S1). We used the previously published synthetic approach (3) to link FAHFAs with various branching positions (5-, 7-, 9-, 10-, and 16-), chain length (C_{16} and C_{18}), and degree of saturation (0 to 2) (34) to dipalmitoylglycerol or dilinoleoylglycerol. As an example, Fig. 1*A* displays the synthesis of the TAG estolide 70:4 subgroup, where 5-, 7-, and 9-PAHSA were esterified to the outer (*sn*-1 or *sn*-3) and inner (*sn*-2) positions of dilinoleoylglycerol, respectively. Since the synthesis was performed with racemic DAGs, the resulting TAG estolides include epimers of the *sn*-2 and the *sn*-1/3 series. Synthesized TAG estolides were analyzed by liquid chromatography tandem mass spectrometry (LC-MS/MS) and NMR. LC-MS/MS analysis involved the initial separation of TAG estolides by reversed-phase LC according to the number of carbon atoms, the number of double bonds, and the position of the branching carbon atom of FAHFAs (exemplified in Fig. 1*B* for the TAG estolide isomers 70:4 and 66:1) and subsequent MS/MS analysis by Q Exactive Plus. Based on these experimental data, we prepared an in silico LC-MS/MS library for MS-DIAL of all theoretical TAG estolides as well as single, double, and triple monoestolides of MAGs, DAGs, and TAGs, respectively. TAG estolides with multiple branching (diestolides and triestolides) were not considered, as such structures have only been detected in plants but not in animals or humans (13, 14).

Glycerol Ester Bond Hydrolysis: ATGL Is the Predominant Hydrolase to Release FAHFAs from TAG Estolides. To explore the substrate specificity of ATGL and HSL for TAG estolides, we overexpressed the respective complementary DNAs (cDNAs) as well as the *LacZ* gene coding for β-galactosidase (β-Gal) as negative control in HEK293T cells and used cell lysates as enzyme sources. Protein expression in lysates was verified by Western blotting analysis (*SI Appendix*, Fig. S2*A*). LC-MS/MS analysis confirmed that ATGL and HSL were enzymatically active (*SI Appendix*, Fig. S2 *B* and *C*). Using standard lipase substrates, ATGL preferentially hydrolyzed triolein, while HSL preferentially hydrolyzed diolein, conforming with the established substrate preference of the enzymes (27). To determine TAG estolide hydrolysis, ATGL- or HSL-overexpressing cell lysates were incubated with phosphatidylcholine/phosphatidylinositol–emulsified TAG estolide substrates and the reaction products were analyzed by LC-MS/MS. The substrate preference of ATGL was assessed in the presence or absence of purified recombinant CGI-58 (21). In the first set of experiments, saturated TAG estolides 66:0 [16:0-(z-O-18:0)/16:0/16:0] with branching positions at z = 5, 7, or 9 were used as substrate. As shown in Fig. 2*A*, ATGL most efficiently catalyzed the release of PAHSAs from the glycerol backbone in the presence of CGI-58 followed by ATGL without coactivator. HSL had only a minor PAHSA-releasing activity compared to ATGL. Interestingly, the PAHSA release via ATGL+ CGI-58 or ATGL alone decreased with increasing distance between the FA-branching carbon atom and the glycerol ester bond.

Similar results were obtained when OAHPA replaced PAHSA within TAG estolide substrates. Again, ATGL+CGI-58 cleaved the glycerol ester bond more efficiently than ATGL alone or HSL (Fig. 2*B*). Also, with OAHPA-containing TAG estolides, the hydrolytic activity of ATGL+CGI-58 decreased with the distance of the branching carbon atom to the glycerol ester bond and was lowest for TAG estolides containing the 9-OAHPA. Thus, the overall lipolytic activity of ATGL+CGI-58 for the cleavage of the FAHFA–glycerol ester bond in branched TAG estolides followed the "branching-point rule" 9-OAHPA < 7-OAHPA < 5-OAHPA. In contrast, the unbranched TAG estolide 66:1 with ω-hydroxy FA (16-OAHPA) did not follow this rule, since the 16-OAHPA release by ATGL+CGI-58 or ATGL alone was higher than the 9-OAHPA release (compare Fig. 2 *B* and *C*), indicating the branching-point rule does not apply to linear TAG estolides like TAG estolide with 16-OAHPA.

ATGL+CGI-58 Hydrolyzes Both *sn*-1,3 and *sn*-2 FAHFA–Glycerol Esters. To evaluate the regioselectivity of ATGL and HSL toward TAG estolides, we prepared positional isomers of the TAG estolide

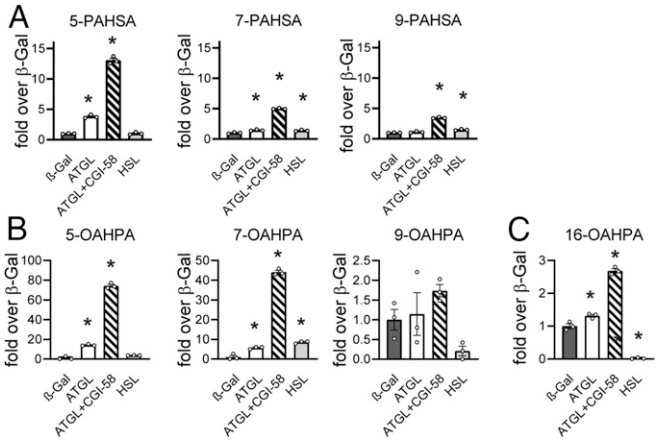

Fig. 2. The FAHFA–glycerol ester bond in TAG estolides is preferentially hydrolyzed by ATGL. (*A*) Release of PAHSAs from TAG estolide 66:0 with 5-, 7-, or 9-PAHSA bound at the *sn*-1/3 position. (*B*) Release of 5-, 7-, or 9-OAHPAs from TAG estolide 66:1 series. (*C*) Release of 16-OAHPA from the TAG estolide 66:1 with 16-OAHPA bound at the *sn*-1/3 position. Data are presented as means ± SEM ($n = 3$). Statistical differences were determined by one-way ANOVA with multiple comparison test (Tukey). *Significantly different at $P < 0.05$ from the β-Gal group. Additional statistics are presented in *SI Appendix*.

70:4 with 5-PAHSA esterified at a primary alcohol position (*sn*-1/3) or at the secondary alcohol position (*sn*-2) in the glycerol. While HSL remained a poor FAHFA–glycerol ester bond hydrolase, ATGL and ATGL+CGI-58 cleaved both *sn*-1,3 and *sn*-2 FAHFA–glycerol ester bonds, leading to the formation of free 5-PAHSA and the corresponding DAG 36:4 (Fig. 3*A*). In addition to the FAHFA–glycerol ester bond, ATGL+CGI-58 also cleaved the FA–glycerol ester bond, leading to the formation of linoleic acid (18:2) and the remaining DAG estolides (Fig. 3*B*). Notably, ATGL+CGI-58 as well as ATGL alone also led to the formation of MAG 18:2 (Fig. 3*A*) and the MAG estolide with 5-PAHSA (Fig. 3*B*), which may either result from DAG lipase or transacylase activities of ATGL (discussed below).

ATGL's Hydrolase and Transacylase Activities Generate TAG Double and Triple Monoestolides. Next, we assessed whether TAG estolide remodeling occurs via transesterification reactions. In addition to its hydrolytic activity, ATGL exhibits marked transacylase activity with MAGs or DAGs acting as acyl donors and DAGs as acyl acceptors, thus creating TAGs and glycerol or TAGs and MAGs, respectively (17, 19). Incubation of the TAG estolide 70:4 (5-PAHSA at the *sn*-1/3 position) with ATGL+CGI-58, but not ATGL alone or HSL, led to the formation of the TAG double monoestolides 84:0, 86:0, and 86:2 with FA 16:0, 18:0, and 18:2 as the third acyl chain as well as the TAG triple monoestolide 102:0 (Fig. 4*A*). Fig. 4*A* also includes the anticipated hydrolysis and transesterification reactions that led to these products. Fig. 4 *B*–*F* summarize a comprehensive analysis of selected reaction products of TAG estolide 70:4 incubation with ATGL+CGI-58. Transesterification and hydrolysis processes involved both the TAG estolide 70:4 substrate and acylglycerols that are present in the ATGL-overexpressing cell lysates, which markedly increased the compositional complexity of detected intermediates. This observation explains, for example, the appearance of monoestolides containing palmitic acid (Fig. 4 *B* and *C*) or myristic acid (Fig. 4*E*), which are not present in the TAG estolide substrate.

Taken together, ATGL+CGI-58 efficiently hydrolyzes the FAHFA–glycerol ester bond in TAG estolides depending on the FAHFA *sn* position and the branching carbon atom. Additionally, ATG+CGI-58 leads to major acylglycerol remodeling reactions that participate in the synthesis of TAG, DAG, and MAG estolides with FAHFAs in all *sn* positions as well as double and triple monoestolides.

Estolide Bond Hydrolysis: HSL Is the Major Estolide Bond Hydrolase. The striking drop of 16-OAHPA levels below control baseline in the HSL group (Fig. 2*C*) urged us to explore the hydrolysis of the estolide bond. Initially, we focused on the estolide bond hydrolysis in TAG estolides 66:1 with OAHPA branching at carbon atom 5, 7, or 9, and the unbranched 16-OAHPA. Estolide bond hydrolysis was monitored by the formation of oleic acid (FA 18:1). HSL-containing HEK293T lysates effectively hydrolyzed the estolide bond of all branched glycerol-bound FAHFAs with similar efficiency (Fig. 5 *A* and *B*). Extremely high hydrolytic activities of the enzyme were observed for the unbranched 16-OAHPA–containing TAG estolide. This profound activity enabled the detection of the second reaction product, TAG-containing 16-HPA [TAG 48:0(OH)] (Fig. 5*B*), which was undetectable when branched TAG estolides (Fig. 5*A*) were used as substrates. In comparison to HSL, ATGL alone or ATGL+CGI-58 did not hydrolyze the estolide bond in branched TAG estolides and exhibited a much weaker activity for the unbranched TAG estolide substrate containing 16-OAHPA (Fig. 5 *A* and *B*).

To investigate whether HSL also hydrolyzes nonesterified FAHFAs, we used the branched 5-, 7-, and 9-OAHPA as well as the unbranched 16-OAHPA as substrate in our lipase assays. HSL released oleic acid (FA 18:1) from all substrates. Highest enzyme activity was observed when the unbranched 16-OAHPA was used as substrate followed by 5-OAHPA, 7-OAHPA, and 9-OAHPA (Fig. 6*A*). Oleic acid release correlated well with the formation of the corresponding HFAs (Fig. 6*B*). In contrast to HSL, ATGL lacks or demonstrates only minor hydrolytic activity against OAHPA substrates.

The Loss of Functional ATGL or HSL Affects the TAG Estolide Metabolism in Mice. Finally, to assess whether the ATGL and HSL play a role in TAG estolide formation or hydrolysis also in vivo, TAG estolide and FAHFA concentrations were determined in white adipose tissue extracts from wild-type (WT), and ATGL and HSL knockout

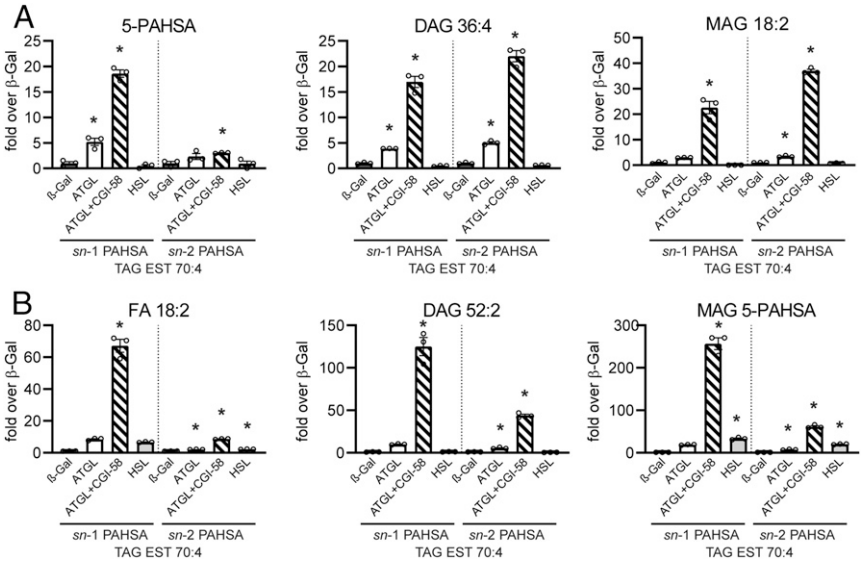

Fig. 3. Regioselectivity of ATGL-, ATGL+CGI-58–, and HSL-mediated glycerol ester bond hydrolysis. (*A* and *B*) Lipolytic products formed by the hydrolysis of TAG estolide (TAG EST) 70:4 with 5-PAHSA bound at *sn*-1/3 (marked *sn*-1 due to ATGL position specificity) or *sn*-2 position are shown. Data are presented as means ± SEM ($n = 3$). Statistical differences were determined by one-way ANOVA with multiple comparison test (Tukey). *Significantly different at $P < 0.05$ from the β-Gal group. Additional statistics are presented in *SI Appendix*. DAG 52:2 stands for DAG 5-PAHSA_18:2.

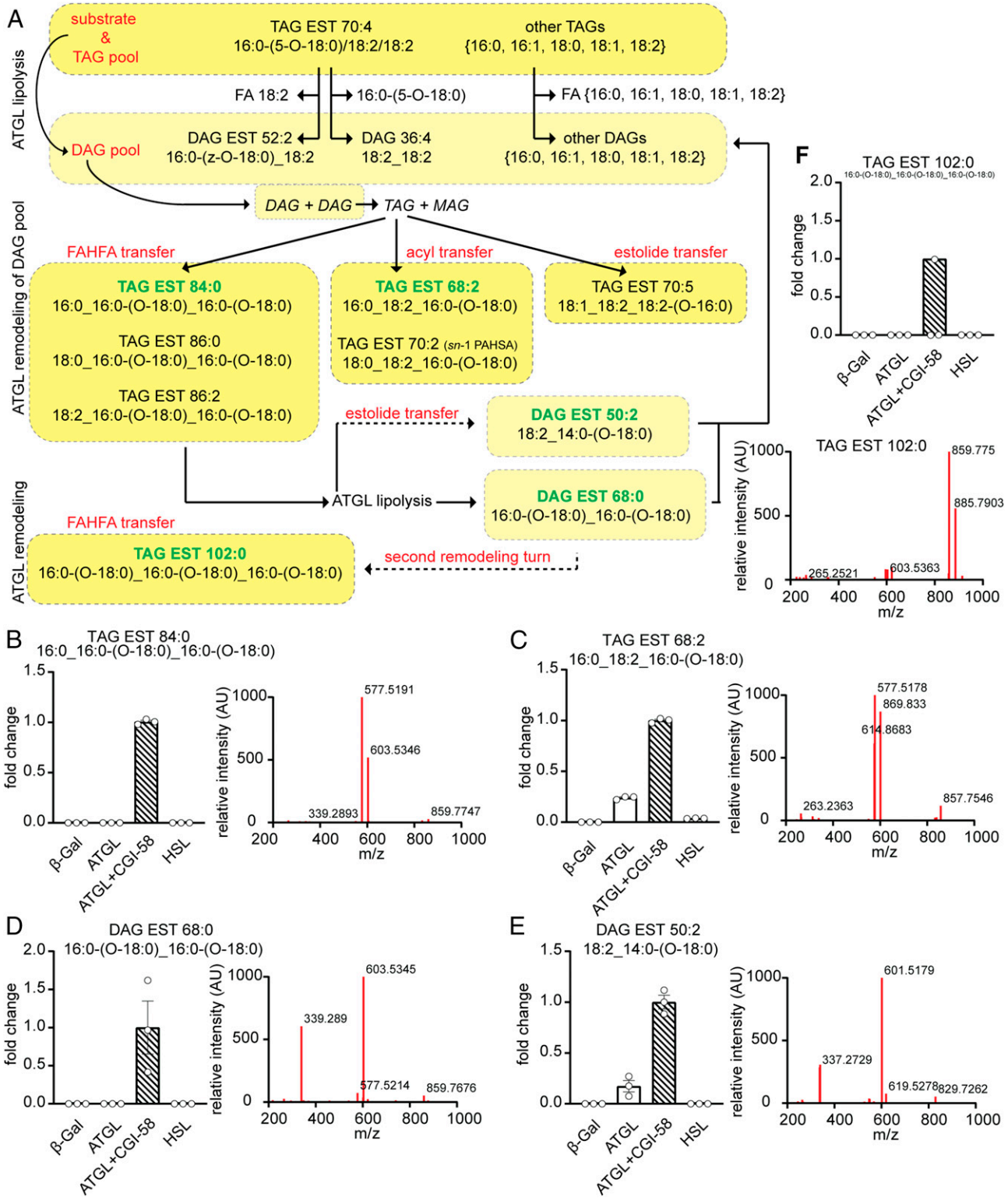

Fig. 4. TAG estolide remodeling yields alternative TAG estolide combinations. (*A*) Schematic representation of the main biochemical reactions running simultaneously or sequentially within the TAG estolide (TAG EST) 70:4 (5-PAHSA at *sn*-1/3) hydrolysis assay. The substrate as well as other substrates present in the cell lysate are metabolized by ATGL and other enzymes in the lysate. These pools of intermediates serve as both acyl donors and acceptors in reactions catalyzed by ATGL (acyltransferase, transacylase reaction). TAG estolides with one, two, or three PAHSAs and alternative estolides originating from FAHFA transfer or estolide remodeling were detected mainly in the samples where ATGL was coactivated by CGI-58. All structures with acyl chain composition were annotated based on MS/MS spectra. (*B*–*F*) Levels of selected estolides from *A* including MS/MS spectra. Data are presented as means ± SEM ($n = 3$). Fold change over ATGL+CGI-58 group.

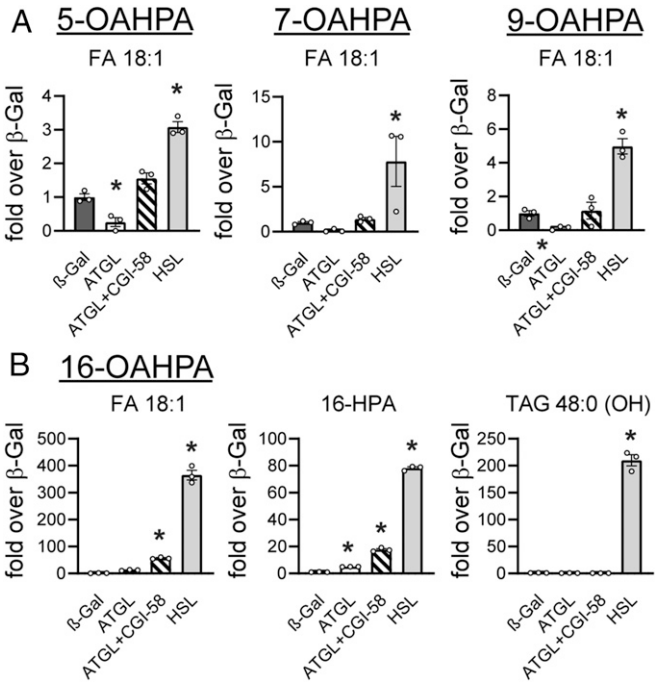

Fig. 5. The estolide bond in TAG estolides is preferentially hydrolyzed by HSL. Hydrolysis of TAG estolide 66:1 series with OAHPA bound at the *sn*-1/3 position and with OAHPA branching at the carbon atom 5, 7, 9 (*A*), and 16 (*B*), respectively. Data are presented as means ± SEM (n = 3). Statistical differences were determined by one-way ANOVA with multiple comparison test (Tukey). *Significantly different at $P < 0.05$ from the β-Gal group. Additional statistics are presented in *SI Appendix*. TAG 48:0(OH), monohydroxylated TAG intermediate; HPA, hydroxy palmitic acid. The 5-, 7-, and 9-HPA and the corresponding TAGs 48:0 (OH) were not found in *A* reactions.

(KO) mice. We previously reported that total TAG estolide levels decrease in ATGL-deficient adipose tissue (3). As shown in Fig. 7*A*, this decrease affects essentially all TAG estolide species in both the fed and the fasted state when compared to WT animals. Additionally, the variety of TAG estolides is reduced in ATGL-deficient adipose tissue, consistent with an essential role of ATGL-mediated transacylation reactions in the synthesis and remodeling of TAG estolides.

In contrast to the results in ATGL KO adipose tissue, essentially all species of TAG estolides increased in mice lacking adipose tissue HSL in both the fed and the fasted condition (Fig. 7*B*). Upon quantitation, total TAG estolide levels in HSL KO adipose tissue were approximately fourfold higher in the fed state and approximately eightfold higher in the fasted state when compared to WT animals (Fig. 7*C*), suggesting a crucial role of the enzyme in the degradation of TAG estolides. Furthermore, the concentrations of nonesterified FAHFAs were also increased in HSL KO adipose tissue (Fig. 7*D*). For example, the physiologically most relevant 5- and 9-PAHSA as well as 5- and 9-OAHPA increased 2- to 10-fold in adipose tissue of HSL KO mice in both the fasted and the fed condition.

Discussion

The current study addressed the question whether and how the principal metabolic lipases ATGL and HSL facilitate the hydrolysis of estolides and TAG estolides. In vitro enzyme activity assays revealed that both enzymes contribute to TAG estolide catabolism but differ in their substrate specificity. ATGL predominantly cleaves the ester bond between glycerol and FAHFAs but represents a relatively poor hydrolase for the estolide ester bond linking FAs to HFAs. ATGL additionally exhibits transacylase activity that is heavily involved in the remodeling of TAG estolides. In contrast, HSL is a much better estolide ester hydrolase (generating FA and HFA) than ATGL but a relatively weak enzyme to release FAHFAs from the glycerol backbone of TAG estolides. Moreover, HSL does not contribute to TAG estolide remodeling via catalysis of transacylase reactions. These findings strongly argue for distinct roles of the main enzymes for neutral lipolysis in estolide and TAG estolide metabolism.

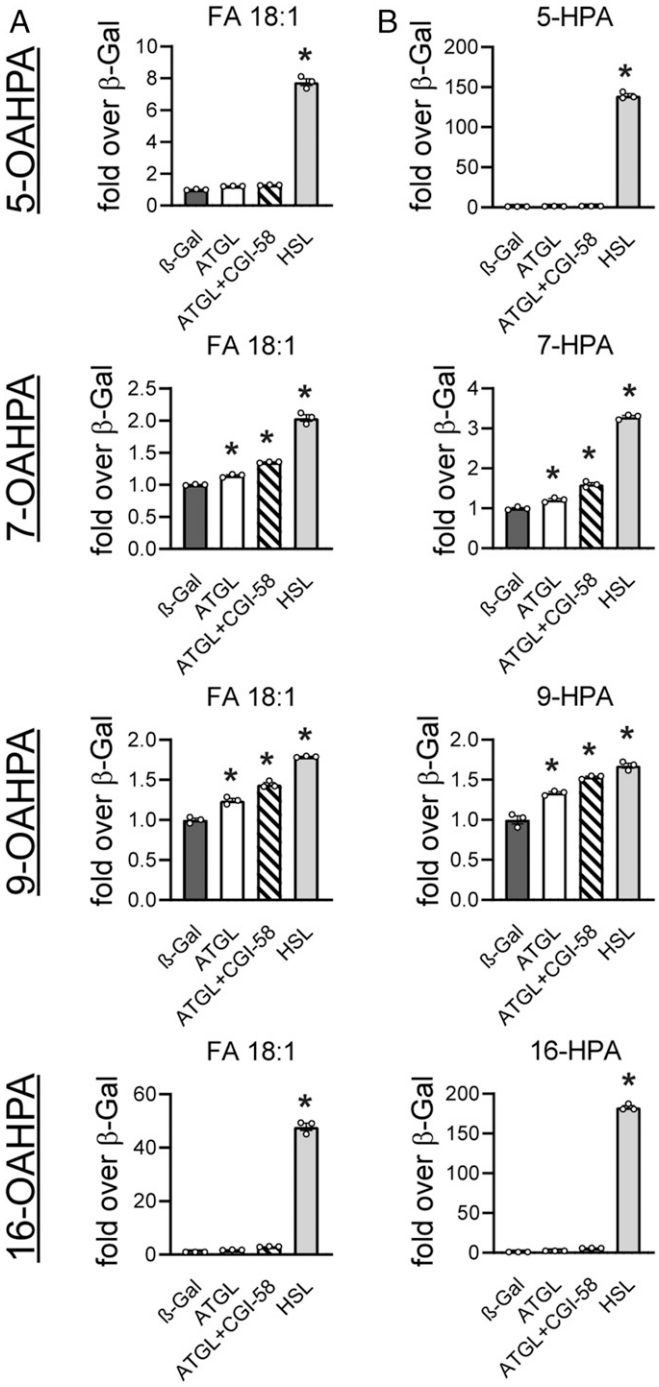

Fig. 6. Hydrolysis of free OAHPAs with branching at the carbon atom 5, 7, 9, or 16. Production of FA 18:1 (*A*) and the corresponding HPA (*B*). Data are presented as means ± SEM (n = 3). Statistical differences were determined by one-way ANOVA with multiple comparison test (Tukey). *Significantly different at $P < 0.05$ from the β-Gal group. Additional statistics are presented in *SI Appendix*.

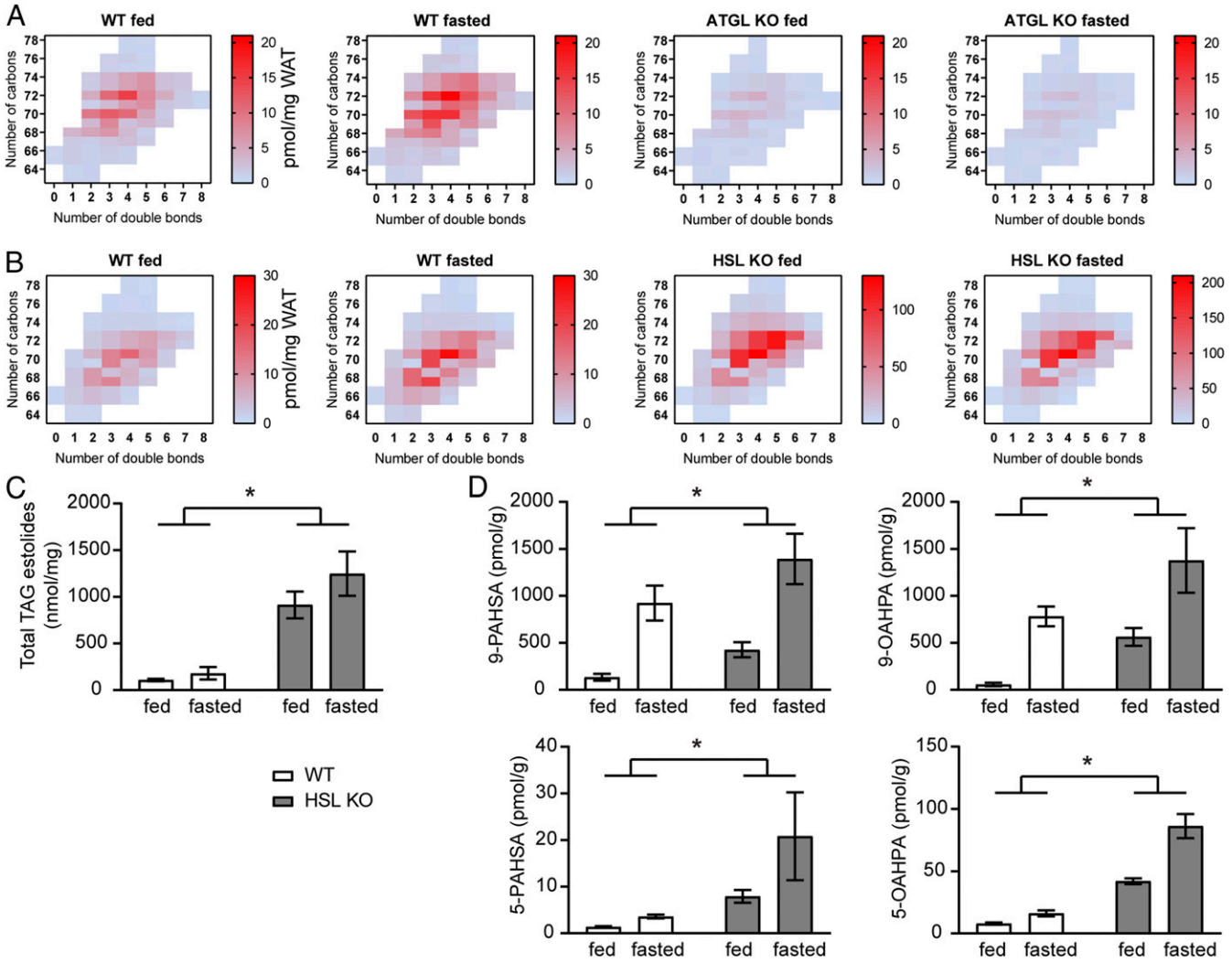

Fig. 7. Concentrations of TAG estolides and free FAHFAs in epididymal white adipose tissue of ATGL and HSL KO mice. Epididymal white adipose tissue from WT, ATGL KO, and HSL KO mice was collected in the ad libitum-fed and 14-h-fasted state. (*A* and *B*) TAG estolide species were quantified and data sorted according to the number of carbon atoms and the number of double bonds. The color scale represents the mean concentration ($n = 5$ to 7). When multiple isomers were detected, the square was divided into sections. (*C*) Concentrations of total TAG estolide and (*D*) various free FAHFAs in HSL KO white adipose tissue compared to WT control samples. Data are presented as means ± SEM ($n = 5$). Statistical differences were determined by two-way ANOVA with multiple comparison test (Tukey). *Significantly different at $P < 0.05$ for genotype. Additional statistics are presented in *SI Appendix*.

ATGL and HSL are highly expressed in white and brown adipose tissue, which are also primary sites of FAHFA and TAG estolide synthesis and metabolism. Nonadipose tissues including the heart, skeletal muscle, liver, pancreas, ovaries, or testes also express both enzymes at a lower level (18). Nevertheless, the severe pathology and increased lethality of ATGL deficiency in humans and mice highlights the functional importance of lipases in nonadipose tissues (35). Although both ATGL and HSL are potent TAG hydrolases, their substrate preferences differ. While ATGL preferentially hydrolyzes TAGs and requires FA chain lengths of eight carbon atoms and above with a modest preference for unsaturated over saturated FAs (26), HSL is much less substrate-specific, efficiently hydrolyzing TAGs, DAGs, MAGs, cholesteryl esters, retinyl ester, and short-chain ester substrates such as *p*-nitrophenylbutyrate (36). Therefore, it was not unexpected to find that ATGL and HSL hydrolyze various ester bonds within TAG estolides with different efficiency.

As observed for ATGL-mediated hydrolysis of regular TAGs, CGI-58 strongly enhanced enzyme activity also for TAG estolides. Our experimental setup did not permit a quantitative comparison of ATGL activities for ester hydrolysis of the TAG FAHFA-glycerol bond vs. TAG FA-glycerol bonds. However, from a rough estimation we can say that estolides are poorer substrates (1 to 10%) than ordinary FA esters. Concerning substrate specificity, ATGL favored branched TAG estolides with more compact structures, in which the branching carbon atom of FAHFAs is located closer to the glycerol backbone. This branching point-specific preference of ATGL may enable the preferential release of a subgroup of FAHFAs with specific biological functions. Unlike the majority of animal and bacterial lipases, ATGL+CGI-58 hydrolyzes ester bonds within TAGs at both the *sn*-1 and the *sn*-2 position (26, 37). This substrate preference was also observed when CGI-58–activated ATGL reacted with both positional isomers of TAG estolide 70:4 with 5-PAHSA bound to the *sn*-1/3 or the *sn*-2 position, resulting in the formation of free 5-PAHSA and the corresponding DAG. HSL also acted as a TAG estolide lipase generating FAHFAs and DAGs. However, compared to ATGL+CGI-58, the hydrolytic activity of HSL for the FAHFA–glycerol ester bond was considerably lower. This finding confirms previous studies using 3T3-L1 adipocytes and

ATGL as well as HSL inhibitors (15). ATGL and HSL are currently the only enzymes known that hydrolyze the FAHFA–glycerol ester bond on TAG estolides. Whether other established TAG hydrolases that are present in adipose tissue including carboxyl esterase-3 (CES3; also named triglyceride hydrolase-1) (38), PNPLA3 (also named adiponutrin) (39), or DDHD2 (40) also contribute to TAG estolide hydrolysis remains to be determined.

In addition to the well-established hydrolytic activity, both ATGL and HSL also exhibit transacylase activities, transferring acyl residues from donor acylglycerols to acceptor acylglycerols (17, 19). We previously demonstrated that although FAHFAs are released from TAG estolides during lipolysis, some FAHFAs and TAG estolides are being resynthesized at the same time (3). Our current data suggest that transacylation reactions catalyzed by CGI-58–activated ATGL are responsible for both processes. Apparently, ATGL reuses DAG estolides as acyl acceptors or donors to generate TAG estolides with an alternative acyl composition. This extensive remodeling process can result in the formation of double or triple estolides with two or three FAHFAs esterified to glycerol. However, the condensation of several FAHFAs on a single glycerol backbone is rare and only observed with PAHSA-containing substrates. Thus, we and others have only detected TAG monoestolides containing various FAHFAs in human and mouse white adipose tissue samples but failed to observe more complex di- and triestolide structures (3, 15, 16). TAG estolide analyses of ATGL-deficient white adipose tissue support the concept of a crucial role of ATGL in the synthesis and remodeling of FAHFAs and TAG estolides. Mice lacking ATGL have very low TAG estolide and nonesterified PAHSA levels in adipose tissue (3). ATGL-dependent PAHSA production may be physiologically relevant because under normal conditions free PAHSA concentrations rise in subcutaneous and perigonadal adipose tissue during fasting when ATGL expression is high in order to gear adipocytes for prospective glucose utilization (2, 3). In the absence of ATGL, low PAHSA concentrations may interfere with this normal fasting response. Taken together, the ATGL-mediated hydrolysis and transacylase reactions contribute to the formation and remodeling of FAHFAs and TAG estolides in vitro and in vivo, although details of these anabolic functions of ATGL remain to be elucidated.

Besides ATGL, other members of the PNPLA family have also been shown to catalyze transacylation reactions (41). PNPLA1 catalyzes the estolide bond formation between amide-linked ultra-long-chain HFAs in ω-hydroxyceramides and linoleic acid generating ω-*O*-acylceramides in keratinocytes. This reaction, utilizing TAG as acyldonor, is activated by CGI-58 and represents an essential step in the formation of the corneocyte lipid envelope to maintain permeability barrier function in the skin (42, 43). The second ATGL paralog, PNPLA3, also exhibits, in addition to its relatively weak TAG hydrolase activity, transacylase and acyltransferase activities (19, 44). Recent findings showed that PNPLA3 competes with ATGL for CGI-58 binding affecting TAG metabolism in adipocytes and hepatocytes (39, 45). In contrast to ATGL, *Pnpla3* gene expression is upregulated by insulin, which suggests a role in glycerolipid synthesis and remodeling rather than its degradation (46). While PNPLA1 expression is essentially restricted to keratinocytes, PNPLA3 is strongly expressed in adipose tissue and the liver. Whether PNPLA1 or 3 participate in FAHFA or TAG estolide synthesis and/or remodeling needs to be elucidated.

Our work identified HSL as a potent hydrolase of the estolide bond in FAHFAs and TAG estolides in vitro and in vivo. The absence of HSL resulted in a marked increase in total TAG estolide concentrations in white adipose tissue from fed and fasted mice. Free FAHFA concentrations also increased in HSL KO adipose tissue, arguing for a functional role of HSL as FAHFA hydrolase in branched FA metabolism also in vivo. Several other hydrolases including androgen-induced gene 1 (AIG1) protein, androgen-dependent TFPI regulating protein (ADTRP), and CES3 have already been identified as potential FAHFA hydrolases (47–49). Induced mutant mouse models proved that AIG1 and ADTRP are active estolide bond hydrolases in vivo (49). HSL adds to this list of hydrolases that affect tissue TAG estolide and FAHFA levels. The quantitative contribution of any of these lipases in different physiological situations is currently difficult to estimate and will depend on concomitant parameters such as tissue-specific expression levels, phosphorylation and activation state, and substrate preferences.

In conclusion, our results indicate that the predominant cellular neutral lipid hydrolases ATGL and HSL differently engage in the hydrolysis and remodeling of TAG estolides and FAHFAs. These distinct differences in hydrolase and transacylase activities, substrate specificity, and ester bond preference as well as a likely interaction with other known and possibly unknown enzymes create a complex enzymology in the formation of signaling FAHFAs that requires better characterization.

Methods

Nomenclature. The lipid nomenclature used throughout the paper is based on general literature recommendations and customized to describe the FAHFA-containing structures (2, 50). Briefly, the notation X:Y refers to an FA chain, where X is the total number of carbon atoms and Y is the number of double bonds.

FAHFAs belong to a family of estolides defined as mono- or oligomers of FAs. An estolide is characterized by the number of estolide linkages per molecule (estolide number, number of oligomers). Therefore, a FAHFA is a monoestolide (e.g., 9-PAHSA). Common (trivial) nomenclature of FAHFAs is used for the most-studied compounds like 9-PAHSA, where 9 defines the ester position relative to carboxylic acid and PA and HSA stand for palmitic acid and hydroxy stearic acid, respectively. Alternatively, to avoid abbreviations for each FA, generalized nomenclature X1:Y1-(z-O-X2:Y2) [e.g., 16:0-(9-O-18:0) for 9-PAHSA] is used for schematic representations.

TAG estolide nomenclature follows the general recommendations and an FAHFA is treated as an acyl group (51). Where only one FAHFA is bound to the glycerol backbone, it is a TAG monoestolide. Where two or three FAHFAs are bound to glycerol, it is a double or triple TAG monoestolide, respectively. As only monoestolides (FAHFAs) were found in mammals, the "mono" prefix is often omitted. The position of the FAHFA or FA acyl chains on the glycerol backbone is reported in the order *sn*-1, *sn*-2, *sn*-3, from left to right. As an example, when 9-PAHSA is esterified at the *sn*-1/3 position of the racemic 1,2-dipalmitoyl glycerol, the structure is written as 16:0-(9-O-18:0)/16:0/16:0, while an unknown position of the 9-PAHSA in the glycerol backbone is written 16:0-(9-O-18:0)_16:0_16:0.

Reagents. All chemical reagents were from Sigma-Aldrich unless stated otherwise. FAHFA standards were from Cayman Europe or synthesized previously (34).

TAG Estolide Library. The TAG estolides were synthesized at the Institute of Biomolecules Max Mousseron (Montpellier) and the Institute of Organic Chemistry and Biochemistry. The procedure for the Steglich esterification reactions is exemplified with the synthesis of TAG estolide 66:0 (*SI Appendix*). The synthesis of TAG estolide 70:4 is outlined in Fig. 1*A*.

cDNA Cloning of Recombinant Proteins and Expression and Purification of SMT-Tagged CGI-58. Mammalian expression vector pcDNA4/HisMax constructs containing the entire open reading frame of murine ATGL, murine HSL, or LacZ (β-Gal) were generated as described in Lass et al. (22). Small ubiquitin-like modifier (SMT)-tagged CGI-58 was expressed and purified as described in Gruber et al. (21).

Expression of Recombinant Proteins. HEK293T cells (ATCC CRL-3216) were cultivated in Dulbecco's modified Eagle's medium (Thermo Fisher Scientific) supplemented with 10% fetal bovine serum on cell culture dishes precoated with 0.1% gelatin in a standard humidified 7% CO_2 atmosphere at 37 °C; 1×10^6 cells were transfected with 2.5 μg plasmid DNA using Metafectene (Biontex GmbH) according to the manufacturer's instructions. The expression of Xpress-tagged proteins was detected using Western blotting analysis as described previously (42).

Preparation of Cell Homogenates. HEK293T cells overexpressing β-Gal, ATGL, or HSL were harvested 24 h after transfection and disrupted in buffer A (0.25 mol/L sucrose, 1 mmol/L ethylenediaminetetraacetic acid, 1 mmol/L dithiothreitol, pH 7.0, supplemented with 1 μg/mL pepstatin, 2 μg/mL antipain, and 20 μg/mL leupeptin) by sonication on ice. Thereafter, the cell lysates were centrifuged at 1,000 × *g* and 4 °C for 10 min to pellet the nuclei and unbroken cells. The protein concentration of the supernatants was determined using the Bradford reagent (Bio-Rad) and bovine serum albumin as a standard.

TAG Estolide Hydrolysis Assay. For the determination of TAG estolide hydrolase activity of HSL and ATGL in the presence or absence of CGI-58, 50 μg of protein from the respective cell homogenates was mixed with 200 ng of purified SMT-tagged CGI-58 or SMT empty vector control in a total volume of 100 μL of buffer A and then incubated with 100 μL of substrate in a water bath at 37 °C for 60 min. The reaction was terminated by adding 1 mL of methyl *tert*-butyl ether/methanol/acetic acid (75/25/1, vol/vol/vol). After centrifugation (7,500 × *g*, 5 min, room temperature), the organic phase was collected, dried under a stream of nitrogen, and finally resuspended in a dichloromethane/methanol/isopropanol (1/2/4, vol/vol/vol) mixture. Reaction products were analyzed using lipidomics platforms. As a control, incubations were performed under identical conditions using homogenates from cells expressing β-Gal that does not exhibit hydrolytic activities. To identify lipid products formed by the reaction of background lipids present in cell homogenates, control reactions were performed under identical conditions without the TAG estolide substrate. The assay substrate contained 250 μmol/L TAG estolide emulsified with 35 μmol/L phosphatidylcholine/phosphatidylinositol (PC/PI, 3:1) in 100 mmol/L potassium phosphate buffer, pH 7.0, by sonication on ice. To prevent product inhibition, bovine serum albumin was added to the reaction at a final concentration of 1%. Assays with free OAHPAs, triolein, or diolein as substrate were processed identically.

Animal Tissues. White adipose tissue was prepared from ad libitum-fed and 12- to 14-h-fasted, 12- to 14-wk-old female global HSL KO (53) and ATGL KO (52) mice as well as corresponding WT controls. Mice were housed under standard conditions (25 °C, 14/10-h light/dark cycle) with ad libitum access to chow diet (11 kJ % fat, V1126; Ssniff Spezialdiäten GmbH) in a specific pathogen-free environment. All animal studies were approved by the Ethics committee of the University of Graz and the Austrian Federal Ministry of Science, Research and Economy.

Lipidomics. The LC-MS system consisted of a Vanquish UHPLC System (Thermo Fisher Scientific) coupled to a Q Exactive Plus mass spectrometer (Thermo Fisher Scientific). For the acylglycerol estolide platform, the MS1 mass range of *m/z* 400 to 2,000 was used. Data were acquired in positive electrospray ionization (ESI) mode with a spray voltage of 3.6 kV and normalized collision energy of 20%. General lipidomic profiling in both positive and negative mode was performed as described before (3). TAG estolides are detectable in positive ion mode, similar to TAGs, as ammoniated adducts, sodium adducts, or ethylamine adducts $[M+CH_3CH_2NH_2+H]^+$ if acetonitrile is used as solvent.

Using this methodology, the TAG estolide mixture could be separated according to the number of carbon atoms and double bonds, and individual superfamilies (e.g., 70:4) could be quantified. For LC-ESI(+)-MS analysis, the mobile phase consisted of (A) 60:40 (vol/vol) acetonitrile:water with ammonium formate (10 mmol/L) and formic acid (0.1%) and (B) 90:10:0.1 (vol/vol/vol) isopropanol:acetonitrile:water with ammonium formate (10 mmol/L) and formic acid (0.1%); the following prolonged gradient was used: 0 min 0% (B); 0 to 12 min from 0 to 95% (B); 12 to 18 min from 95 to 99% (B); 18 to 25 min at 99% (B); 25 to 27 min from 99 to 0% (B); and 27 to 35 min 0% (B) (3). TAG estolide quantification was performed using deuterated TAG internal standards (TAG 51:1-$^2H_5$, TAG 60:1-$^2H_5$) and confirmed by the method of standard addition of pure TAG estolide 70:4 (3). The FA composition of the TAG estolide (or the main contributor) within the superfamily can be deduced from the MS/MS spectra, thus allowing the assessment of TAG estolide acyl composition as before (3). See the extracted ion chromatograms in *SI Appendix*, pages S60–S61.

Bioinformatics and Statistical Analyses. LC-MS and LC-MS/MS data were processed with the software MS-DIAL v. 4.0 (54). Metabolites were annotated using an in-house retention time–*m/z* library, and an in silico library of theoretical acylglycerol estolides was calculated using Python scripts. GraphPad Prism 8.0.2 was used to compare groups (ANOVA, Tukey's multiple comparisons test).

Data Availability. All study data are included in the paper and *SI Appendix*.

ACKNOWLEDGMENTS. This work was supported by grants from the Czech Science Foundation (20-00317S) and the Czech Academy of Sciences (LQ200111901; RVO Grant 61388963), projects P 32225-B (to F.P.W.R.) and F7302 SFB LIPID HYDROLYSIS (to R.Z.) funded by the Austrian Funds zur Förderung der Wissenschaftlichen Forschung, the Fondation Leducq Transatlantic Network grant 12CVD04 (R.Z.), the Louis-Jeantet Prize for Medicine 2015 (R.Z.), and the European Research Council (ERC) under the European Union's Seventh Framework Programme (FP/2007-2013)/ERC Grant Agreement 340896 (R.Z.). We thank Dr. Martin Dracinsky for measuring samples.

1. J. Lee *et al*., Branched fatty acid esters of hydroxy fatty acids (FAHFAs) protect against colitis by regulating gut innate and adaptive immune responses. *J. Biol. Chem.* **291**, 22207–22217 (2016).
2. M. M. Yore *et al*., Discovery of a class of endogenous mammalian lipids with anti-diabetic and anti-inflammatory effects. *Cell* **159**, 318–332 (2014).
3. V. Paluchova *et al*., Lipokine 5-PAHSA is regulated by adipose triglyceride lipase and primes adipocytes for de novo lipogenesis in mice. *Diabetes* **69**, 300–312 (2020).
4. A. Hammarstedt *et al*., Adipose tissue dysfunction is associated with low levels of the novel Palmitic Acid Hydroxystearic Acids. *Sci. Rep.* **8**, 15757 (2018).
5. B. Bandak, L. Yi, M. G. Roper, Microfluidic-enabled quantitative measurements of insulin release dynamics from single islets of Langerhans in response to 5-palmitic acid hydroxy stearic acid. *Lab Chip* **18**, 2873–2882 (2018).
6. I. Syed *et al*., PAHSAs attenuate immune responses and promote β cell survival in autoimmune diabetic mice. *J. Clin. Invest.* **129**, 3717–3731 (2019).
7. O. Kuda *et al*., Docosahexaenoic acid-derived fatty acid esters of hydroxy fatty acids (FAHFAs) with anti-inflammatory properties. *Diabetes* **65**, 2580–2590 (2016).
8. I. Syed *et al*., Palmitic acid hydroxystearic acids activate GPR40, which is involved in their beneficial effects on glucose homeostasis. *Cell Metab.* **27**, 419–427.e4 (2018).
9. K. Brejchova *et al*., Understanding FAHFAs: From structure to metabolic regulation. *Prog. Lipid Res.* **79**, 101053 (2020).
10. Y. Z. Chen *et al*., Fatty acid estolides: A review. *J. Am. Oil Chem. Soc.* **97**, 231–241 (2020).
11. O. Kuda *et al*., Nrf2-Mediated antioxidant defense and peroxiredoxin 6 are linked to biosynthesis of palmitic acid ester of 9-hydroxystearic acid. *Diabetes* **67**, 1190–1199 (2018).
12. M. Brezinova *et al*., Levels of palmitic acid ester of hydroxystearic acid (PAHSA) are reduced in the breast milk of obese mothers. *Biochim. Biophys. Acta Mol. Cell Biol. Lipids* **1863**, 126–131 (2018).
13. J. T. Lin, A. Arcinas, L. R. Harden, C. K. Fagerquist, Identification of (12-ricinoleoylricinoleoyl)diricinoleoylglycerol, an acylglycerol containing four acyl chains, in castor (Ricinus communis L.) oil by LC-ESI-MS. *J. Agric. Food Chem.* **54**, 3498–3504 (2006).
14. H. X. Zhang, D. J. H. Olson, D. Van, R. W. Purves, M. A. Smith, Rapid identification of triacylglycerol-estolides in plant and fungal oils. *Ind. Crops Prod.* **37**, 186–194 (2012).
15. D. Tan *et al*., Discovery of FAHFA-containing triacylglycerols and their metabolic regulation. *J. Am. Chem. Soc.* **141**, 8798–8806 (2019).
16. M. Brezinova *et al*., Exercise training induces insulin-sensitizing PAHSAs in adipose tissue of elderly women. *Biochim. Biophys. Acta Mol. Cell Biol. Lipids* **1865**, 158576 (2020).
17. C. M. Jenkins *et al*., Identification, cloning, expression, and purification of three novel human calcium-independent phospholipase A2 family members possessing triacylglycerol lipase and acylglycerol transacylase activities. *J. Biol. Chem.* **279**, 48968–48975 (2004).
18. R. Zimmermann *et al*., Fat mobilization in adipose tissue is promoted by adipose triglyceride lipase. *Science* **306**, 1383–1386 (2004).
19. X. Zhang *et al*., An epistatic interaction between *Pnpla2* and *lipe* reveals new pathways of adipose tissue lipolysis. *Cells* **8**, 395 (2019).
20. A. C. Lake *et al*., Expression, regulation, and triglyceride hydrolase activity of Adiponutrin family members. *J. Lipid Res.* **46**, 2477–2487 (2005).
21. A. Gruber *et al*., The N-terminal region of comparative gene identification-58 (CGI-58) is important for lipid droplet binding and activation of adipose triglyceride lipase. *J. Biol. Chem.* **285**, 12289–12298 (2010).
22. A. Lass *et al*., Adipose triglyceride lipase-mediated lipolysis of cellular fat stores is activated by CGI-58 and defective in Chanarin-Dorfman syndrome. *Cell Metab.* **3**, 309–319 (2006).
23. C. Lefèvre *et al*., Mutations in CGI-58, the gene encoding a new protein of the esterase/lipase/thioesterase subfamily, in Chanarin-Dorfman syndrome. *Am. J. Hum. Genet.* **69**, 1002–1012 (2001).
24. Z. H. Jebessa *et al*., The lipid droplet-associated protein ABHD5 protects the heart through proteolysis of HDAC4. *Nat. Metab.* **1**, 1157–1167 (2019).
25. G. Montero-Moran *et al*., CGI-58/ABHD5 is a coenzyme A-dependent lysophosphatidic acid acyltransferase. *J. Lipid Res.* **51**, 709–719 (2010).
26. T. O. Eichmann *et al*., Studies on the substrate and stereo/regioselectivity of adipose triglyceride lipase, hormone-sensitive lipase, and diacylglycerol-O-acyltransferases. *J. Biol. Chem.* **287**, 41446–41457 (2012).
27. G. Fredrikson, H. Tornqvist, P. Belfrage, Hormone-sensitive lipase and monoacylglycerol lipase are both required for complete degradation of adipocyte triacylglycerol. *Biochim. Biophys. Acta* **876**, 288–293 (1986).

28. M. Sekiya *et al*., Hormone-sensitive lipase is involved in hepatic cholesteryl ester hydrolysis. *J. Lipid Res.* **49**, 1829–1838 (2008).
29. J. A. Rodriguez *et al*., In vitro stereoselective hydrolysis of diacylglycerols by hormone-sensitive lipase. *Biochim. Biophys. Acta* **1801**, 77–83 (2010).
30. S. Wei *et al*., Retinyl ester hydrolysis and retinol efflux from BFC-1beta adipocytes. *J. Biol. Chem.* **272**, 14159–14165 (1997).
31. J. G. Granneman *et al*., Analysis of lipolytic protein trafficking and interactions in adipocytes. *J. Biol. Chem.* **282**, 5726–5735 (2007).
32. C. Krintel, M. Mörgelin, D. T. Logan, C. Holm, Phosphorylation of hormone-sensitive lipase by protein kinase A in vitro promotes an increase in its hydrophobic surface area. *FEBS J.* **276**, 4752–4762 (2009).
33. C. Krintel *et al*., Ser649 and Ser650 are the major determinants of protein kinase A-mediated activation of human hormone-sensitive lipase against lipid substrates. *PLoS One* **3**, e3756 (2008).
34. L. Balas *et al*., Regiocontrolled syntheses of FAHFAs and LC-MS/MS differentiation of regioisomers. *Org. Biomol. Chem.* **14**, 9012–9020 (2016).
35. M. Schweiger, A. Lass, R. Zimmermann, T. O. Eichmann, R. Zechner, Neutral lipid storage disease: Genetic disorders caused by mutations in adipose triglyceride lipase/PNPLA2 or CGI-58/ABHD5. *Am. J. Physiol. Endocrinol. Metab.* **297**, E289–E296 (2009).
36. T. Tsujita, H. Ninomiya, H. Okuda, p-nitrophenyl butyrate hydrolyzing activity of hormone-sensitive lipase from bovine adipose tissue. *J. Lipid Res.* **30**, 997–1004 (1989).
37. E. Rogalska, C. Cudrey, F. Ferrato, R. Verger, Stereoselective hydrolysis of triglycerides by animal and microbial lipases. *Chirality* **5**, 24–30 (1993).
38. K. G. Soni *et al*., Carboxylesterase 3 (EC 3.1.1.1) is a major adipocyte lipase. *J. Biol. Chem.* **279**, 40683–40689 (2004).
39. A. Yang, E. P. Mottillo, L. Mladenovic-Lucas, L. Zhou, J. G. Granneman, Dynamic interactions of ABHD5 with PNPLA3 regulate triacylglycerol metabolism in brown adipocytes. *Nat. Metab.* **1**, 560–569 (2019).
40. M. Araki *et al*., Enzymatic characterization of recombinant rat DDHD2: A soluble diacylglycerol lipase. *J. Biochem.* **160**, 269–279 (2016).
41. P. C. Kienesberger, M. Oberer, A. Lass, R. Zechner, Mammalian patatin domain containing proteins: A family with diverse lipolytic activities involved in multiple biological functions. *J. Lipid Res.* **50** (suppl.), S63–S68 (2009).
42. B. Kien *et al*., ABHD5 stimulates PNPLA1-mediated ω-*O*-acylceramide biosynthesis essential for a functional skin permeability barrier. *J. Lipid Res.* **59**, 2360–2367 (2018).
43. Y. Ohno, A. Nara, S. Nakamichi, A. Kihara, Molecular mechanism of the ichthyosis pathology of Chanarin-Dorfman syndrome: Stimulation of PNPLA1-catalyzed ω-O-acylceramide production by ABHD5. *J. Dermatol. Sci.* **92**, 245–253 (2018).
44. M. Kumari *et al*., Adiponutrin functions as a nutritionally regulated lysophosphatidic acid acyltransferase. *Cell Metab.* **15**, 691–702 (2012).
45. Y. Wang, N. Kory, S. BasuRay, J. C. Cohen, H. H. Hobbs, PNPLA3, CGI-58, and inhibition of hepatic triglyceride hydrolysis in mice. *Hepatology* **69**, 2427–2441 (2019).
46. E. E. Kershaw *et al*., Adipose triglyceride lipase: Function, regulation by insulin, and comparison with adiponutrin. *Diabetes* **55**, 148–157 (2006).
47. M. J. Kolar *et al*., Branched fatty acid esters of hydroxy fatty acids are preferred substrates of the MODY8 protein carboxyl ester lipase. *Biochemistry* **55**, 4636–4641 (2016).
48. W. H. Parsons *et al*., AIG1 and ADTRP are atypical integral membrane hydrolases that degrade bioactive FAHFAs. *Nat. Chem. Biol.* **12**, 367–372 (2016).
49. M. Erikci Ertunc *et al*., AIG1 and ADTRP are endogenous hydrolases of fatty acid esters of hydroxy fatty acids (FAHFAs) in mice. *J. Biol. Chem.* **295**, 5891–5905 (2020).
50. Y. Ma *et al*., An in silico MS/MS library for automatic annotation of novel FAHFA lipids. *J. Cheminform.* **7**, 53 (2015).
51. R. A. Moreau *et al*., The identification of mono-, di-, tri-, and tetragalactosyldiacylglycerols and their natural estolides in oat kernels. *Lipids* **43**, 533–548 (2008).
52. G. Haemmerle *et al*., Defective lipolysis and altered energy metabolism in mice lacking adipose triglyceride lipase. *Science* **312**, 734–737 (2006).
53. G. Haemmerle *et al*., Hormone-sensitive lipase deficiency in mice causes diglyceride accumulation in adipose tissue, muscle, and testis. *J. Biol. Chem.* **277**, 4806–4815 (2002).
54. H. Tsugawa *et al*., MS-DIAL: Data-independent MS/MS deconvolution for comprehensive metabolome analysis. *Nat. Methods* **12**, 523–526 (2015).

Free Radical Biology and Medicine 193 (2022) 787–794

Contents lists available at ScienceDirect

Free Radical Biology and Medicine

journal homepage: www.elsevier.com/locate/freeradbiomed

The role of peroxiredoxin 6 in biosynthesis of FAHFAs

Veronika Paluchova [a,b], Tomas Cajka [a], Thierry Durand [c], Claire Vigor [c], Chandra Dodia [d], Shampa Chatterjee [d], Aron B. Fisher [d], Ondrej Kuda [a,*]

[a] Institute of Physiology of the Czech Academy of Sciences, Videnska 1083, 14220, Prague 4, Czech Republic
[b] First Faculty of Medicine, Charles University, Katerinska 32, Prague, 12108, Czech Republic
[c] Institut des Biomolecules Max Mousseron, CNRS, ENSCM, University Montpellier, 34093, Montpellier, France
[d] Institute for Environmental Medicine of the Department of Physiology, University of Pennsylvania, 3620 Hamilton Walk, 1 John Morgan Building, USA

ARTICLE INFO

Keywords:
Peroxiredoxin
FAHFA
Lipid oxidation
Adipose tissue
Linoleic acid

ABSTRACT

Peroxiredoxin 6 (Prdx6) is a multifunctional enzyme, a unique member of the peroxiredoxin family, with an important role in antioxidant defense. Moreover, it has also been linked with the biosynthesis of anti-inflammatory and anti-diabetic lipids called fatty acid esters of hydroxy fatty acids (FAHFAs) and many diseases, including cancer, inflammation, and metabolic disorders. Here, we performed metabolomic and lipidomic profiling of subcutaneous adipose tissue from mouse models with genetically modified Prdx6. Deletion of Prdx6 resulted in reduced levels of FAHFAs containing 13-hydroxylinoleic acid (13-HLA). Mutation of Prdx6 C47S impaired the glutathione peroxidase activity and reduced FAHFA levels, while D140A mutation, responsible for phospholipase A2 activity, showed only minor effects. Targeted analysis of oxidized phospholipids and triacylglycerols in adipocytes highlighted a correlation between FAHFA and hydroxy fatty acid production by Prdx6 or glutathione peroxidase 4. FAHFA regioisomer abundance was negatively affected by the Prdx6 deletion, and this effect was more pronounced in longer and more unsaturated FAHFAs. The predicted protein model of Prdx6 suggested that the monomer-dimer transition mechanism might be involved in the repair of longer-chain peroxidized phospholipids bound over two monomers and that the role of Prdx6 in FAHFA synthesis might be restricted to branching positions further from carbon 9. In conclusion, our work linked the peroxidase activity of Prdx6 with the levels of FAHFAs in adipose tissue.

1. Introduction

During conditions of oxidative stress, reactive oxygen species readily attack phospholipids (PLs), which results in their peroxidation and consequently leads to disruption of the membrane lipid bilayer arrangement [1]. Peroxiredoxin 6 (Prdx6), also called 1-Cys peroxiredoxin (UniProt ID O08709, EC:1.11.1.27), exists as a dimer and it is the last identified mammalian enzyme of the peroxiredoxin family [2,3]. It has been assumed to play an important role in several health disorders, including acute lung injury and inflammation [4–6], type 1 diabetes [7], male fertility [8], and ferroptosis, which is highly related to cancer [9–11]. The mechanism of the catalytic activity is based on a single active cysteine, in contrast to a 2-cys mechanism common for most other members of the peroxiredoxin family. Moreover, Prdx6 uses glutathione (GSH) as a reducing agent for peroxidase activity rather than thioredoxin unlike most other peroxiredoxins [2,12]. It also plays a crucial role in antioxidant defense as it can bind to peroxidized phospholipids (PL-OOHs) and repair them through its enzymatic activities [12] (Fig. 1A). Three enzymatic activities of Prdx6 have been described: a) glutathione peroxidase activity, b) phospholipase A_2 (PLA_2) activity, and c) lysophosphatidylcholine acyltransferase (LPCAT) activity [13].

1.1. Peroxidase activity

Prdx6 can reduce peroxidized phospholipids to the corresponding alcohols (PL-OHs) through its peroxidase activity, which involves three main steps: peroxidation, resolution, and recycling [3,14,15]. The phospholipid hydroperoxidase GSH peroxidase (PHGPx) activity is dependent on catalytic cysteine (Cys) at position 47 (C47). Mutating cysteine to serine (C47S) abolishes the ability of Prdx6 to reduce hydroperoxides but does not affect PLA_2 activity [16,17] (Fig. 1B).

1.2. Phospholipase A2 activity

Prdx6 is the only member of the Prdx family that possesses PLA_2

* Corresponding author. Metabolism of Bioactive Lipids, Institute of Physiology of the Czech Academy of Sciences, Videnska 1083, 142 20, Prague, Czech Republic.
E-mail address: ondrej.kuda@fgu.cas.cz (O. Kuda).

https://doi.org/10.1016/j.freeradbiomed.2022.11.015
Received 11 October 2022; Accepted 9 November 2022
Available online 18 November 2022
0891-5849/

Abbreviations

FAHFA	fatty acid ester of hydroxy fatty acid
GSH	glutathione
GSSG	oxidized glutathione
Gpx4	glutathione peroxidase 4
HFA	hydroxy fatty acid
(H)PA	(hydroxy) palmitic acid
(H)PO	(hydroxy) palmitoleic acid
(H)SA	(hydroxy) stearic acid
(H)OA	(hydroxy) oleic acid
(H)LA	(hydroxy) linoleic acid
(H)AA	(hydroxy) arachidonic acid
(H)DHA	(hydroxy) docosahexaenoic acid
HODE	hydroxy octadecadienoic acid
HpETE	hydroperoxy eicosatetraenoic acid
HpFA	hydroperoxy fatty acid
HpODE	hydroperoxy octadecadienoic acid
HpSA	hydroperoxy stearic acid
IsoP	isoprostanes
LPC	lysophosphatidylcholine
LPCAT	lysophosphatidylcholine acyltransferase activity
PC	phosphatidylcholine
PE	phosphatidylethanolamine
PHGPx	phospholipid hydroperoxidase GSH peroxidase activity
PLOOH	phospholipid hydroperoxide
scWAT	subcutaneous adipose tissue
TAG	triacylglycerol

activity, which also participates in the phospholipid turnover by hydrolyzing an oxidized fatty acid (FA) bound at the *sn*-2 position, thus generating lysoPLs [3,18]. It is a calcium-independent activity and requires a catalytic triad serine at position 32 (S32), histidine at position 26 (H26), and aspartate at position 140 (D140). Since H26 and S32 are necessary for binding Prdx6 to the phospholipid, a mutation of aspartate to alanine (D140A) was found to be the most suitable one for abolishing the PLA_2 activity [19,20] (Fig. 1B).

1.3. Lysophosphatidylcholine acyltransferase activity

Lysophosphatidylcholine acyltransferase (LPCAT) activity is coupled to the PLA_2 activity and re-acylates the *sn*-2 position of lysoPLs with an FA-CoA. This activity generates remodeled phosphatidylcholine (PC), a lung surfactant [3,21].

1.4. Biosynthesis of FAHFA

A previous study linked Prdx6 with the biosynthesis of FAHFAs (fatty acid esters of hydroxy fatty acids) via the nuclear factor E2-related factor 2-related pathway, suggesting that PL-OH, generated during the process of peroxidized phospholipid repair, could serve as a source of the hydroxy fatty acid (HFA) in FAHFA structure [22]. FAHFAs represent a diverse group of lipids. The position of the ester bond between the HFA and the FA defines the regioisomer and biological activities, mainly anti-diabetic and anti-inflammatory [23,24]. A recent review summarizing current knowledge about their metabolism, biological effects, and synthesis has been published [25]. The adipose tissue depots are the main sources of FAHFAs and we focused on subcutaneous white adipose tissue (scWAT) [23,26].

Here, we present a study exploring the effects of specific enzymatic activities of Prdx6 on FAHFA levels. We hypothesize that the glutathione peroxidase activity is important for the generation of HFA for FAHFA synthesis. For this purpose, we used mouse models with genetically altered Prdx6: one knock-out model (Prdx6 null), two knock-in models (C47S, D140A), and wild type (WT) mice as a control group.

2. Materials and methods

2.1. Materials and reagents

LC–MS-grade solvents and mobile phase modifiers were purchased from VWR International (Czech Republic). FAHFA standards were from Cayman Europe (Tallinn, Estonia), and all other chemicals, including selective Glutathione peroxidase 4 (GPX4) inhibitor ML210, were ordered from Merck (Czech Republic) unless stated otherwise. GPX4 functions as a phospholipid hydroperoxidase to reduce specific phospholipid hydroperoxides (20:4- or 22:4-PE-OOH) to the corresponding phospholipid alcohol (PL-OH) [28]. MJ33 (1-hexadecyl-3-trifluoroethylglycero-*sn*-2-phosphomethanol) is an inhibitor of the PLA_2 activity of Prdx6 [29].

2.2. Animal studies

Mouse models (Prdx6 null, Prdx6 D140A, and C47S knock-in mice) used in this study were bred in animal care facilities of the Institute for Environmental Medicine, Department of Physiology, Perelman School of Medicine of the University of Pennsylvania. The generation and characterization of these mouse models has been described previously [13,19,22,30,31]. These mice have been fully backcrossed to the C57Bl/6J background to achieve >99.9% homozygosity. Wild type mice C57Bl/6J were obtained from the Jackson Laboratory (Bar Harbor, ME). We used male and female mice 10–13 weeks old in this study. Mice were maintained at 22 °C on a 12 h light/dark cycle while feeding a standard chow diet and having unlimited access to water. Mice were fasted for 24 h and then re-fed overnight with 15% sucrose in drinking water before scarification to stimulate de novo lipogenesis. All tissue samples (scWAT and the liver) were collected into cryovials, immediately frozen in liquid

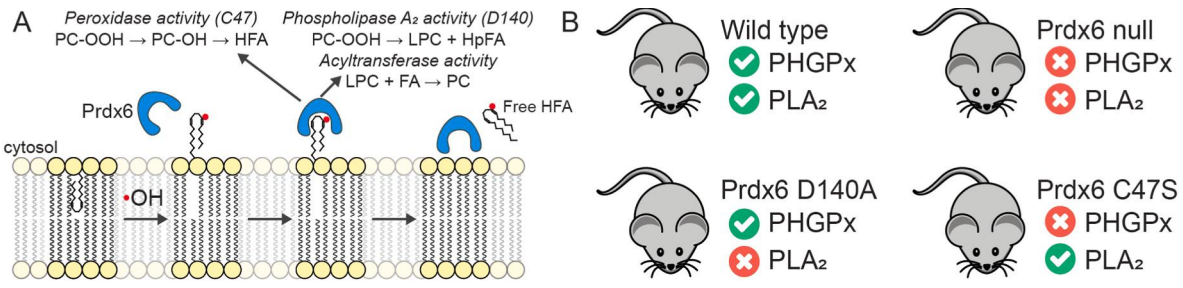

Fig. 1. Illustrative overview (A) Scheme of the function of Prdx6 and its enzymatic activities. Adapted from Manevich, 2009 [27]. (B) Overview of mouse models used in the study – wild type mice and mice with genetically altered Prdx6 (Prdx6 null, D140A, and C47S).

nitrogen, and stored at – 80 °C freezer. The University of Pennsylvania Animal Care and Use Committee (IACUC) approved all procedures involving mice.

2.3. Cell culture experiments

The 3T3-L1 cell line was differentiated according to the standard protocol [32]. Differentiated adipocytes were incubated in a DMEM complete medium (25 mmol/L glucose, 10% FBS, 850 nM insulin, penicillin/streptomycin) supplemented with a 40 μM mixture of poly-unsaturated FAs (OA, LA, AA, DHA; 10 μM each, complexed to BSA at the ratio 3:1) for 96 h to provide building blocks for more complex FAHFAs. For the last 24 h, inhibitors MJ33 and ML210 were added to the medium (10 μM) separately or combined.

2.4. Sample processing

Tissue samples were divided into aliquots in liquid nitrogen and three different extraction protocols and LC–MS analyzes were applied. Liquid nitrogen or ice was used during sample processing to prevent the degradation of oxidized PLs (PL-OOHs, PL-OHs). All samples were used for lipidomic profiling and targeted methods, including FAHFA analysis. However, only the liver samples were used to measure isoprostanes (IsoP) as oxidative stress biomarkers due to limited sample amounts. WAT IsoPs were measured in a previous study [22].

2.4.1. FAHFA analysis

FAHFAs extraction was based on liquid-liquid extraction followed by solid-phase extraction performed according to the published methods [23,33]. The final dried and purified extract was re-suspended in methanol and immediately analyzed using an UltiMate 3000 RSLC UHPLC system coupled to a QTRAP 5500/SelexION mass spectrometer (SCIEX, Darmstadt, Germany) with Triart C18 ExRS 250 × 2.0 mm; 3 μm column (YMC, Japan). FAHFAs were detected in negative electrospray ionization mode as before [32].

2.4.2. Metabolomic/lipidomic profiling and targeted analysis

Analytes were extracted using a mixture of cold water, methanol, and methyl *tert*-butyl ether (MTBE), as published before, with some modifications [34]. A Vanquish UHPLC System (Thermo Fisher Scientific, Bremen, Germany) coupled to a Q Exactive Plus mass spectrometer (Thermo Fisher Scientific, Bremen, Germany) together with LIMeX (Lipids, Metabolites, and eXposome compounds) LC–MS workflow was used for the untargeted analysis of complex lipids and polar metabolites (e.g. glutathione) [35]. In addition, MS/MS methods with inclusion lists were used to annotate oxidized phospholipids.

2.4.3. Isoprostane analysis

Extraction of IsoPs was based on a published protocol [36] with certain modifications for the liver (see Supplementary material). An Eksigent microLC 200 Plus system coupled to a QTRAP 5500 (Sciex, Darmstadt, Germany) was used to analyze IsoPs [37].

2.5. Prdx6 protein model

ColabFold pipeline v1.3 including MMseqs2 with AlphaFold2-multimer engine (databases UniRef30 2022_02 and PDB/PDB70 220313) was used to predict human Prdx6 dimer model (Uniprot # P30041, reduced form) [38]. Original crystal structure of human Prdx6 (PDB:5B6M) expressed in *E. coli* was solved using Prx6 from *Arenicola marina* at 2.5–2.9 Å resolution [39]. MatchMaker in Chimera was used to compare the dimer model created by the machine learning approach and 5B6M. RMSD between 221 pruned atom pairs was 0.519 Å. Chimera 1.16, ChimeraX v1.4 and VinaDock v1.2 were used to dock the oxidized ligands to the dimer model: a collection of phosphatidylcholines (PC) containig palmitic acid at *sn*-1 position and peroxidized stearic acid (HpSA) at *sn*-2 position (with –OOH position 5-, 7-, 8-, 9-, 10-, 11-, and 12- from alpha carbon), and PC 16:0/13-HpODE, PC 16:0/9-HpODE, PC 16:0/15-HpETE known Prdx6 ligands [17,40]. Twenty poses for each ligand were calculated. Structure PDB:5B6M was used only for the known ligands as a control. The PDB dimer model is included in SI material (ZIP file).

2.6. Data processing and statistics

LC-MS data from the LIMeX workflow were processed using MS-DIAL ver. 4.70 [41]. Metabolites were annotated using in-house retention time–*m/z* library and using MS/MS libraries available from public sources (MassBank, MoNA, LipidBlast). Raw data were filtered using blank samples, serial dilution samples, and quality control (QC) pool samples with relative standard deviation (RSD) $< 30\%$, and then normalized using the LOESS approach by means of QC pool samples for each matrix regularly injected between 10 actual samples. LC–MS/MS data from targeted analysis of FAHFAs and IsoPs were processed using MultiQuant software (SCIEX). Data were further processed via MetaboAnalyst [42] and GraphPad Prism to compare groups (ANOVA, Dunnett's multiple comparison test vs Control group, $p < 0.05$ was considered significant). Over-representation analysis (lipid class enrichment) was calculated using Fisher's test and LipidMaps classification system as before [43].

3. Results

3.1. Mild effect of Prdx6 deletion on scWAT lipidome

We explored the role of Prdx6 in scWAT lipid metabolism. We used a mouse model of *Prdx6* deletion (global knockout), *Prdx6* C47S, and D140A knock-in mice to target the particular enzymatic activities. Deletion of *Prdx6* resulted in mild changes in the scWAT lipidome and we did not find any specific pattern in the downregulated lipids but enrichment in TAG class and more specifically oxidized TAGs (Fig. 2A and D). These oxidized TAGs contained oxidized FA 18:2. Mice harboring the C47S mutation showed several downregulated and upregulated lipid species. The downregulated cluster was enriched in short chain TAG species containing saturated FAs with 8–14 carbons. The upregulated lipid cluster was characterized by ether phosphatidylenthanolamines (PE) containing mainly O-20:1 chains and steroid sulfate conjugates (Fig. 2B). The D140A mutation showed the weakest effect compared to wild type mice and only a few steroid sulfate conjugates were upregulated (Fig. 2C). Based on the original hypothesis, we focused only on the lipids related to oxidation and FAHFA synthesis.

3.2. Oxidative stress markers were unaltered by deletion of Prdx6

Next, we checked the markers of oxidative stress. Levels of oxidized glutathione in scWAT were similar between all genotypes and only the reduced glutathione was increased in C47S mutation (Fig. 2E). The marker of susceptibility to ferroptosis (PE O-16:1/20:4) was not altered in scWAT (Fig. 2F), levels of TBARS and F2-isoprostanes were unaltered [22]. Also the levels of IsoP did not suggest oxidative stress condition in the liver (Fig. S1). Therefore, we concluded that other general antioxidant mechanisms compensated for the missing Prdx6 enzymatic activities.

3.3. Prdx6 Cys47 is important for FAHFA biosynthesis

TAGs downregulated in Prdx6 null mice contained oxidized linoleic acid (FA 18:2;O). Therefore, we explored the levels of highly abundant FAHFAs containing 13-hydroxylinoleic acid (HLA or 18:2;O chain). The scheme in Fig. 3A illustrates the putative metabolic pathway of FAHFA synthesis. Oxidized membrane phospholipids are a source of hydroxylated FAs which are then incorporated into TAGs or serve as lone

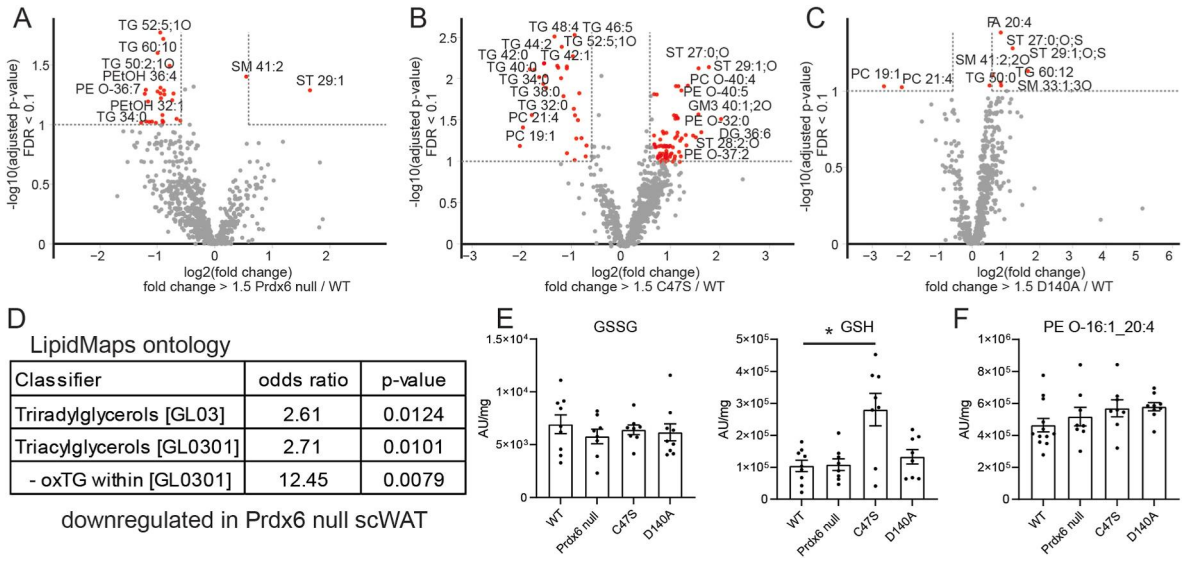

Fig. 2. scWAT lipidome alterations. (A) Volcano plot comparing Prdx6 null mice and wild type mice (WT). Metabolites with fold change >1.5 and FDR <0.1 were highlighted in red. (B) Volcano plot for C47S and WT. (C) Volcano plot for D140A and WT. (D) Over-representation analysis of the downregulated lipid cluster in Prdx6 null scWAT. (E) Levels of oxidized and reduced glutathione in scWAT. (F) Levels of PE O-16:1/20:4 in scWAT. Data are mean ± S.E., $n = 8–9$. * Significantly different at $p < 0.05$, ANOVA, Dunnett's multiple comparison test. (For interpretation of the references to colour in this figure legend, the reader is referred to the Web version of this article.)

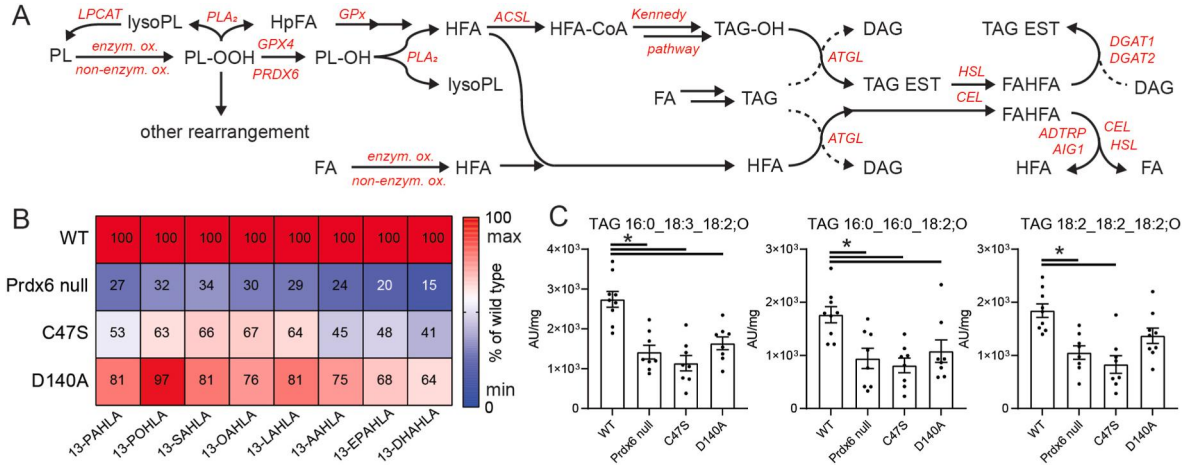

Fig. 3. FAHLA synthesis in scWAT. (A) Proposed scheme of FAHFA synthesis. ADTRP, Androgen-dependent TFPI-regulating protein; AIG1, Androgen-induced protein 1; ATGL, adipose triglyceride lipase; CEL, carboxyl ester lipase; DAG, diacylglycerol; DGAT, diacylglycerol acyltransferase; FA, fatty acid; GPx, peroxidase activity; GPX4, glutathione peroxidase 4; HFA, hydroxy fatty acid, e.g. 13-HLA; HpFA, hydroperoxy FA; HSL, hormone-sensitive lipase; LPCAT, acyltransferase activity; lysoPL, lysophospholipid; PLA2, phospholipase A2 activity; PL, phospholipid, e.g. PC; PL-OH, hydroxylated PC; PL-OOH, peroxidated PL; TAG, triacylglycerol; TAG EST, triacylglycerol estolide (TG-FAHFA). (B) Levels of FAHLA (containing 13-HLA) in scWAT expressed as percentage of wild type (WT) group. (C) Levels of TAGs containing hydroxylated 18:2 (HLA in general) in scWAT. Data are mean ± S.E., $n = 8–9$, * significantly different at $p < 0.05$, ANOVA, Dunnett's multiple comparison test.

precursors. The ATGL biosynthetic transacylase activity combines a TAG and HFA or two TAGs and creates a free FAHFA or a TAG estolide (TG-FAHFA), respectively. Free FAHFAs are liberated from TAG estolides by hormone-sensitive lipase or carboxyl ester lipase or further degraded by specific hydrolases [26,43,44] (Fig. 3A). Levels of 13-HLA-containing FAHFAs were significantly downregulated in Prdx6 null scWAT and this effect was also observed in C47S mice. The lack of PLA_2 activity in D140A mice had the weakest effect on FAHFA levels. Interestingly, the longer and more unsaturated FAHFAs were affected more than the shorter and saturated species (Fig. 3B). The untargeted lipidomic analysis also showed several TAG species containing HLA, which could be the intermediates in FAHFA synthesis (Figs. 3C and 2D). Their profiles were similar to the FAHFA profiles.

The untargeted lipidomic profiling cannot capture the peroxidized phospholipid species (putative intermediates in HFA synthesis). Therefore, we performed the targeted analysis using 3T3-L1 adipocytes exposed to ML210 (inhibitor of phospholipid peroxidase activity [28]) and or MJ33 (inhibitor of PLA_2 activity of Prdx6 [29]). Although the specific peroxidase inhibitor of Prdx6 is not available, this situation mimics impaired PL-OOH repair. We selected the PC 16:0/18:2 as the tracer molecule. Peroxidized PC 16:0/18:2;O2 and hydroxylated PC 16:0/18:2;O showed profiles that resembled the pattern observed in mouse scWAT (Fig. 4A). Levels of 13-HLA were downregulated only by the combination of both inhibitors (Fig. 4B), while the levels of HLA-containing FAHFAs were similar to the animal profiles (Figs. 4C and 3). The animal and in vitro data suggest that Prdx6 participates in

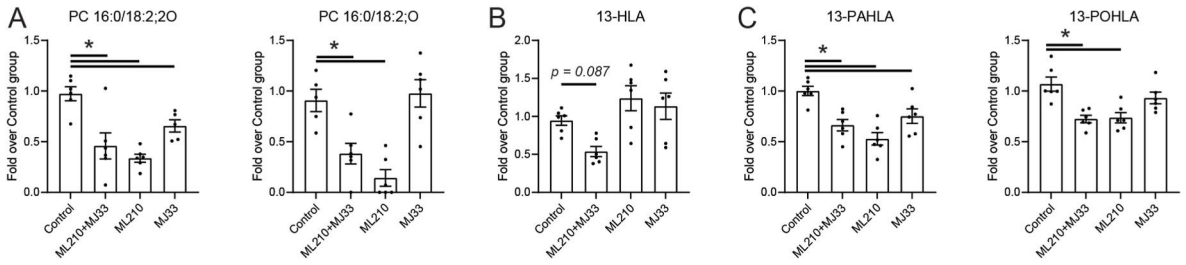

Fig. 4. Targeted analysis of 3T3-L1 cells. (A) Levels of peroxidized and hydroxylated PC 16:0/18:2. (B) Levels of 13-HLA (FA 18:2;O). (C) FAHFA levels. Data are mean ± S.E., $n = 5$-6, * significantly different at $p < 0.05$, ANOVA & Dunnett's multiple comparison test.

FAHFA biosynthesis and that peroxidase activity, either of Prdx6 or Gpx4 or both, is involved in this process.

3.4. *Prdx6 deletion affects FAHFA regioisomer abundance*

To explore Prdx6 regioselectivity and substrate specificity affecting potential FAHFA precursors, we explored FAHFAs with different branching positions in wild type and Prdx6 null groups (Fig. 5). Although the HFAs might come from Prdx6-independent pathways and the FA availability could be affected by many factors, we observed a trend in FAHFA levels: the further the hydroxyl group from α carbon atom of HFA, the more significant the effect of Prdx6 deletion on FAHFA levels was observed (Fig. 5A and B). This trend was more pronounced when we pooled relative FAHFA levels according to the position from the HFA α carbon (Fig. 5B). No such clear trend was seen in C47S and D140A groups.

3.5. *Prdx6 protein model supports phospholipid binding over two monomers*

Prdx6′s activity is a conformation-driven process involving monomer–dimer transition [45,46]. To visualize the process and the key amino acid residues, we used AlphaFold2-multimer algorithm implemented as ColabFold pipeline to predict Prdx6 dimer structure [38]. Next, we used ChimeraX to dock an oxidized PC ligand (PC 16:0/13-HpODE) and explore the putative active sites [40] (Fig. 6A). The prediction showed that two monomers created a deep valley at their interface to fit the oxidized 13-HpODE chain close to the peroxidatic Cys47 residue (Fig. 6A and B). Simultaneously, the glycerol backbone and the ester bonds were positioned close to the Asp140 residue, important for the PLA_2 activity, on the flat surface of the protein [20]. While the peroxidase activity was localized within the monomer B, the PLA_2 activity residues were localized within the A chain (Fig. 6C). This confirms the monomer ↔ dimer transition mechanism and the proposed phospholipid binding over two monomers [39].

Next, we performed docking of other PC regioisomers where the peroxidized carbon is closer or further to the α carbon. The ligands took either a pose with FA 16:0 in the valley close to Cys47 or a pose with the peroxidized chain close to Cys47. Therefore, it was not possible to clearly evaluate root-mean-square deviation (RMSD), which is calculated relative to the first pose. The RMSD for the poses with peroxidized chain close to Cys47 were between 0.8 and 3.1 Å (lower bound) and 1.1–7.8 Å (upper bound), and the scores from −4.9 to −7.3 kcal/mol. To evaluate the effect of regioisomers, we recorded the distance between the second oxygen within –OOH group and the sulphur atom in Cys47 residue. The poses with the shortest distance were plotted against the regioisomer position (Fig. 6D). Red dots represent the PC ligands with HpSA chains and the blue dots known Prdx6 substrates (Fig. 6E). Green dots represent the known substrates docked to Prdx6 (PDB:5B6M) as control. Unsaturated ligands fitted into better poses than HpSA-containing ligands and the –OOH groups close to the α carbon were inaccessible for the Cys47. The trend partially explained the effect on regioisomer branching position (Fig. 5) when the peroxidation at carbon atoms further from the α carbon could be more easily processed by Prdx6 peroxidase activity. However, the acyl chain (un)saturation, free or PC-bound chain, type of oxidation, etc. might further modify the substrate specificity at positions higher than 9, thus affect the final FAHFA levels via multiple (parallel) ways.

4. Discussion

Elucidation of FAHFA metabolism has been one of the main goals since their discovery in 2014 [23]. The synthesis of FAHFAs, FAHFA storage, degradation, and metabolic regulations [26,44,47,48] have been described and summarized in a review [49]. However, the mechanism of HFA synthesis has not been fully elucidated yet. Here, we report the role of the glutathione peroxidase activity of Prdx6 in the biosynthesis of FAHFA.

Lipidomic profiling of mouse models showed that whole body Prdx6 knockout had only a mild impact on the general lipidome of scWAT. We did not observe any massive increase in oxidized lipids, but the targeted methods highlighted that levels of specific oxidized lipids were lower in Prdx6 null mice. We speculate that the antioxidant defense system for lipids, mainly Gpx4, compensated for the loss of Prdx6 in scWAT and that only Prdx6-specific role was dysregulated. This is supported by the unaltered oxidative stress and ferroptosis susceptibility markers in scWAT.

The knock-in model C47S showed more dysregulated scWAT lipidome than the Prdx6 knockout and the D140A model was nearly identical to wild type mice. The physical presence of mutated Prdx6 protein might participate in the signaling cascades (phosphorylation at T177 by MAPK results in 11-fold increase in PLA_2 activity, translocation to cellular compartments, etc. [21,50]), the PLA_2 activity might remove HpFA even in the absence of PHGPx activity, or the effect of the

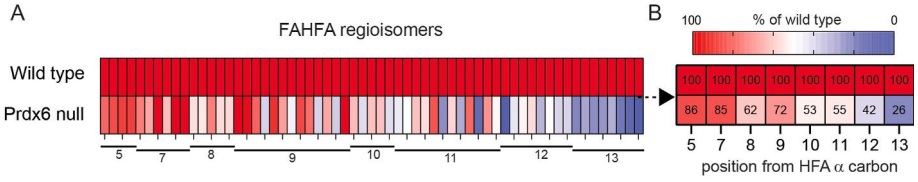

Fig. 5. FAHFA regioisomers in scWAT. (A) Levels of FAHFA regioisomers expressed as percentage of wild type group and sorted according to the position from HFA α carbon. Data are means, relative to wild type, $n = 8$–9. (B) Heatmap of average values per regioisomers, $n = 4$–13 (number of regioisomers).

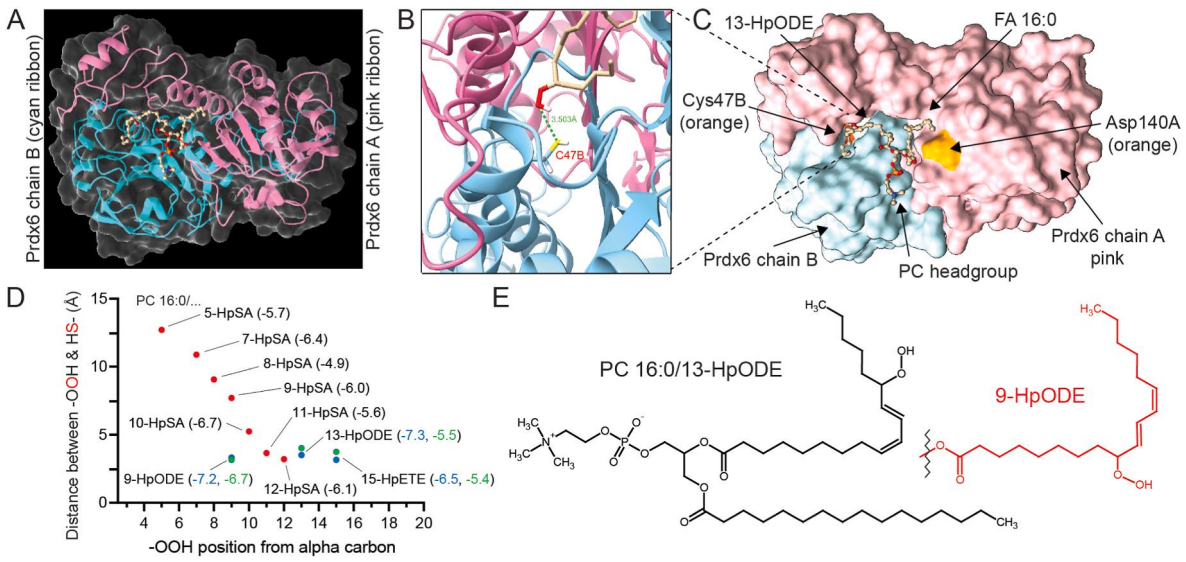

Fig. 6. Model of Prdx6 dimer. (A) Chain A in pink and chain B in cyan within the transparent protein surface. Ligand PC 16:0/18:2;O2 is shown as balls & sticks model. (B) Detail of the active site within chain B. The distance between oxygen in –OOH in 13-HpODE and sulphur in thiol group of C47B is approx. 3.5 Å. (C) The annotated surface structure of the Prdx6 dimer. (D) Minimal modelled distance between the –OOH group of the ligand and Cys47 according to the position from α carbon of HpFA. Values in brackets are AutoDock Vina scores (kcal/mol). Red dots, PC 16:0/x-HpSA ligands; blue dots, known Prdx6 ligands on modelled dimer. Green dots, known ligands docked to PDB:5B6M. (E) Structures of two known substrates of Prdx6 [17]. (For interpretation of the references to colour in this figure legend, the reader is referred to the Web version of this article.)

mutation could be more pronounced in the tissues that are primarily under oxidative stress, e.g., lungs [30].

The cluster of downregulated lipids in Prdx6 null mice highlighted altered metabolism of FA 18:2;O (HLA). We explored FAHFAs containing HLA, specifically the most abundant 13-HLA, and found significantly lower levels in Prdx6 null mice. C47S mouse model confirmed that the peroxidase activity is linked to FAHFA levels while the PLA_2 is dispensable. Next, we explored the putative metabolic intermediates in the synthesis of FA-HLAs, the hydroxy-TAGs containing 13-HLA, and found the same concentration patterns. In general, the hydroxy-TAGs should be used by ATGL to generate TAG estolides [26,44]. However, this neutral lipid remodeling process creates a huge number of isomeric structures (TAG *sn* position, FAHFA regioisomers) and acyl combinations (FAHFA and two FAs) [44]. There is currently no analytical approach for this challenge and we detected only pooled signals for TAG estolide families that are approximately 100-times more concentrated than the free FAHFAs [48]. Therefore, we could not track the fate of hydroxy-TAGs any further.

To explore the other branch of FAHFA synthesis pathway, we focused on oxidized PCs, the preferred substrates of Prdx6 [17,51]. We used a cell culture model of adipocytes to precisely control the extraction procedure of oxidized lipids (freezing in liquid nitrogen) and a combination of inhibitors to simulate impaired PL-OOH repair. The levels of peroxidized PC 16:0/18:2;O2, hydroxylated PC 16:0/18:2;O, and 13-HLA-containing FAHFA showed similar profiles to FAHFAs we previously detected in mice. This suggests a mechanistic link between Prdx6 peroxidase activity and FAHFA levels, but it also suggests that Gpx4, primary target of ML210 inhibitor, might be involved in FAHFA precursor synthesis [28]. The suppression of peroxidase activities did not result in increased levels of lipid hydroperoxides targeted by our analysis. Using the current methodology, we were not able to measure all possible combinations of oxidized lipids (epilipidome signature) within the samples [52]. We can speculate that in oxidative stress condition, e.g. obesity and type 2 diabetes, the (per)oxidized phospholipid species containing oxidized octadecanoids decrease while those containing oxidized eicosanoids increase as was shown in human plasma [52]. Oxidative stress can also initiate ferroptosis, and the oxidized phospholipid remodeling could change the balance between octadecanoid and eicosanoid/docosanoid species, as was recently reported for ether lipids [53].

We could speculate that the antioxidant system in adipose tissue compensated for the loss of Prdx6 action and degraded the oxidized lipids [54], or converted the oxidized lipids to species we did not measure, while the alternative pathway storing oxidized acyls within lipid droplets was scaled down [55]. The adipose tissue could store the oxidized lipids in lipid droplets in the form of oxidized TAGs or lipid droplet surface phospholipid monolayer, providing the substrates for TAG estolide synthesis. Inhibition of this process could limit the availability of hydroxy-TAGs and further affect FAHFA levels. The inability to produce FAHFAs due to alterations in Prdx6 might compromise the anti-diabetic and anti-inflammatory effects of FAHFAs, the link between glycemic and lipogenic metabolism, and lead to obesity-related metabolic disorders such as liver diseases and diabetes [56]. However, the effect might be restricted to branching positions further from 9 and preserve the anti-diabetic potential of FAHFAs with lower branching positions [24].

The trend suggesting a stronger negative effect of Prdx6 deletion on FAHFAs with the branching carbon farther from α carbon indicated a preference of Prdx6 for HpFAs with –OOH group farther from the α carbon. This trend was not observed in C47S group in which the FAHFA profile was highly dysregulated. While the PHGPx activity was absent in C47S, the PLA_2 activity could compensate and remove peroxidized chains to be reduced by other enzymatic or non-enzymatic ways later [30].

The protein model of Prdx6 dimer and Fig. 5 heatmaps suggested that the peroxidase active residue Cys47 can repair oxidized carbon atoms from position nine further to the tail of the PC acyl chain, preferentially the HpODE species. The dimer also showed that the PHGPx and PLA_2 activities were localized within the A and B monomers, respectively. The substrate binding might rely on the presence of all critical residues within the dimer and affect the prevailing product – either free HpFA by PLA_2 or PC-HFA/HFA by PHGPx activity [13]. Furthermore, the specific distribution of acyl composition in PCs and TAGs, adipose tissue depot, substrate preference of ATGL, and feeding status might affect the biosynthesis of FAHFAs within the lipid remodeling cycle [22,26,33,44,47].

In conclusion, our work linked the peroxidase activity of Prdx6 with the levels of FAHFAs in adipose tissue. However, the fate of oxidized acyl chains within the lipid remodeling cycle, specificity of the enzymatic machinery, and the co-regulation with the antioxidant defense system remains unknown for future research.

Declaration of competing interest

The authors declare that there are no competing interests associated with the manuscript.

Funding

This work was supported by a grant from the Ministry of Education, Youth and Sports of the Czech Republic [LTAUSA18104] and by a grant from the Czech Academy of Sciences [Lumina quaeruntur LQ200111901].

Acknowledgment

Conceptualization: A.B.F. and O.K.; Data curation: V.P.; Formal analysis: V.P., T.C. and O.K.; Funding acquisition: T.D., A.B.F. and O.K.; Investigation: V.P., C.V., C.D., S.C., A.B.F. and O.K.; Methodology: V.P., T.D., C.V., C.D. and S.C.; Project administration: V.P., A.B.F. and O.K.; Resources: C.D., S.C., A.B.F. and O.K.; Software: O.K.; Supervision: A.B.F. and O.K.; Validation: T.C. and O.K.; Visualization: V.P. and O.K.; Writing – original draft: V.P., A.B.F. and O.K.; Writing - review & editing: V.P., T.C., T.D., C.V., C.D., S.C., A.B.F. and O.K.;

The authors would like to acknowledge the Metabolomics Core Facility at the Institute of Physiology of the Czech Academy of Sciences for lipidomics profiling and Camille Oger, Jean-Marie Galano and Bingqing Zhou for their help with IsoP analysis.

Appendix A. Supplementary data

Supplementary data to this article can be found online at https://doi.org/10.1016/j.freeradbiomed.2022.11.015.

References

[1] E. Birben, U.M. Sahiner, C. Sackesen, S. Erzurum, O. Kalayci, Oxidative stress and antioxidant defense, World Allergy Organ J 5 (1) (2012) 9–19, https://doi.org/10.1097/WOX.0b013e3182439613.

[2] S.W. Kang, I.C. Baines, S.G. Rhee, Characterization of a mammalian peroxiredoxin that contains one conserved cysteine, J. Biol. Chem. 273 (11) (1998) 6303–6311, https://doi.org/10.1074/jbc.273.11.6303.

[3] S. Zhou, E.M. Sorokina, S. Harper, H. Li, L. Ralat, C. Dodia, D.W. Speicher, S. I. Feinstein, A.B. Fisher, Peroxiredoxin 6 homodimerization and heterodimerization with glutathione S-transferase pi are required for its peroxidase but not phospholipase A2 activity, Free Radic. Biol. Med. 94 (2016) 145–156, https://doi.org/10.1016/j.freeradbiomed.2016.02.012.

[4] A.B. Fisher, C. Dodia, J.Q. Tao, S.I. Feinstein, S. Chatterjee, Inhibition of peroxiredoxin 6 PLA2 activity decreases oxidative stress and the severity of acute lung injury in the mouse cecal ligation and puncture model, Antioxidants 10 (11) (2021), https://doi.org/10.3390/antiox10111676.

[5] D.X. Li, W. Chen, Y.L. Jiang, J.Q. Ni, L. Lu, Antioxidant protein peroxiredoxin 6 suppresses the vascular inflammation, oxidative stress and endothelial dysfunction in angiotensin II-induced endotheliocyte, Gen. Physiol. Biophys. 39 (6) (2020) 545–555, https://doi.org/10.4149/gpb_2020029.

[6] X. Wang, X. An, X. Wang, X. Hu, J. Bi, L. Tong, D. Yang, Y. Song, C. Bai, Peroxiredoxin 6 knockout aggravates cecal ligation and puncture-induced acute lung injury, Int. Immunopharm. 68 (2019) 252–258, https://doi.org/10.1016/j.intimp.2018.12.053.

[7] E.G. Novoselova, O.V. Glushkova, S.M. Lunin, M.O. Khrenov, S.B. Parfenyuk, T. V. Novoselova, M.G. Sharapov, A.E. Gordeeva, V.I. Novoselov, E.E. Fesenko, Thymulin and peroxiredoxin 6 have protective effects against streptozotocin-induced type 1 diabetes in mice, Int. J. Immunopathol. Pharmacol. 35 (2021), 20587384211005645, https://doi.org/10.1177/20587384211005645.

[8] E. Bumanlag, E. Scarlata, C. O'Flaherty, Peroxiredoxin 6 peroxidase and Ca(2+)-independent phospholipase A2 activities are essential to support male-mouse fertility, Antioxidants 11 (2) (2022), https://doi.org/10.3390/antiox11020226.

[9] B. Lu, X.B. Chen, Y.C. Hong, H. Zhu, Q.J. He, B. Yang, M.D. Ying, J. Cao, Identification of PRDX6 as a regulator of ferroptosis, Acta Pharmacol. Sin. 40 (10) (2019) 1334–1342, https://doi.org/10.1038/s41401-019-0233-9.

[10] J. Xu, Q. Su, M. Gao, Q. Liang, J. Li, X. Chen, Differential expression and effects of peroxiredoxin-6 on drug resistance and cancer stem cell-like properties in non-small cell lung cancer, OncoTargets Ther. 12 (2019) 10477–10486, https://doi.org/10.2147/OTT.S211125.

[11] X. Xu, D. Lu, R. Zhuang, X. Wei, H. Xie, C. Wang, Y. Zhu, J. Wang, C. Zhong, X. Zhang, Q. Wei, Z. He, L. Zhou, S. Zheng, The phospholipase A2 activity of peroxiredoxin 6 promotes cancer cell death induced by tumor necrosis factor alpha in hepatocellular carcinoma, Mol. Carcinog. 55 (9) (2016) 1299–1308, https://doi.org/10.1002/mc.22371.

[12] A.B. Fisher, Peroxiredoxin 6 in the repair of peroxidized cell membranes and cell signaling, Arch. Biochem. Biophys. 617 (2017) 68–83, https://doi.org/10.1016/j.abb.2016.12.003.

[13] S.I. Feinstein, Mouse models of genetically altered peroxiredoxin 6, Antioxidants 8 (4) (2019), https://doi.org/10.3390/antiox8040077.

[14] A. Hall, K. Nelson, L.B. Poole, P.A. Karplus, Structure-based insights into the catalytic power and conformational dexterity of peroxiredoxins, Antioxidants Redox Signal. 15 (3) (2011) 795–815, https://doi.org/10.1089/ars.2010.3624.

[15] L.A. Ralat, Y. Manevich, A.B. Fisher, R.F. Colman, Direct evidence for the formation of a complex between 1-cysteine peroxiredoxin and glutathione S-transferase pi with activity changes in both enzymes, Biochemistry 45 (2) (2006) 360–372, https://doi.org/10.1021/bi0520737.

[16] J.W. Chen, C. Dodia, S.I. Feinstein, M.K. Jain, A.B. Fisher, 1-Cys peroxiredoxin, a bifunctional enzyme with glutathione peroxidase and phospholipase A2 activities, J. Biol. Chem. 275 (37) (2000) 28421–28427, https://doi.org/10.1074/jbc.M005073200.

[17] A.B. Fisher, C. Dodia, Y. Manevich, J.W. Chen, S.I. Feinstein, Phospholipid hydroperoxides are substrates for non-selenium glutathione peroxidase, J. Biol. Chem. 274 (30) (1999) 21326–21334, https://doi.org/10.1074/jbc.274.30.21326.

[18] A.B. Fisher, C. Dodia, S.I. Feinstein, Y.S. Ho, Altered lung phospholipid metabolism in mice with targeted deletion of lysosomal-type phospholipase A2, J. Lipid Res. 46 (6) (2005) 1248–1256, https://doi.org/10.1194/jlr.M400499-JLR200.

[19] H. Li, B. Benipal, S. Zhou, C. Dodia, S. Chatterjee, J.Q. Tao, E.M. Sorokina, T. Raabe, S.I. Feinstein, A.B. Fisher, Critical role of peroxiredoxin 6 in the repair of peroxidized cell membranes following oxidative stress, Free Radic. Biol. Med. 87 (2015) 356–365, https://doi.org/10.1016/j.freeradbiomed.2015.06.009.

[20] Y. Manevich, K.S. Reddy, T. Shuvaeva, S.I. Feinstein, A.B. Fisher, Structure and phospholipase function of peroxiredoxin 6: identification of the catalytic triad and its role in phospholipid substrate binding, J. Lipid Res. 48 (10) (2007) 2306–2318, https://doi.org/10.1194/jlr.M700299-JLR200.

[21] A.B. Fisher, C. Dodia, E.M. Sorokina, H. Li, S. Zhou, T. Raabe, S.I. Feinstein, A novel lysophosphatidylcholine acyl transferase activity is expressed by peroxiredoxin 6, J. Lipid Res. 57 (4) (2016) 587–596, https://doi.org/10.1194/jlr.M064758.

[22] O. Kuda, M. Brezinova, J. Silhavy, V. Landa, V. Zidek, C. Dodia, F. Kreuchwig, M. Vrbacky, L. Balas, T. Durand, N. Hubner, A.B. Fisher, J. Kopecky, M. Pravenec, Nrf2-Mediated antioxidant defense and peroxiredoxin 6 are linked to biosynthesis of palmitic acid ester of 9-hydroxystearic acid, Diabetes 67 (6) (2018) 1190–1199, https://doi.org/10.2337/db17-1087.

[23] M.M. Yore, I. Syed, P.M. Moraes-Vieira, T. Zhang, M.A. Herman, E.A. Homan, R. T. Patel, J. Lee, S. Chen, O.D. Peroni, A.S. Dhaneshwar, A. Hammarstedt, U. Smith, T.E. McGraw, A. Saghatelian, B.B. Kahn, Discovery of a class of endogenous mammalian lipids with anti-diabetic and anti-inflammatory effects, Cell 159 (2) (2014) 318–332, https://doi.org/10.1016/j.cell.2014.09.035.

[24] P. Aryal, I. Syed, J. Lee, R. Patel, A.T. Nelson, D. Siegel, A. Saghatelian, B.B. Kahn, Distinct biological activities of isomers from different families of branched fatty acid esters of hydroxy fatty acids (FAHFAs), J. Lipid Res. (2021), 100108, https://doi.org/10.1016/j.jlr.2021.100108.

[25] K. Brejchova, L. Balas, V. Paluchova, M. Brezinova, T. Durand, O. Kuda, Understanding FAHFAs: from structure to metabolic regulation, Prog. Lipid Res. 79 (2020), 101053, https://doi.org/10.1016/j.plipres.2020.101053.

[26] R. Patel, A. Santoro, P. Hofer, D. Tan, M. Oberer, A.T. Nelson, S. Konduri, D. Siegel, R. Zechner, A. Saghatelian, B.B. Kahn, ATGL is a biosynthetic enzyme for fatty acid esters of hydroxy fatty acids, Nature 606 (7916) (2022) 968–975, https://doi.org/10.1038/s41586-022-04787-x.

[27] Y. Manevich, T. Shuvaeva, C. Dodia, A. Kazi, S.I. Feinstein, A.B. Fisher, Binding of peroxiredoxin 6 to substrate determines differential phospholipid hydroperoxide peroxidase and phospholipase A(2) activities, Arch. Biochem. Biophys. 485 (2) (2009) 139–149, https://doi.org/10.1016/j.abb.2009.02.008.

[28] V.E. Kagan, G. Mao, F. Qu, J.P. Angeli, S. Doll, C.S. Croix, H.H. Dar, B. Liu, V. A. Tyurin, V.B. Ritov, A.A. Kapralov, A.A. Amoscato, J. Jiang, T. Anthonymuthu, D. Mohammadyani, Q. Yang, B. Proneth, J. Klein-Seetharaman, S. Watkins, I. Bahar, J. Greenberger, R.K. Mallampalli, B.R. Stockwell, Y.Y. Tyurina, M. Conrad, H. Bayir, Oxidized arachidonic and adrenic PEs navigate cells to ferroptosis, Nat. Chem. Biol. 13 (1) (2017) 81–90, https://doi.org/10.1038/nchembio.2238.

[29] A.B. Fisher, C. Dodia, A. Chander, M. Jain, A competitive inhibitor of phospholipase A2 decreases surfactant phosphatidylcholine degradation by the rat lung, Biochem. J. 288 (Pt 2) (1992) 407–411, https://doi.org/10.1042/bj2880407.

[30] Y.C. Lien, S.I. Feinstein, C. Dodia, A.B. Fisher, The roles of peroxidase and phospholipase A2 activities of peroxiredoxin 6 in protecting pulmonary microvascular endothelial cells against peroxidative stress, Antioxidants Redox Signal. 16 (5) (2012) 440–451, https://doi.org/10.1089/ars.2011.3950.

[31] J.P. Vazquez-Medina, J.Q. Tao, P. Patel, R. Bannitz-Fernandes, C. Dodia, E. M. Sorokina, S.I. Feinstein, S. Chatterjee, A.B. Fisher, Genetic inactivation of the phospholipase A2 activity of peroxiredoxin 6 in mice protects against LPS-induced

acute lung injury, Am. J. Physiol. Lung Cell Mol. Physiol. 316 (4) (2019) L656–L668, https://doi.org/10.1152/ajplung.00344.2018.
[32] O. Kuda, M. Brezinova, M. Rombaldova, B. Slavikova, M. Posta, P. Beier, P. Janovska, J. Veleba, J. Kopecky Jr., E. Kudova, T. Pelikanova, J. Kopecky, Docosahexaenoic acid-derived fatty acid esters of hydroxy fatty acids (FAHFAs) with anti-inflammatory properties, Diabetes 65 (9) (2016) 2580–2590, https://doi.org/10.2337/db16-0385.
[33] V. Paluchova, A. Vik, T. Cajka, M. Brezinova, K. Brejchova, V. Bugajev, L. Draberova, P. Draber, J. Buresova, P. Kroupova, K. Bardova, M. Rossmeisl, J. Kopecky, T.V. Hansen, O. Kuda, Triacylglycerol-rich oils of marine origin are optimal nutrients for induction of polyunsaturated docosahexaenoic acid ester of hydroxy linoleic acid (13-DHAHLA) with anti-inflammatory properties in mice, Mol. Nutr. Food Res. 64 (11) (2020), e1901238, https://doi.org/10.1002/mnfr.201901238.
[34] M. Brezinova, T. Cajka, M. Oseeva, M. Stepan, K. Dadova, L. Rossmeislova, M. Matous, M. Siklova, M. Rossmeisl, O. Kuda, Exercise training induces insulin-sensitizing PAHSAs in adipose tissue of elderly women, BBA MCBL 1865 (2) (2020), 158576, https://doi.org/10.1016/j.bbalip.2019.158576.
[35] M. Lopes, K. Brejchova, M. Riecan, M. Novakova, M. Rossmeisl, T. Cajka, O. Kuda, Metabolomics atlas of oral 13C-glucose tolerance test in mice, Cell Rep. 37 (2) (2021), 109833, https://doi.org/10.1016/j.celrep.2021.109833.
[36] A. Dupuy, P. Le Faouder, C. Vigor, C. Oger, J.M. Galano, C. Dray, J.C. Lee, P. Valet, C. Gladine, T. Durand, J. Bertrand-Michel, Simultaneous quantitative profiling of 20 isoprostanoids from omega-3 and omega-6 polyunsaturated fatty acids by LC-MS/MS in various biological samples, Anal. Chim. Acta 921 (2016) 46–58, https://doi.org/10.1016/j.aca.2016.03.024.
[37] K.M. Rund, A.I. Ostermann, L. Kutzner, J.M. Galano, C. Oger, C. Vigor, S. Wecklein, N. Seiwert, T. Durand, N.H. Schebb, Development of an LC-ESI(-)-MS/MS method for the simultaneous quantification of 35 isoprostanes and isofurans derived from the major n3- and n6-PUFAs, Anal. Chim. Acta 1037 (2018) 63–74, https://doi.org/10.1016/j.aca.2017.11.002.
[38] M. Mirdita, K. Schutze, Y. Moriwaki, L. Heo, S. Ovchinnikov, M. Steinegger, ColabFold: making protein folding accessible to all, Nat. Methods 19 (6) (2022) 679–682, https://doi.org/10.1038/s41592-022-01488-1.
[39] K.H. Kim, W. Lee, E.E. Kim, Crystal structures of human peroxiredoxin 6 in different oxidation states, Biochem. Biophys. Res. Commun. 477 (4) (2016) 717–722, https://doi.org/10.1016/j.bbrc.2016.06.125.
[40] E.F. Pettersen, T.D. Goddard, C.C. Huang, E.C. Meng, G.S. Couch, T.I. Croll, J. H. Morris, T.E. Ferrin, U.C.S.F. ChimeraX, Structure visualization for researchers, educators, and developers, Protein Sci. 30 (1) (2021) 70–82, https://doi.org/10.1002/pro.3943.
[41] T. Cajka, J.T. Smilowitz, O. Fiehn, Validating quantitative untargeted lipidomics across nine liquid chromatography-high-resolution mass spectrometry platforms, Anal. Chem. 89 (22) (2017) 12360–12368, https://doi.org/10.1021/acs.analchem.7b03404.
[42] J. Chong, O. Soufan, C. Li, I. Caraus, S. Li, G. Bourque, D.S. Wishart, J. Xia, MetaboAnalyst 4.0: towards more transparent and integrative metabolomics analysis, Nucleic Acids Res. 46 (W1) (2018) W486–W494, https://doi.org/10.1093/nar/gky310.
[43] K. Brejchova, V. Paluchova, M. Brezinova, T. Cajka, L. Balas, T. Durand, M. Krizova, Z. Stranak, O. Kuda, Triacylglycerols containing branched palmitic acid ester of hydroxystearic acid (PAHSA) are present in the breast milk and hydrolyzed by carboxyl ester lipase, Food Chem. 388 (2022), 132983, https://doi.org/10.1016/j.foodchem.2022.132983.
[44] K. Brejchova, F.P.W. Radner, L. Balas, V. Paluchova, T. Cajka, H. Chodounska, E. Kudova, M. Schratter, R. Schreiber, T. Durand, R. Zechner, O. Kuda, Distinct roles of adipose triglyceride lipase and hormone-sensitive lipase in the catabolism of triacylglycerol estolides, Proc. Natl. Acad. Sci. U.S.A. 118 (2) (2021), https://doi.org/10.1073/pnas.2020999118.
[45] R.K. Chowhan, H. Rahaman, L.R. Singh, Structural basis of peroxidase catalytic cycle of human Prdx6, Sci. Rep. 10 (1) (2020), 17416, https://doi.org/10.1038/s41598-020-74052-6.
[46] R.F. Rivera-Santiago, S.L. Harper, S. Zhou, S. Sriswasdi, S.I. Feinstein, A.B. Fisher, D.W. Speicher, Solution structure of the reduced form of human peroxiredoxin-6 elucidated using zero-length chemical cross-linking and homology modelling, Biochem. J. 468 (1) (2015) 87–98, https://doi.org/10.1042/BJ20141463.
[47] V. Paluchova, M. Oseeva, M. Brezinova, T. Cajka, K. Bardova, K. Adamcova, P. Zacek, K. Brejchova, L. Balas, H. Chodounska, E. Kudova, R. Schreiber, R. Zechner, T. Durand, M. Rossmeisl, N.A. Abumrad, J. Kopecky, O. Kuda, Lipokine 5-PAHSA is regulated by adipose triglyceride lipase and primes adipocytes for de novo lipogenesis in mice, Diabetes 69 (3) (2020) 300–312, https://doi.org/10.2337/db19-0494.
[48] D. Tan, M.E. Ertunc, S. Konduri, J. Zhang, A.M. Pinto, Q. Chu, B.B. Kahn, D. Siegel, A. Saghatelian, Discovery of FAHFA-containing triacylglycerols and their metabolic regulation, J. Am. Chem. Soc. 141 (22) (2019) 8798–8806, https://doi.org/10.1021/jacs.9b00045.
[49] M. Riecan, V. Paluchova, M. Lopes, K. Brejchova, O. Kuda, Branched and linear fatty acid esters of hydroxy fatty acids (FAHFA) relevant to human health, Pharmacol. Ther. 231 (2022), 107972, https://doi.org/10.1016/j.pharmthera.2021.107972.
[50] Y. Wu, S.I. Feinstein, Y. Manevich, I. Chowdhury, J.H. Pak, A. Kazi, C. Dodia, D. W. Speicher, A.B. Fisher, Mitogen-activated protein kinase-mediated phosphorylation of peroxiredoxin 6 regulates its phospholipase A(2) activity, Biochem. J. 419 (3) (2009) 669–679, https://doi.org/10.1042/BJ20082061.
[51] S. Akiba, C. Dodia, X. Chen, A.B. Fisher, Characterization of acidic Ca(2+)-independent phospholipase A2 of bovine lung, Comp. Biochem. Physiol. B Biochem. Mol. Biol. 120 (2) (1998) 393–404, https://doi.org/10.1016/s0305-0491(98)10046-9.
[52] A. Criscuolo, P. Nepachalovich, D.F. Garcia-del Rio, M. Lange, Z. Ni, M. Blüher, M. Fedorova, Epilipidomics Platform for Holistic Profiling of Oxidized Complex Lipids in Blood Plasma of Obese Individuals, biorxiv, 2021, https://doi.org/10.1101/2021.12.23.473968.
[53] A. Reed, T. Ware, H. Li, J.F. Bazan, B.F. Cravatt, TMEM164 Is an Acyltransferase that Forms Ferroptotic Polyunsaturated Ether Phospholipids, biorXiv, 2022, https://doi.org/10.1101/2022.07.06.498872.
[54] D. Chen, B. Chu, X. Yang, Z. Liu, Y. Jin, N. Kon, R. Rabadan, X. Jiang, B. R. Stockwell, W. Gu, iPLA2beta-mediated lipid detoxification controls p53-driven ferroptosis independent of GPX4, Nat. Commun. 12 (1) (2021) 3644, https://doi.org/10.1038/s41467-021-23902-6.
[55] E. Jarc, T. Petan, A twist of FATe: lipid droplets and inflammatory lipid mediators, Biochimie 169 (2020) 69–87, https://doi.org/10.1016/j.biochi.2019.11.016.
[56] R. Arriga, F. Pacifici, B. Capuani, A. Coppola, A. Orlandi, M.G. Scioli, D. Pastore, A. Andreadi, P. Sbraccia, M. Tesauro, N.D. Daniele, G. Sconocchia, G. Donadel, A. Bellia, D. Della-Morte, D. Lauro, Peroxiredoxin 6 is a key antioxidant enzyme in modulating the link between glycemic and lipogenic metabolism, Oxid. Med. Cell. Longev. (2019), 9685607, https://doi.org/10.1155/2019/9685607, 2019.

Food Chemistry 388 (2022) 132983

Contents lists available at ScienceDirect

Food Chemistry

journal homepage: www.elsevier.com/locate/foodchem

Triacylglycerols containing branched palmitic acid ester of hydroxystearic acid (PAHSA) are present in the breast milk and hydrolyzed by carboxyl ester lipase

Kristyna Brejchova [a], Veronika Paluchova [a,b], Marie Brezinova [a,b], Tomas Cajka [a], Laurence Balas [c], Thierry Durand [c], Marcela Krizova [d], Zbynek Stranak [d], Ondrej Kuda [a,*]

[a] Institute of Physiology of the Czech Academy of Sciences, Videnska 1083, 14220 Praha 4, Czech Republic
[b] First Faculty of Medicine, Charles University, Katerinska 1660/32, 12108 Praha, Czech Republic
[c] Institut des Biomolecules Max Mousseron, University Montpellier, CNRS, ENSCM, Montpellier, France
[d] Institute for the Care of Mother and Child, Prague, Czech Republic

ARTICLE INFO

Keywords:
Human breast milk
Lipidomics
PAHSA
Colostrum
Elective caesarean section
Preterm birth

ABSTRACT

Breast milk is a complex mixture containing underexplored bioactive lipids. We performed an observational case-control study to compare the impact of delivery mode: caesarean section (CS) and vaginal birth (VB); and term (preterm and term delivery) on the levels of lipokines in human milk at different stages of lactation. Metabolomic analysis of the milk identified triacylglycerol estolides as a metabolic reservoir of the anti-inflammatory lipid mediator 5-palmitic acid ester of hydroxystearic acid (5-PAHSA). We found that triacylglycerol estolides were substrates of carboxyl ester lipase and 5-PAHSA-containing lipids were the least preferred substrates among tested triacylglycerol estolide isomers. This explained exceptionally high colostrum levels of 5-PAHSA in the VB group. CS and preterm birth negatively affected colostrum lipidome, including 5-PAHSA levels, but the lipidomic profiles normalized in mature milk. Mothers delivering term babies vaginally produce colostrum rich in 5-PAHSA, which could contribute to the prevention of intestinal inflammation in newborns.

1. Introduction

Nourishment plays a key role in the early stage of life. Breast milk provides the ideal cocktail of nutrients for infants in this period of rapid development and growth, and breastfeeding has a long-term impact on health (Floris, Stahl, Abrahamse-Berkeveld, & Teller, 2020). Although total contents of milk macronutrients are relatively stable, the levels of distinct components can be altered by several factors such as maternal dietary habits, mode of delivery, time of delivery, and/or stage of lactation (Hobbs, Mannion, McDonald, Brockway, & Tough, 2016; Koletzko, 2016; H. Lee et al., 2018).

The milk-producing mammary gland is a dynamic organ embedded in the mammary fat pad (Morroni et al., 2004). The first fluid produced after delivery – colostrum – is rich in proteins, immunologic components, and developmental factors, and it plays a primary role in immunomodulation and the promotion of intestinal development. In a few days postpartum (3–6 days), transitional milk replaces colostrum, and fully mature milk is produced after two weeks postpartum.

Human milk lipids provide a major energy supply for infants, and the main lipid species are triacylglycerols (TAGs) which form the core of the milk fat globule covered by phospholipid tri-layer membrane (H. Lee et al., 2018). The membrane comprises predominantly amphipathic lipids that originate from mammary gland epithelia (Koletzko, 2016; H. Lee et al., 2018). Besides the structural and nutritional lipids, lipid-based bioactive components such as specialized pro-resolving mediators and fatty acid esters of hydroxy fatty acids (FAHFA) were identified in human and bovine milk at concentrations comparable to human plasma (Arnardottir, Orr, Dalli, & Serhan, 2016; Brezinova et al., 2018; Matamoros, Harsch, Salfer, Shepardson, Shearer, & Harvatine, 2020).

FAHFAs belong to a family of branched lipids, some of which have

Abbreviations: CEL, carboxyl ester lipase; CS, caesarean section; FAHFA, fatty acid ester of hydroxy fatty acid; PAHSA, palmitic acid ester of hydroxystearic acid; PB, preterm birth; TAG, triacylglycerol; VB, vaginal birth.

* Corresponding author at: Laboratory of Metabolism of Bioactive Lipids, Institute of Physiology of the Czech Academy of Sciences, Videnska 1083, 14220 Prague, Czech Republic.
E-mail address: ondrej.kuda@fgu.cas.cz (O. Kuda).

https://doi.org/10.1016/j.foodchem.2022.132983
Received 24 November 2021; Received in revised form 24 March 2022; Accepted 12 April 2022
Available online 15 April 2022

anti-inflammatory and anti-diabetic properties (Aryal et al., 2021; Brejchova, Balas, Paluchova, Brezinova, Durand, & Kuda, 2020). One specific FAHFA family called palmitic acid ester of hydroxystearic acid (PAHSAs) could stimulate glucagon-like peptide 1 (GLP-1) secretion in the gut and improve systemic glucose homeostasis (Yore et al., 2014). Oral administration of 5-PAHSA isomer prevented gut mucosal damage and colitis in mice (J. Lee et al., 2016). Maternal body mass index and FAHFA milk content were implied in developmental programming (Brezinova et al., 2018; Enstad et al., 2019). Milk levels of 5-PAHSA were higher relative to other regioisomers, positively associated with weight gain during pregnancy, and reduced in the milk from obese mothers (Brezinova et al., 2018).

FAHFAs are either de novo synthesized in cells capable of (de novo) lipogenesis or supplied by dietary sources (Brezinova et al., 2018; Paluchova et al., 2020; Yore et al., 2014). Free FAHFAs can be esterified to glycerol giving rise to FAHFA acylglycerols, which in combination with other two fatty acids (FAs), result in the formation of TAG estolides (TAG EST) (Brejchova et al., 2021; Brezinova et al., 2020; Paluchova et al., 2020; Tan et al., 2019). FAHFAs can be released from the TAG estolide storage pool by adipose triglyceride lipase (ATGL), which is also free FAHFA hydrolase and the enzyme responsible for acyl-remodeling reaction among acylglycerols (Brejchova et al., 2021; Tan et al., 2019). In free FAHFAs, the estolide bond can be hydrolyzed by carboxyl ester lipase (CEL) (Kolar et al., 2016), androgen-induced gene 1, androgen-dependent TFPI-regulating protein (Parsons et al., 2016), and hormone-sensitive lipase (Brejchova et al., 2021). Importantly, CEL is one of the abundant proteins in human milk, and it contributes to TAG digestion in the immature gut of infants (Miller & Lowe, 2008).

Infant formula is a manufactured food designed as a complete or partial substitute for human milk, and its structure affects its digestion (Bourlieu et al., 2015). Human milk TAGs contain a conserved proportion of saturated FAs (mainly palmitic acid) at the *sn*-2 position unique to humans (Innis, 2011). Infant formulas with high *sn*-2 palmitate (β-palmitate) content have superior health outcomes compared to less humanized formulas (Miles & Calder, 2017). Saturated FAHFAs (e.g., 5-PAHSA) can be considered a special type of saturated FAs, and TAG EST containing FAHFAs at *the sn*-2 position could be potentially important components of the formula (Tan et al., 2019).

The aim of our study was to explore the metabolome and lipidome of human milk and focus on one specific group of FAHFA-related lipids. Identification of the biological role of FAHFAs and TAG EST in the milk could help with optimizations of infant formulas.

2. Hypothesis

We have previously identified 5-PAHSA as a signaling lipid, which was reduced in the colostrum of obese mothers. In the present study, we hypothesized that 1) timing, mode of delivery, and stage of lactation have an impact on the levels of bioactive FAHFAs, and 2) TAG estolides are present in human milk, and FAHFA could be released by the CEL in the milk.

3. Methods

3.1. Chemicals

Liquid chromatography and mass spectrometry (LC–MS)-grade solvents and mobile phase modifiers were obtained from VWR International, Merck, and J.T.Baker (Czech Republic). FAHFA standards were from Cayman Europe (Tallinn, Estonia), 5-PAHSA and $^{13}C_{16}$-5-PAHSA were synthesized as previously described (Balas et al., 2016). Internal standards for LC–MS were purchased from Avanti Polar Lipids (USA). The TAG estolides were synthesized at the Institute of Biomolecules Max Mousseron (Montpellier) (Brejchova et al., 2021). All other chemicals were obtained from Merck (Czech Republic) unless stated otherwise.

3.2. Study design and sample collection

Milk samples from healthy lactating mothers who delivered spontaneously in term (VB, vaginal birth, controls), or by caesarean section (CS), or preterm (PB, preterm birth) were collected at the Institute for Mother and Child Care in Prague, Czech Republic. The inclusions criteria were: body mass index 19–24, gestational age (38–41 weeks and $<32^{nd}$ week), type of delivery (CS or VB), maternal age $>$ 18 years, no symptoms of acute infection (i.e., respiratory, urinary tract infection, otitis, chorioamnionitis), absence of any diabetes mellitus and sufficient amounts of breast milk to achieve adequate breastfeeding. Mothers, who delivered spontaneously in term or underwent caesarean section, gave birth between 38 and 41 weeks of gestation (Table 1). Their newborns had a chronological age of 72 h and 28 days at the time of milk collection, respectively. Preterm infants were delivered before the 32^{nd} week of gestation (Table 1), and samples of milk were collected after 72 h and 28 days. Moreover, another milk sample was acquired at the time when the infants would have reached the 36^{th} week of gestation. We considered the preterm delivery condition (before the 32^{nd} week) more relevant for data interpretation than the mode of preterm delivery (Table 1). Therefore, the PB group contains both vaginal birth and caesarean section cases. Milk samples were frozen at −20 °C within 30 min after collection and transported to a −80 °C freezer in 1–3 days. All donors signed informed consent before inclusion in the study. The study protocols were approved by the Research Ethics Board of the Institute for Mother and Child Care (Approval number: 2016–12-19/3).

3.3. Sample extraction

LIMeX (LIpids, Metabolites, and eXposome compounds) LC–MS workflow was used for the untargeted analysis of complex lipids and polar metabolites as before with a few modifications (Lopes et al., 2021). Targeted milk FAHFA analysis was performed as before (Brezinova et al., 2018). In more detail, before the extraction, frozen milk samples were warmed up to 37 °C in a water bath and homogenized within 3 min using an ultrasonic bath to ensure sample homogeneity. Total lipids were extracted using a biphasic solvent system of cold methanol, methyl *tert*-butyl ether (MTBE), and water according to the published method (Brezinova et al., 2020; Brezinova et al., 2018). In brief, 300 μL of milk was mixed with pre-chilled 660 μL of methanol, 2.4 mL of MTBE, and 500 μL of 10% methanol containing internal standards. Samples were

Table 1
Maternal and infant anthropometrics.

	Term delivery		Preterm delivery
	Vaginal birth (VB)	Caesarean section (CS)	Preterm birth (PB)
Maternal characteristics			
Sample size (n)	27	26	20
Age at birth (years)	32.4 ± 0.8	32.6 ± 0.8	31.0 ± 0.9
BMI (kg/m^2)	22.2 ± 0.5	23.0 ± 0.5	21.7 ± 0.6
Gestational weight gain (kg)	12.2 ± 1.0	14.4 ± 1.3	8.9 ± 0.9
Gravidity	2.4 ± 0.2	2.2 ± 0.2	1.5 ± 0.1
Parity	1.7 ± 0.1	1.7 ± 0.1	1.3 ± 0.1
Delivery method			
Vaginal	27	0	6
Caesarean section	0	26	14
Milk sample			
72 h	27	26	20
28 days	18	21	15
36^{th} gestational week	–	–	10
Newborn characteristics			
Gestational age at delivery (wk + d)	40 + 3 ± 1d	39 + 2 ± 1d	29 + 4 ± 1d
Sex (M/F)	11 / 16	17 / 9	8 / 12
Birth weight (g)	3613 ± 67	3323 ± 74	1255 ± 65
Birth height (cm)	50.4 ± 0.3	50.0 ± 0.3	–

centrifuged at 5,200×*g*, 10 min at 4 °C, and aliquots of the organic phase for lipidomics (100 μL) and TAG estolide/FAHFA (2 mL) analysis were collected. The water phase (70 μL) was used for metabolomics and protein pellets for proteomic analysis. FAHFA extraction was performed using SPE columns (HyperSep Silica 500 mg/10 mL, 40–60 μm, 60 Å, ThermoFisher Scientific, Czech Republic) similarly as was described before (Brezinova et al., 2018), see Supplemental Methods.

3.4. CEL activity assay

To determine CEL hydrolase affinity to TAG estolide substrates, the previously published CEL activity assay method was modified and performed (Kolar et al., 2016; Xiao, Mukherjee, Ross, & Lowe, 2011). Positional isomers of TAG EST 70:4 containing either 5- or 9-PAHSA esterified at *sn-1/sn-3* (e.g. 5-PAHSA/18:2/18:2) or *sn-2* positions of glycerol backbone (e.g. 18:2/5-PAHSA/18:2) as well as trilinolein (18:2/18:2/18:2) were used as CEL substrates. In brief, 3.8 μg of purified CEL (BioVendor R&D, Czech Republic) was used per reaction in the assay buffer containing 150 mM NaCl, 1 mM Tris-HCl, 2 mM $CaCl_2$, pH 8. TAG estolide substrate (250 μM) was emulsified in the assay buffer with 10 mM sodium cholate. To prevent product inhibition, fatty acid-free bovine serum albumin (MP Biomedicals, France) was added to the reaction at a final concentration of 1%. Volume 100 μL of the enzyme solution and 100 μL of the substrate were mixed and incubated at 37 °C for 60 min. The reaction was terminated in an ice-cold water bath. MTBE extraction was performed as before (Brejchova et al., 2021). Control reactions were performed under identical conditions without the enzyme. Reaction products were analyzed using lipidomics platforms.

3.5. LC–MS analyzes

For untargeted metabolomics and lipidomics, the LC–MS systems consisted of a Vanquish UHPLC System (Thermo Fisher Scientific, Bremen, Germany) coupled to a Q Exactive Plus mass spectrometer (Thermo Fisher Scientific, Bremen, Germany). Six different LC–MS platforms were used: (i) lipidomics of high-abundant TAG in positive ion mode; (ii) lipidomics of low-abundant TAG EST in positive ion mode; (iii) lipidomics of minor polar lipids in positive ion mode; (iv) lipidomics of minor polar lipids in negative ion mode; (v) metabolomics of polar metabolites in positive ion mode; and (vi) metabolomics of polar metabolites in negative ion mode. LC–MS instrumental files from metabolomic and lipidomic profiling were processed through MS-DIAL v. 4.16 software (Brezinova et al., 2020). Metabolites were annotated using in-house retention time–*m/z* library and using MS/MS libraries (NIST20, MassBank, MoNA, LipidBlast). Raw data were filtered using blank samples, serial dilution samples, and quality control (QC) pool samples with relative standard deviation (RSD) < 30%, normalized using LOESS approach by means of QC pool samples injected regularly between 10 actual samples. Samples were randomized across the platform run. Targeted FAHFA analysis was conducted on an UltiMate 3000 RSLC UHPLC system coupled to a QTRAP 5500/SelexION mass spectrometer (SCIEX, Darmstadt, Germany) as before (Brezinova et al., 2018).

Standards of TAG estolides reported previously were used for the identification of milk TAG estolides (Brejchova et al., 2021; Brezinova et al., 2020; Tan et al., 2019). Following internal standards were used for quantification: $^{2}H_5$ TG (17:0/17:1/17:0), $^{2}H_5$ DG (18:1/0:0/18:1), MG (17:0/0:0/0:0), $^{2}H_5$ TG (20:0/20:1/20:0), $^{13}C_4$ 9-PAHSA, $^{13}C_{16}$ 5-PAHSA, $^{2}H_9$ FA 18:1 based on chemical similarity between analytes. No suitable internal standards were available for the quantification of hydroxylated acylglycerols. Currently, it is impossible to prepare chemically pure substrates at chiral levels (*sn*-1 or *sn*-3 position at the glycerol combined with *R/S* isomers within the PAHSA structure). Therefore, we did not further characterize the structures of the intermediates.

3.6. Milk metabolome and lipidome dataset analysis

Metabolomics data were analyzed using a statistical enrichment approach based on chemical similarity (Barupal & Fiehn, 2017). Customized ChemRICH software was used to generate metabolite clusters annotated according to Medical Subject Headings classes. Kolmogorov–Smirnov test was used to calculate adjusted cluster *p*-value and *z*-score for each cluster. The sign of *z*-score defines whether the clustered metabolites are downregulated (*z*-score < 0) or upregulated (*z*-score > 0). Clusters with |*z*-score| > 2 and $-\log_{10}$ (adjusted cluster *p*-value) > 1 were considered significantly altered. ChemRICH uses classic 881-bit molecular fingerprints defined by PubChem, which is not optimal for lipid-rich datasets. Therefore, the algorithm generated one big cluster of TAGs (n = 140). To overcome this limitation, we performed the enrichment analysis of the TAG cluster using a 1024-bit 'hybridization' type of fingerprint, which explored the 'depth' of 7 atoms and considered the presence of double bonds. The final 8 TAG sub-clusters were annotated using Lipid Mini-On, and the TAG double bond number was considered as the significant sub-cluster discriminator (q values < 0.05) (Clair et al., 2019).

3.7. Statistics

GraphPad Prism 9.2.0 statistical tools were used for bar graphs. Table 1 values and bar graph data are means ± SEM. Results of One-way ANOVA (Tukey's multiple comparison test) and Students *t*-test were considered significant at $p < 0.05$. Based on published differences in serum 5-PAHSA concentrations in humans (Yore et al., 2014), the minimum sample size of 19 per group was calculated using G*Power software (*t*-test, two groups, one tail, power 0.95, α = 0.05) (Faul, Erdfelder, Lang, & Buchner, 2007).

4. Results

4.1. Impact of lactation stage, gestational age, and mode of delivery on metabolite composition of breast milk

We analyzed the metabolite composition of breast milk by LC–MS in the three groups of mothers at different time points of lactation and selected VB samples at 72 h after childbirth as a reference group. The metabolome consisted of 148 water-soluble compounds (amino acids, nucleosides, etc.) and 541 simple and complex lipids (acylglycerols, fatty acids, etc.), summarized in Fig. S1. First, we focused on the differences between the groups at the level of the whole metabolome. Annotated metabolites were sorted into 55 clusters using the chemical similarity approach, and up- or down-regulated clusters were visualized (Fig. 1A, Table S1). Enrichment analysis showed that CS colostrum had significantly lower levels of TAGs and higher levels of several phosphatidylinositol (PI) and phosphatidylserine (PS) classes than VB. In contrast, PB colostrum was highly enriched in several phospholipid and sphingomyelin classes as compared to the VB group (Fig. 1B, Table S2).

The largest cluster of TAGs was further sub-clustered based on acyl chain composition to gain a better insight into the changes of milk lipid composition in time (Fig. 2). Heatmap representation of the clusters showed that metabolic profiles in all three groups followed similar patterns – a decrease of phospholipids and an increase of unsaturated acylglycerols. The composition of PB mature milk caught up with the VB and CS groups after 28 days and remained stable until gestational week 36.

4.2. Milk FAHFA isomer profiles change in time

We have previously shown that human colostrum contains several FAHFA species and that 5-PAHSA levels were lower in obese compared to lean mothers (Brezinova et al., 2018). Here we also explored other FAHFA with documented biological activities (Aryal et al., 2021;

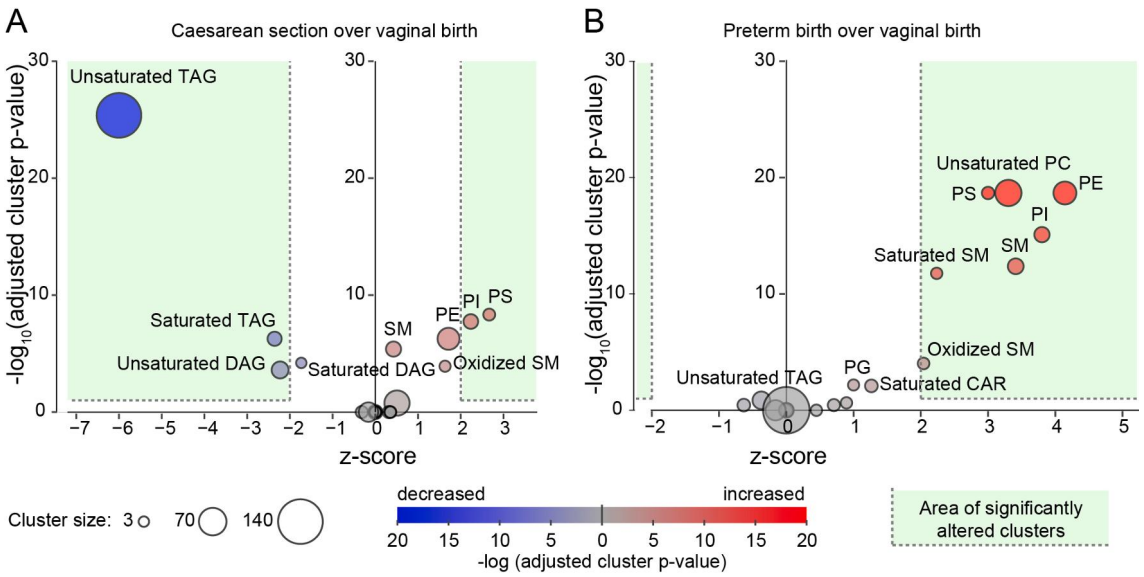

Fig. 1. Differences in metabolic profiles of colostrum. Chemical similarity enrichment analysis of CS 72 h over VB 72 h (A); and PB 72 h over VB 72 h (B). CAR, carnitines; DAG, diacylglycerols; PE, phosphatidylethanolamines; PG, phosphatidylglycerols; PI, phosphatidylinositols; PS, phosphatidylserines; SM, sphingomyelins; TAG, triacylglycerols.

Brejchova et al., 2020; Yore et al., 2014).

First, we tested whether the term or mode of delivery affects FAHFA concentration. We detected significantly lower levels of both 5- and 9-PAHSA in colostrum samples of mothers who delivered preterm compared to those who gave birth spontaneously in term. A significantly lower concentration of 5-PAHSA was also found in milk samples of mothers in the CS group (Fig. 3A). The levels of both PAHSAs normalized in mature milk (28 days). The only difference was detected in the PB group, in which the concentration of 5-PAHSA was still significantly reduced in comparison with the VB group. None of the other bioactive FAHFAs in colostrum and mature milk revealed significant differences among groups of delivery (Fig. 3B).

Second, we looked into the change of FAHFAs levels during different stages of lactation. In the VB group, the only significant change observed was a decrease in 5-PAHSA and a rise in 13-LAHLA levels in mature milk compared to colostrum (Fig. 3B). Significantly increased concentrations of seven FAHFAs (5-PAHSA, 10-PAHSA, 9-PAHPA, 9-, 10-, 12/13-OAHSA and 13-LAHLA) and three FAHFAs (5-PAHSA, 10- and 12/13-OAHSA) were found in mature milk from CS and PB groups, respectively (Fig. 3B).

4.3. TAG estolides are present in the milk

Milk fat globule TAG core is synthesized from cytoplasmic lipid droplets by mammary gland alveolar epithelial cells. Metabolism of FAHFAs and their storage form, TAG estolides, is closely associated with ATGL, which acts on the lipid droplet surface. Therefore, we tested whether the milk contains TAG estolides present in human adipose tissue (Brezinova et al., 2020). We confirmed the presence of TAG estolides in the milk, specifically TAG EST 68:1, 68:2, 68:3, 68:4, 70:2, 70:3, 70:4, and 70:5. However, their levels were very variable and low or undetectable in some samples, and no significant difference was found among the groups. The most abundant TAG estolides represented a mixture of isomers containing PAHSAs, palmitic acid esters of hydroxylinoleic acid, OAHSA, and oleic acid esters of hydroxyoleic acids in agreement with free FAHFA species (Fig. 4).

4.4. CEL hydrolyzes glycerol ester bonds and FAHFA estolide bond in TAG estolides

We hypothesized that the TAG estolides in the milk could be degraded by the CEL because PAHSAs are known CEL substrates (Kolar et al., 2016). We tested the affinity of purified CEL to TAG estolides with a small combinatorial library of one PAHSA and two linoleic acids (LA, FA 18:2) bound to the glycerol backbone and compared it with a common CEL substrate, glyceryl trilinoleate. The assay was focused on three main TAG estolide structural features (Fig. 5A). First, to evaluate substrate preference to different TAG estolide/FAHFA regioisomers, we used TAG estolides containing either 5-PAHSA or 9-PAHSA. Second, to evaluate *sn*-position preference, we used two positional isomers, in which PAHSA was esterified either at the primary (*sn-1/3*) alcohol position or at secondary alcohol position (*sn-2*) of glycerol. Third, to test whether CEL hydrolyzes FAHFA estolide bond when bound to TAG estolide, we monitored hydroxylated acylglycerol intermediates (Fig. 5A).

CEL metabolized all substrates giving rise to several intermediates and products of the cleavage (Fig. 5A). CEL can cleave LA–glycerol bond, release LA and produce an intermediate - diacylglycerol estolide (DAG EST) (Fig. 5A, green cloud). This could also serve as a CEL substrate generating another molecule of LA and a monoacylglycerol estolide (MAG EST). Our results showed that CEL effectively released LA from both TAG EST regioisomers and their positional isomers, as well as from trilinolein. Corresponding reaction products such as DAG EST and MAG EST were also found in all TAG EST substrate samples (Fig. 5B).

CEL can also cleave the PAHSA-glycerol bond resulting in the production of a PAHSA and a DAG (Fig. 5A, orange cloud). The presence of free PAHSA found in all reactions confirms the ability of the lipase to release 5- and 9-PAHSA from both TAG estolide positional isomers, although CEL was more effective when PAHSA was bound at the *sn-2* position. This preference is evident not only from significantly higher PAHSAs but also from lower levels of MAG ESTs in samples of these positional isomers (Fig. 5B, C). Moreover, considerably lower values of MAG EST 9P than MAG EST 5P of both positional isomers ($p < 0.0001$ for both positional isomers, compare absolute values between panels) indicate higher affinity of CEL to 9-PAHSA- than 5-PAHSA-glycerol ester bond (Fig. 5B).

The reaction scheme in the blue cloud (Fig. 5A, blue cloud) depicts

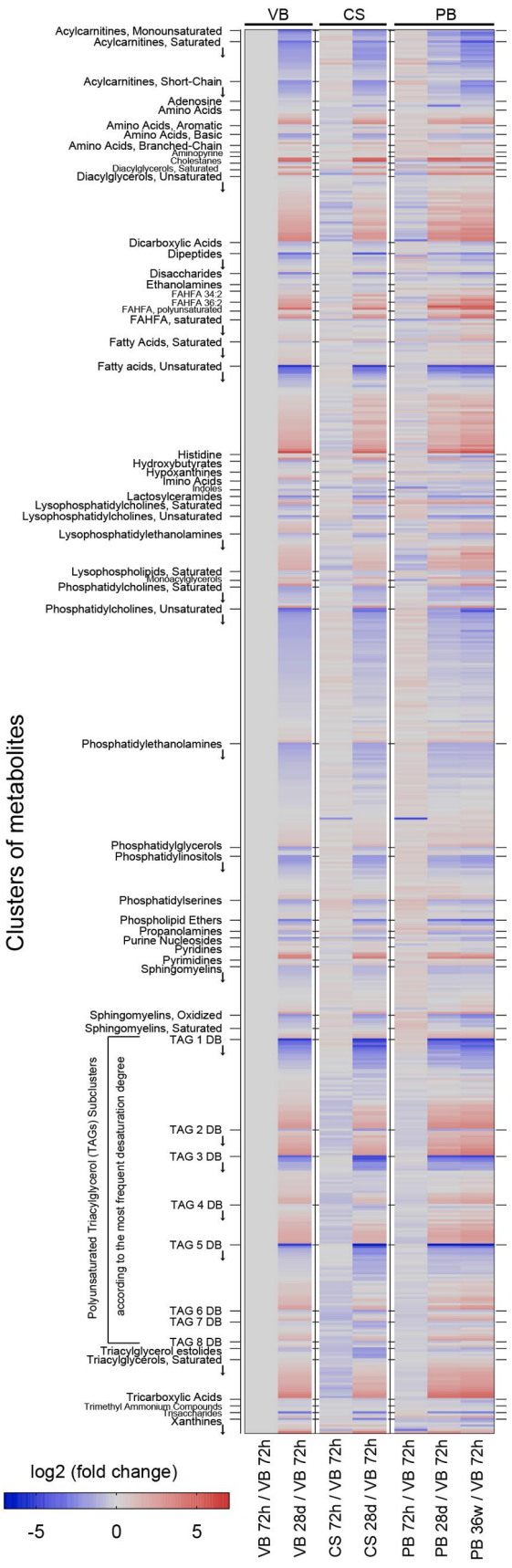

Fig. 2. Milk metabolomics profiles. Columns represent groups as fold change over VB 72 h group. Cluster labels on the left side span over cluster members, indicated by arrows. Each line within the column heatmap represents a metabolite; $n = 636$ metabolites; for n per group see Table 1.

possible cleavage of PAHSA estolide bond within TAG estolide structure resulting in the release of free palmitic acid (PA, FA 16:0) and hydroxylated TAG. LA could be subsequently hydrolyzed from this intermediate, and hydroxylated DAGs and MAGs may arise (Fig. 5A, blue cloud). However, CEL could also react with a pool of intermediate products (DAG EST and MAG EST) in the same way (Fig. 5A, green cloud) and generate hydroxylated DAGs and MAGs. The presence of all of these products in samples with TAG estolide containing 5-PAHSA provided evidence that CEL has such ability and prefers TAG estolide with 5-PAHSA bound at the primary (*sn-1,3*) alcohol position in the glycerol (Fig. 5D).

Since hydrolysis of 9-PAHSA TAG estolide substrates gave rise to negligible levels of hydroxylated DAG, DAGs, and MAGs, it is plausible that CEL rather cleaves 9-PAHSA-glycerol ester bond than FAHFA estolide bond (Fig. 5D). It has been shown that free 9-PAHSA is more effectively hydrolyzed by CEL than 5-PAHSA (Kolar et al., 2016). This rule also applies to TAG estolide substrates (Fig. 5E), as significantly higher levels of the final products (9-HSA and PA, $p < 0.0001$), as well as lower levels of free 9-PAHSA ($p < 0.0001$), were found compared to reactions with TAG EST containing 5-PAHSA substrate (Fig. 5C).

5. Discussion

Our data suggest that milk from the VB group has an optimally balanced combination of free FAHFAs and TAG estolides. Premature birth and/or caesarean section represents a situation in which the mammary gland is not ideally stimulated or ready for milk production, but the milk lipid composition normalizes in time.

The caesarean section rate is expected to increase above the medically necessary threshold in the future, neglecting the potentially negative effects for the mother and the child (Betran, Ye, Moller, Souza, & Zhang, 2021). The caesarean section has a negative impact on breastfeeding initiation, duration, and difficulties (Hobbs et al., 2016). Prior et al. systematically reviewed the association between CS and breastfeeding and concluded that rates of early breastfeeding initiation were lower in CS compared with the VB group (Prior, Santhakumaran, Gale, Philipps, Modi, & Hyde, 2012). Delayed initiation of milk production could affect lipid composition of the colostrum acquired at 72 h postpartum (Fig. 1A), resulting in higher phospholipid levels and lower TAG levels in the CS group. Higher levels of phospholipid and sphingomyelin classes that form the milk fat globule tri-layer were observed also in PB colostrum in agreement with previous publications (Pérez-Gálvez, Calvo, Megino-Tello, Aguayo-Maldonado, Jiménez-Flores, & Fontecha, 2020). Differences in TAG and phospholipid levels or their ratio could be linked to milk fat globule size and potential digestibility (Garcia, Antona, Robert, Lopez, & Armand, 2014). In comparison to colostrum samples, mature milk metabolomic and lipidomic profiles were affected by multiple factors (diet, sample acquisition, etc.), but the differences vanished with advancing lactation.

The logical source of both free FAHFAs and TAG estolides in the milk is the breast white adipose tissue that transdifferentiated into milk-secreting glands during pregnancy (Morroni et al., 2004). FAHFA levels produced into the milk are comparable to serum/plasma FAHFA concentrations (Brejchova et al., 2020), and the structure of milk fat globules (H. Lee et al., 2018) suggests that the TAG lipid core could store TAG estolides.

FAHFA production is dependent on de novo lipogenesis and/or dietary lipids (Brejchova et al., 2020; Yore et al., 2014). However, the de novo lipogenesis in the mammary gland is different from white adipose tissue, and the pathway produces mainly saturated fatty acids with 6–14 carbons (Libertini & Smith, 1978; Mohammad, Sunehag, & Haymond, 2014). This medium-chain fatty acid synthesis in the human mammary gland starts with parturition, irrespective of the length of pregnancy (Spear, Bitman, Hamosh, Wood, Gavula, & Hamosh, 1992). Therefore, fatty acids for FAHFAs containing longer acyl chains (e.g., C16:0 and C18:0 for PAHSAs) are acquired from endogenous sources (liver and

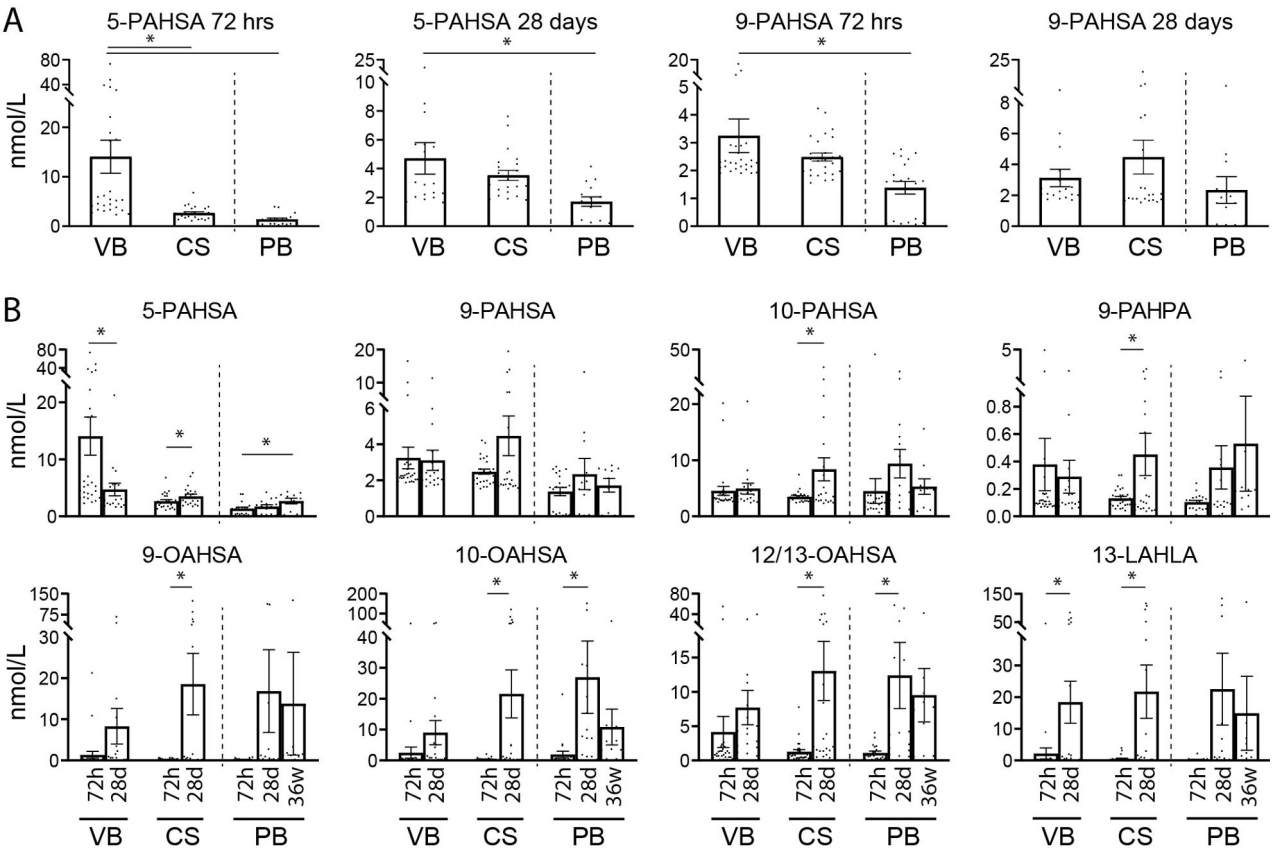

Fig. 3. PAHSA concentrations in human breast milk differ among groups of delivery. (A) The levels of 5- and 9-PAHSA were analyzed and compared in milk samples obtained 72 h (72 h) and 28 days (28d) after delivery from mothers who delivered vaginally in term (VB), by caesarean section in term (CS), or preterm (PB). One-way ANOVA, Tukey's multiple comparison test, *, statistically significant at $p < 0.05$. (B) Bioactive FAHFA levels change during the lactation period. In the PB group, FAHFA levels were measured also at the time when the infants would have reached the 36th week of gestation age (36w). Concentrations of each FAHFA in milk from each time point were compared within each group. Moreover, FAHFA levels in milk samples from the PB group at 36w were compared with mature milk from the VB group. OAHSA, oleic acid ester of hydroxystearic acids; PAHPA, palmitic acid ester of hydroxypalmitic acid; LAHLA, linoleic acid ester of hydroxylinoleic acid; *, statistically significant at $p < 0.05$, *t*-test (comparison within VB and CS groups) or One-way ANOVA, Tukey's multiple comparison test (PB group). Data are means ± SEM, $n = 27–10$ (see Table 1).

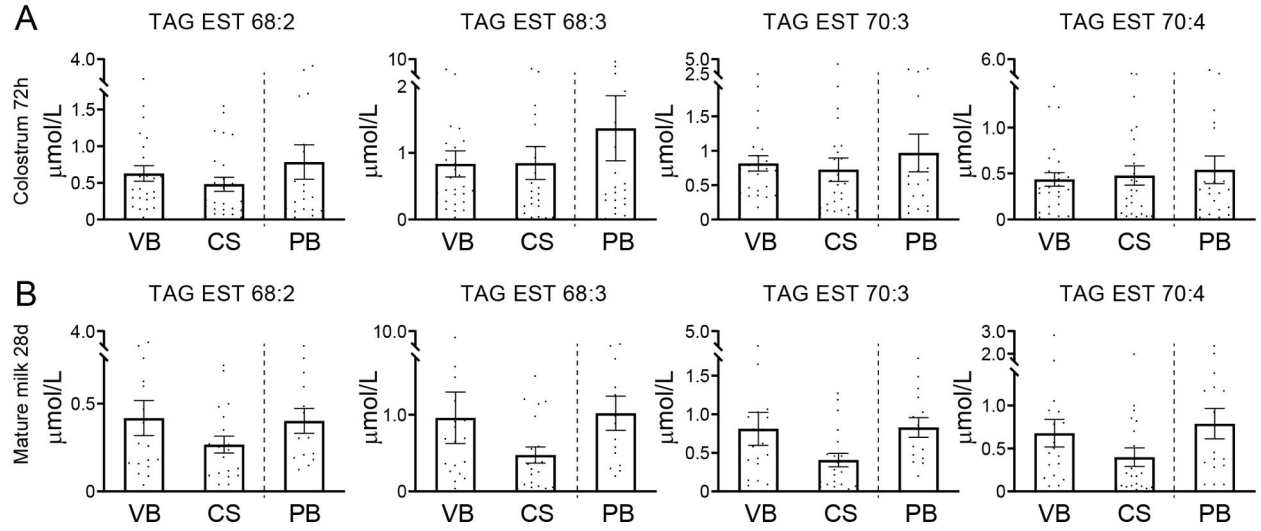

Fig. 4. TAG estolides are present in the milk of all groups and persist during the lactation period. The levels of TAG estolides were analyzed in milk samples obtained 72 h (A) and 28 days (B) after delivery from mothers who delivered vaginally in term (VB), by caesarean section (CS) in term, and from mothers who delivered preterm (PB). Data are means ± SEM, $n = 26–14$ (see Table 1).

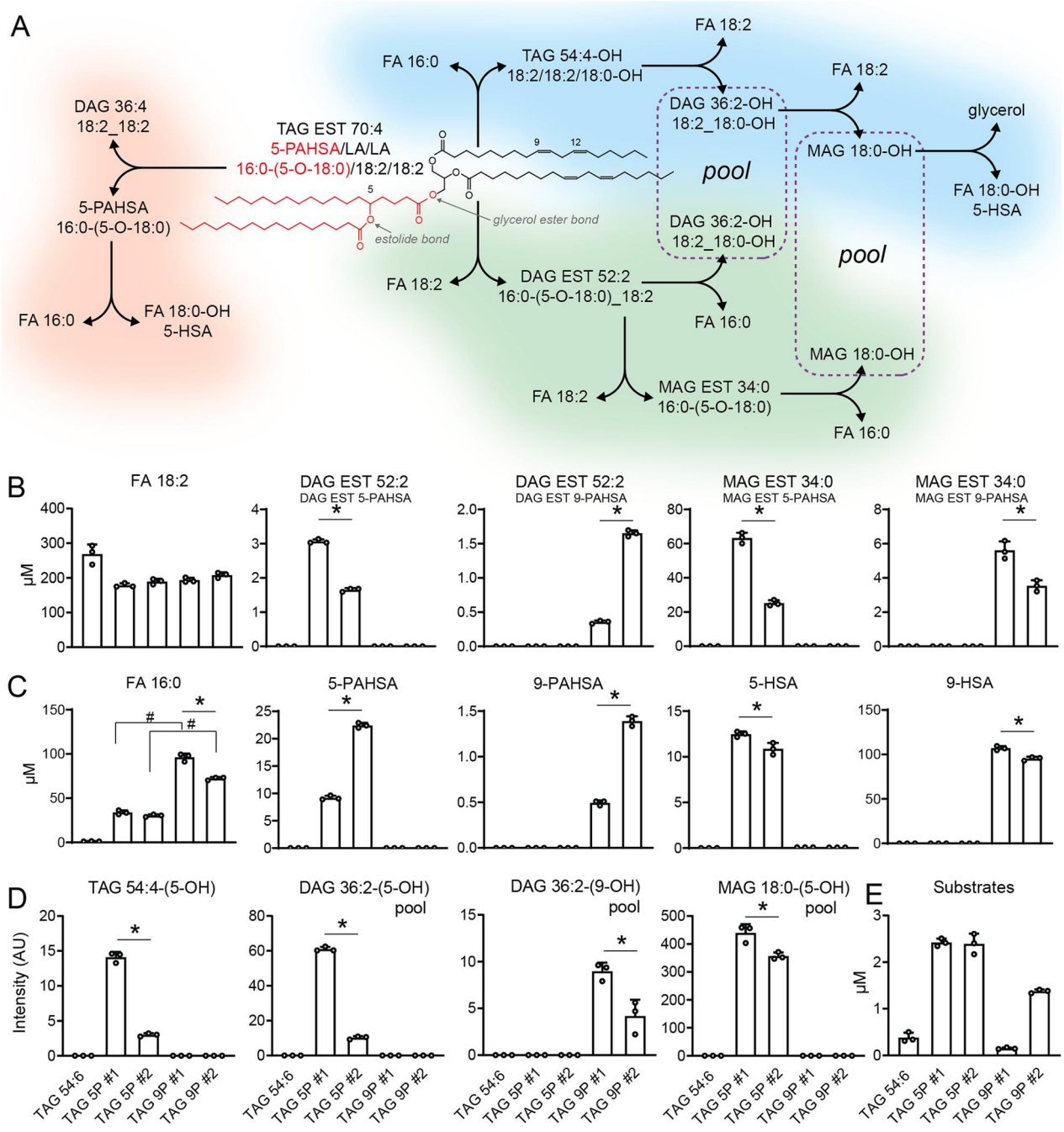

Fig. 5. Scheme of TAG estolide substrate and theoretical reactions catalyzed by CEL (A) and CEL degradation products of TAG EST 70:4 containing either 5-PAHSA (5P) or 9-PAHSA (9P). Reaction products of LA-glycerol bond cleavage (B). Reaction products of PAHSA-glycerol and estolide bond hydrolysis (C). Products of estolide bond disruption within the TAG EST molecule (D). Residual concentration of primary substrates after the assay (E). TAG 5P #1 columns indicate samples, in which TAG EST 70:4 containing 5-PAHSA bound at *sn*-1/3 alcohol position of glycerol was used as a substrate; TAG 5P #2 represents samples with TAG EST 70:4 and 5-PAHSA at *sn*-2 position. TAG 9P #1 and #2 mark positional isomers of TAG EST containing 9-PAHSA. TAG 54:6 stands for trilinolein; TAG, triacylglycerol; DAG, diacylglycerol; MAG, monoacylglycerol; FA, fatty acid; DAG EST, diacylglycerol estolide; MAG EST, monoacylglycerol estolide; HSA, hydroxystearic acid; TAG (OH), hydroxylated triacylglycerol; DAG (OH), hydroxylated diacylglycerol; and MAG (OH), hydroxylated monoacylglycerol. X:Y stands for the number of carbon atoms: the number of double bonds. Data are means ± SEM, $n = 3$. T-test was used to compare *sn* positions (* marks) or regioisomers (# marks), $p < 0.05$. Regioisomer comparison between panels is described in the text for clarity. No suitable internal standards were available for quantification of hydroxylated acylglycerols.

adipose tissue de novo lipogenesis) or diet, and probably only the estolide bond formation takes place in the mammary gland. Preferential handling of fatty acids for TAG or FAHFA synthesis remains enigmatic. Although colostrum contains comparable levels of, e.g., TAG-bound essential LA to mature milk, LA-derived polyunsaturated 13-LAHLA appeared only in mature milk. This might be linked to the unique TAG stereo-specific composition of human milk TAGs which contain a conserved proportion of saturated FAs (mainly palmitic acid) at the *sn*-2 position (Innis, 2011; Miles & Calder, 2017).

TAG cores of milk fat globules are synthesized from cytoplasmic lipid droplets budding from the endoplasmic reticulum (H. Lee et al., 2018). This pathway could also produce TAG estolides that have been detected only in adipose tissue (presumably in lipid droplets) and not in circulation (Brezinova et al., 2020; Paluchova et al., 2020; Tan et al., 2019).

ATGL is one of several known FAHFA hydrolases, but this enzyme can also remodel acyl chains on TAGs and synthesize FAHFA-TAG combinations (Brejchova et al., 2021). ATGL is highly expressed in the goat mammary gland, induced during lactation, and regulates TAG formation (Li et al., 2015). Therefore, both FAHFAs and TAG estolides can be present within the lipid droplets, and their levels can be controlled via ATGL within the epithelial cells or via CEL in the milk. However, it is currently unknown why are FAHFAs and TAG estolides exported to the milk together with their hydrolase CEL.

CEL activity could modulate free FAHFA levels because TAG estolide concentration is an order of magnitude higher than free FAHFA levels. CEL concentrations are higher in mature milk than in colostrum, but no difference was observed between full-term and preterm colostrum (Sha, Zhou, Xi, Li, & Li, 2019). We randomly selected 4 and 4 colostrum samples from the VB and PB groups, respectively, and performed proteomic analysis. Relative protein levels of CEL in colostrum were similar in VB and PB groups (Fig. S1) in agreement with published data (Sha et al., 2019). However, the CEL activity was reported higher in preterm colostrum, resulting in a higher fat-digesting potential during the early postnatal phase (Pamblanco, Ten, & Comín, 1987). Therefore, preterm colostrum might be optimized to help with fat digestion at the expense of TAG estolides and FAHFAs.

The CEL in vitro assay showed that the enzyme hydrolyzes the glycerol ester and the estolide bonds at all positions of TAG estolide substrates. In agreement with data on CEL substrate preferences (Kolar et al., 2016), we observed a lower affinity to 5-PAHSA than 9-PAHSA isomer. This preference explains high levels of 5-PAHSA in VB colostrum samples and also high 5-PAHSA levels in colostrum from an independent study (Brezinova et al., 2018). In mouse experiments, 5-PAHSA successfully passed the gastrointestinal tract and reached circulation (Brezinova et al., 2018; Paluchova et al., 2020). The privileged presence of 5-PAHSA in the colostrum could be linked to its anti-inflammatory effects and protection against ulcerative colitis (J. Lee et al., 2016). A recent screening study concluded that FAHFAs with lower branching position are more likely to be anti-inflammatory (Aryal et al., 2021), thus could help to prevent necrotizing enterocolitis in a newborn. Future studies will be needed to define whether FAHFA-rich milk from milk banks could be the preferred substitute for preterm newborns at risk for conditions such as necrotizing colitis (J. Lee et al., 2016).

6. Conclusion

Here we identified TAG estolides as a new component of human milk and broadened substrate specificity of CEL that can modulate milk FAHFA composition. Mothers and health care professionals should be aware of the indication that CS and associated delayed breastfeeding initiation could negatively affect levels of anti-inflammatory lipid mediators in the milk. Identification of TAG EST containing saturated FAHFAs at specific *sn* position could be potentially applied in infant formula design.

6.1. Limitations of the study

Qualified personnel processed the colostrum samples at the maternity hospital, but mature milk samples were collected by the nursing mothers at home. Therefore, higher variability in milk composition has to be anticipated (mode and time of sample collection, diet, etc.). Our analytical approach is unable to separate TAG estolide isomers, and we report the acyl composition of major species based on MS/MS data. The CEL lipolytic activities were measured under optimal in vitro assay conditions. However, the expected physical form of the TAG estolide substrate is a TAG lipid droplet core of a milk fat globule surrounded by a tri-layer phospholipid membrane. Digestion of the substrate in this unique microenvironment is a complex process and cannot be simulated in vitro. We have no means to incorporate labeled FAHFAs into milk fat globules in humans to mimic the unique TAG *sn*-2 composition (Innis, 2011).

Funding

This work was supported by a grant from the Czech Science Foundation (20-00317S) and by the Czech Academy of Sciences (Lumina quaeruntur LQ200111901).

CRediT authorship contribution statement

Kristyna Brejchova: Data curation, Investigation, Methodology, Visualization, Writing – original draft, Writing – review & editing. **Veronika Paluchova:** Data curation, Formal analysis, Investigation, Methodology. **Marie Brezinova:** Formal analysis. **Tomas Cajka:** Data curation, Methodology, Validation, Writing – review & editing. **Laurence Balas:** Resources, Writing – review & editing. **Thierry Durand:** Resources, Writing – review & editing. **Marcela Krizova:** Project administration, Supervision, Writing – review & editing. **Zbynek Stranak:** Project administration, Supervision, Writing – review & editing. **Ondrej Kuda:** Conceptualization, Formal analysis, Funding acquisition, Investigation, Project administration, Resources, Validation, Visualization, Writing – review & editing.

Declaration of Competing Interest

The authors declare that they have no known competing financial interests or personal relationships that could have appeared to influence the work reported in this paper.

Acknowledgements

The authors would like to acknowledge the Metabolomics Core Facility at the Institute of Physiology of the Czech Academy of Sciences for metabolomics and lipidomics profiling and Proteomics service laboratory at the Institute of Physiology and the Institute of Molecular Genetics of the Czech Academy of Sciences for proteomics profiling. The authors wish to thank Jana Kollarova for help with milk sampling and are grateful to all the mothers who took part in the study.

Appendix A. Supplementary data

Supplementary data to this article can be found online at https://doi.org/10.1016/j.foodchem.2022.132983.

References

Arnardottir, H., Orr, S. K., Dalli, J., & Serhan, C. N. (2016). Human milk proresolving mediators stimulate resolution of acute inflammation. *Mucosal Immunology, 9*(3), 757–766. https://doi.org/10.1038/mi.2015.99

Aryal, P., Syed, I., Lee, J., Patel, R., Nelson, A. T., Siegel, D., … Kahn, B. B. (2021). Distinct Biological Activities of Isomers from Different Families of Branched Fatty Acid Esters of Hydroxy Fatty Acids (FAHFAs). *Journal of Lipid Research, 100108*. https://doi.org/10.1016/j.jlr.2021.100108

Balas, L., Bertrand-Michel, J., Viars, F., Faugere, J., Lefort, C., Caspar-Bauguil, S., … Durand, T. (2016). Regiocontrolled syntheses of FAHFAs and LC-MS/MS differentiation of regioisomers. *Organic & Biomolecular Chemistry, 14*(38), 9012–9020. https://doi.org/10.1039/c6ob01597b

Barupal, D. K., & Fiehn, O. (2017). Chemical Similarity Enrichment Analysis (ChemRICH) as alternative to biochemical pathway mapping for metabolomic datasets. *Scientific Reports, 7*(1), 14567. https://doi.org/10.1038/s41598-017-15231-w

Betran, A. P., Ye, J., Moller, A.-B., Souza, J. P., & Zhang, J. (2021). Trends and projections of caesarean section rates: Global and regional estimates. *BMJ Global Health, 6*(6), Article e005671. https://doi.org/10.1136/bmjgh-2021-005671

Bourlieu, C., Menard, O., De La Chevasnerie, A., Sams, L., Rousseau, F., Madec, M. N., … Dupont, D. (2015). The structure of infant formulas impacts their lipolysis, proteolysis and disintegration during in vitro gastric digestion. *Food Chemistry, 182*, 224–235. https://doi.org/10.1016/j.foodchem.2015.03.001

Brejchova, K., Balas, L., Paluchova, V., Brezinova, M., Durand, T., & Kuda, O. (2020). Understanding FAHFAs: From structure to metabolic regulation. *Progress in Lipid Research, 79*, Article 101053. https://doi.org/10.1016/j.plipres.2020.101053

Brejchova, K., Radner, F. P. W., Balas, L., Paluchova, V., Cajka, T., Chodounska, H., … Kuda, O. (2021). Distinct roles of adipose triglyceride lipase and hormone-sensitive lipase in the catabolism of triacylglycerol estolides. In *Proceedings of the National Academy of Sciences of the United States of America*. https://doi.org/10.1073/pnas.2020999118

Brezinova, M., Cajka, T., Oseeva, M., Stepan, M., Dadova, K., Rossmeislova, L., … Kuda, O. (2020). Exercise training induces insulin-sensitizing PAHSAs in adipose tissue of elderly women. *BBA MCBL, 1865*(2), Article 158576. https://doi.org/10.1016/j.bbalip.2019.158576

Brezinova, M., Kuda, O., Hansikova, J., Rombaldova, M., Balas, L., Bardova, K., … Kopecky, J. (2018). Levels of palmitic acid ester of hydroxystearic acid (PAHSA) are reduced in the breast milk of obese mothers. *BBA MCBL, 1863*(2), 126–131. https://doi.org/10.1016/j.bbalip.2017.11.004

Clair, G., Reehl, S., Stratton, K. G., Monroe, M. E., Tfaily, M. M., Ansong, C., & Kyle, J. E. (2019). Lipid Mini-On: Mining and ontology tool for enrichment analysis of lipidomic data. *Bioinformatics, 35*(21), 4507–4508. https://doi.org/10.1093/bioinformatics/btz250

Enstad, S., Cheema, S., Thomas, R., Turner, D., Wagner, C., Isesele, P., … Sen, S. (2019). Maternal body mass index influence on breast milk fatty acid esters of hydroxy fatty acids and their potential role in developmental programming. *Current Developments in Nutrition, 3*. doi: 10.1093/cdn/nzz048.OR30-07-19.

Faul, F., Erdfelder, E., Lang, A. G., & Buchner, A. (2007). G*Power 3: A flexible statistical power analysis program for the social, behavioral, and biomedical sciences. *Behavior Research Methods, 39*(2), 175–191. https://doi.org/10.3758/bf03193146

Floris, L. M., Stahl, B., Abrahamse-Berkeveld, M., & Teller, I. C. (2020). Human milk fatty acid profile across lactational stages after term and preterm delivery: A pooled data analysis. *Prostaglandins, Leukotrienes, and Essential Fatty Acids, 156*, Article 102023. https://doi.org/10.1016/j.plefa.2019.102023

Garcia, C., Antona, C., Robert, B., Lopez, C., & Armand, M. (2014). The size and interfacial composition of milk fat globules are key factors controlling triglycerides bioavailability in simulated human gastro-duodenal digestion. *Food Hydrocolloids, 35*, 494–504. https://doi.org/10.1016/j.foodhyd.2013.07.005

Hobbs, A. J., Mannion, C. A., McDonald, S. W., Brockway, M., & Tough, S. C. (2016). The impact of caesarean section on breastfeeding initiation, duration and difficulties in the first four months postpartum. *BMC Pregnancy and Childbirth, 16*, 90. https://doi.org/10.1186/s12884-016-0876-1

Innis, S. M. (2011). Dietary triacylglycerol structure and its role in infant nutrition. *Advances in Nutrition, 2*(3), 275–283. https://doi.org/10.3945/an.111.000448

Kolar, M. J., Kamat, S. S., Parsons, W. H., Homan, E. A., Maher, T., Peroni, O. D., … Saghatelian, A. (2016). Branched fatty acid esters of hydroxy fatty acids are preferred substrates of the MODY8 protein carboxyl ester lipase. *Biochemistry, 55*(33), 4636–4641. https://doi.org/10.1021/acs.biochem.6b00565

Koletzko, B. (2016). Human milk lipids. *Annals of Nutrition and Metabolism, 69*(Suppl 2), 28–40. https://doi.org/10.1159/000452819

Lee, H., Padhi, E., Hasegawa, Y., Larke, J., Parenti, M., Wang, A., … Slupsky, C. (2018). Compositional dynamics of the milk fat globule and its role in infant development. *Frontiers in Pediatrics, 6*, 313. https://doi.org/10.3389/fped.2018.00313

Lee, J., Moraes-Vieira, P. M., Castoldi, A., Aryal, P., Yee, E. U., Vickers, C., … Kahn, B. B. (2016). Branched fatty acid esters of hydroxy fatty acids (FAHFAs) protect against colitis by regulating gut innate and adaptive immune responses. *Journal of Biological Chemistry, 291*(42), 22207–22217. https://doi.org/10.1074/jbc.M115.703835

Li, J., Luo, J., Wang, H., Shi, H., Zhu, J., Sun, Y., … Yao, D. (2015). Adipose triglyceride lipase regulates lipid metabolism in dairy goat mammary epithelial cells. *Gene, 554*(1), 125–130. https://doi.org/10.1016/j.gene.2014.10.020

Libertini, L. J., & Smith, S. (1978). Purification and properties of a thioesterase from lactating rat mammary gland which modifies the product specificity of fatty acid synthetase. *Journal of Biological Chemistry, 253*(5), 1393–1401. https://doi.org/10.1016/s0021-9258(17)34879-2

Lopes, M., Brejchova, K., Riecan, M., Novakova, M., Rossmeisl, M., Cajka, T., & Kuda, O. (2021). Metabolomics atlas of oral 13C-glucose tolerance test in mice. *Cell Reports, 37*(2), Article 109833. https://doi.org/10.1016/j.celrep.2021.109833

Matamoros, C., Harsch, B., Salfer, I., Shepardson, R., Shearer, G., & Harvatine, K. (2020). Characterization of fatty acid esters of hydroxy fatty acids, a novel class of bioactive lipids, in milk fat of cows supplemented with stearic and palmitic acid. *Journal of Dairy Science, 103*(Suppl. 1), 99. https://openprairie.sdstate.edu/dairy_pubdb/2257.

Miles, E. A., & Calder, P. C. (2017). The influence of the position of palmitate in infant formula triacylglycerols on health outcomes. *Nutrition Research, 44*, 1–8. https://doi.org/10.1016/j.nutres.2017.05.009

Miller, R., & Lowe, M. E. (2008). Carboxyl ester lipase from either mother's milk or the pancreas is required for efficient dietary triglyceride digestion in suckling mice. *Journal of Nutrition, 138*(5), 927–930. https://doi.org/10.1093/jn/138.5.927

Mohammad, M. A., Sunehag, A. L., & Haymond, M. W. (2014). De novo synthesis of milk triglycerides in humans. *American Journal of Physiology: Endocrinology and Metabolism, 306*(7), E838–847. https://doi.org/10.1152/ajpendo.00605.2013

Morroni, M., Giordano, A., Zingaretti, M. C., Boiani, R., De Matteis, R., Kahn, B. B., … Cinti, S. (2004). Reversible transdifferentiation of secretory epithelial cells into adipocytes in the mammary gland. *Proceedings of the National Academy of Sciences of the United States of America, 101*(48), 16801–16806. https://doi.org/10.1073/pnas.0407647101

Paluchova, V., Oseeva, M., Brezinova, M., Cajka, T., Bardova, K., Adamcova, K., … Kuda, O. (2020). Lipokine 5-PAHSA is regulated by adipose triglyceride lipase and primes adipocytes for de novo lipogenesis in mice. *Diabetes, 69*(3), 300–312. https://doi.org/10.2337/db19-0494

Pamblanco, M., Ten, A., & Comín, J. (1987). Bile salt-stimulated lipase activity in human colostrum from mothers of infants of different gestational age and birthweight. *Acta Paediatrica Scandinavica, 76*(2), 328–331. https://doi.org/10.1111/j.1651-2227.1987.tb10469.x

Parsons, W. H., Kolar, M. J., Kamat, S. S., Cognetta, A. B., 3rd, Hulce, J. J., Saez, E., … Cravatt, B. F. (2016). AIG1 and ADTRP are atypical integral membrane hydrolases that degrade bioactive FAHFAs. *Nature Chemical Biology, 12*(5), 367–372. https://doi.org/10.1038/nchembio.2051

Pérez-Gálvez, A., Calvo, M. V., Megino-Tello, J., Aguayo-Maldonado, J., Jiménez-Flores, R., & Fontecha, J. (2020). Effect of gestational age (preterm or full term) on lipid composition of the milk fat globule and its membrane in human colostrum. *Journal of Dairy Science, 103*(9), 7742–7751. https://doi.org/10.3168/jds.2020-18428

Prior, E., Santhakumaran, S., Gale, C., Philipps, L. H., Modi, N., & Hyde, M. J. (2012). Breastfeeding after cesarean delivery: A systematic review and meta-analysis of world literature. *American Journal of Clinical Nutrition, 95*(5), 1113–1135. https://doi.org/10.3945/ajcn.111.030254

Sha, L., Zhou, S., Xi, Y., Li, R., & Li, X. (2019). The level of bile salt-stimulated lipase in the milk of Chinese women and its association with maternal BMI. *Journal of Biomedical Research, 34*(2), 122–128. https://doi.org/10.7555/JBR.33.20180107

Spear, M. L., Bitman, J., Hamosh, M., Wood, D. L., Gavula, D., & Hamosh, P. (1992). Human mammary gland function at the onset of lactation: Medium-chain fatty acid synthesis. *Lipids, 27*(11), 908–911. https://doi.org/10.1007/BF02535871

Tan, D., Ertunc, M. E., Konduri, S., Zhang, J., Pinto, A. M., Chu, Q., … Saghatelian, A. (2019). Discovery of FAHFA-containing triacylglycerols and their metabolic regulation. *Journal of the American Chemical Society, 141*(22), 8798–8806. https://doi.org/10.1021/jacs.9b00045

Xiao, X., Mukherjee, A., Ross, L. E., & Lowe, M. E. (2011). Pancreatic lipase-related protein-2 (PLRP2) can contribute to dietary fat digestion in human newborns. *Journal of Biological Chemistry, 286*(30), 26353–26363. https://doi.org/10.1074/jbc.M111.249813

Yore, M. M., Syed, I., Moraes-Vieira, P. M., Zhang, T., Herman, M. A., Homan, E. A., … Kahn, B. B. (2014). Discovery of a class of endogenous mammalian lipids with anti-diabetic and anti-inflammatory effects. *Cell, 159*(2), 318–332. https://doi.org/10.1016/j.cell.2014.09.035